LHC Phenomenology of a Z' decaying into supersymmetric particles

Masterarbeit

von

Manuel Krauß

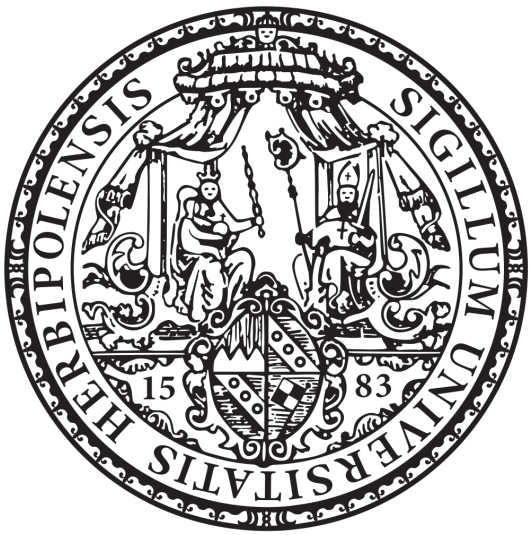

vorgelegt bei

Prof. Dr. Werner Porod

10. Juli 2012

Lehrstuhl für Theoretische Physik II
Institut für Theoretische Physik und Astrophysik
Julius-Maximilians-Universität Würzburg

Zusammenfassung

Diese Arbeit beschäftigt sich mit einer $U(1)_{B-L}$-Erweiterung der Standardmodell-Eichgruppe. Modelle dieser Art sind besonders attraktiv, da zusätzliche $U(1)$-Eichgruppen mit geladener Baryonzahl minus Leptonzahl im Niederenergielimes einer großen Anzahl von vereinheitlichten Theorien entspringen. Da die Supersymmetrie zudem Lösungen zu fundamentalen Problemen des Standardmodells bietet, betrachten wir eine supersymmetrische Version des Modells.

Eine direkte Folge der zusätzlichen lokalen Eichsymmetrie ist die Existenz eines weiteren neutralen Eichbosons, des Z', dessen Eigeschaften hier näher untersucht werden. Ein besonderes Augenmerk wird hierbei auf eine Eigenschaft gelegt, die durch die Existenz zweier Abelscher Eichgruppen auftritt: die eichkinetische Mischung. Diese beeinflusst sowohl die Kopplungen als auch die Produktion des Z' am LHC, was wir explizit zeigen. Desweiteren berechnen wir die Massenbeschränkung auf das Z' für unser Modell unter Benutzung von Dilepton-Produktionsdaten der ATLAS-Kollaboration. Die Beschränkung wird hierbei einerseits durch die Anwesenheit der kinetischen Mischung als auch durch offene Zerfallskanäle in supersymmetrische Teilchen im Vergleich zu verwandten Modellen gelockert, sodass die untere Massenschranke im betrachteten Modell bei etwa 1.7 TeV liegt.

Im letzten Teil der Arbeit wird untersucht, wie eine Z'-Resonanz sich auf die Smyonen-Produktion am LHC auswirkt. Ein wichtiger Entdeckungskanal hiervon enthält zwei Myonen sowie nicht detektierbare Teilchen. Um das Entdeckungspotential der Smyonen über eine Z'-Resonanz an einem Hadronenbeschleuniger zu testen, führen wir eine Monte-Carlo-Studie durch. Hierbei wird festgestellt, dass bei einer Schwerpunktsenergie von 14 TeV und einer integrierten Luminosität von 100 fb^{-1} (300 fb^{-1}) Smyonen mit einer Masse von bis zu 800 GeV (900 GeV) potentiell entdeckt werden können.

Abstract

In this thesis we consider a $U(1)_{B-L}$ extension of the Standard Model gauge group. The investigation of such models is motivated by the fact that a $U(1)$ with charged baryon number minus lepton number emerges out of various Grand Unified Theories as an effective theory at low energy scales. We further consider the model to be supersymmetric as supersymmetry helps solving various problems of the Standard Model.

Since we consider a local $U(1)_{B-L}$, there arises an additional neutral gauge boson, the Z', and its properties and especially decays into supersymmetric particles are the main topic of this work. We investigate the effects of gauge kinetic mixing which is the consequence of a mixing term between the $U(1)$ field strength tensors in the Lagrangian of the model. The influence on the branching ratios of the Z' and the production at the LHC is shown. We further constrain the Z' mass using the latest ATLAS data on dilepton production. It is found that the bound gets reduced substantially by the effect of gauge kinetic mixing as well as open decay channels into supersymmetric partcles such that the Z' must be heavier than about 1.7 TeV in the considered model.

In the last part of this work we examine the impact of a Z' resonance on smuon production and discovery. In a Monte Carlo study searching for two muons and missing energy at 100 fb^{-1} (300 fb^{-1}) of integrated luminosity and $\sqrt{s} = 14$ TeV, we find that smuons with masses up to 800 GeV (900 GeV) can potentially be discovered at the LHC.

Contents

Chapter 1

Introduction

With the start of data-taking at the Large Hadron Collider (LHC) [1] at the CERN in Geneva, particle physics has entered a new era: for the first time, the TeV scale is experimentally accessible in collider experiments. Presently, it is very likely that the much-anticipated Higgs boson has finally been discovered, which is the last particle not yet found in the so far greatly affirmed Standard Model of particle physics[1] (SM). Even more interestingly, most theories that go beyond the SM predict new particles at the TeV scale. Thus, the LHC has the unique possibility to confirm or to strongly constrain appealing models.

One class of these models under frequent discussion imposes supersymmetry (SUSY) [4, 5], which is a symmetry between fermionic and bosonic degrees of freedom. Hence, a bosonic partner to each fermion is postulated and vice versa. High hopes are invested in SUSY as supersymmetric models are able to provide solutions to some problems of the SM and to eradicate some disfigurements. Thus, SUSY is among the most favoured extensions to the SM. We consider a constrained model, *i.e.* we impose boundary conditions on the free parameters at a high energy scale, which is determined by the energy where all gauge couplings unify to a single value, which is possible in SUSY due to the additional field content.

However, minimal constrained models like the CMSSM are for one thing not complete – *e.g.* neutrino masses can still not be explained within their framework – and for another thing, more and more parameter space has been excluded by LHC measurements, direct and indirect ones. A way out of this misery is an extension of the gauge group of the model. One of the simplest and best-motivated extensions is an extra $U(1)$ symmetry group which has a rich variety of phenomenological consequences.

In this thesis we study a $U(1)$ extension of the MSSM with charged $B - L$, where B and L are baryon and lepton number. We further impose CMSSM-like boundary conditions. An immediate consequence of the additional local symmetry group is the existence of an additional neutral vector boson, the Z', the decays and production of which at the LHC we are about to discuss here.

[1] For an overview of the SM, see *e.g.* [2, 3].

The work is organized as follows: first we will introduce the Z' as a product of the additional $U(1)_{B-L}$ symmetry. Afterwards, an overview of supersymmetry and the MSSM as well as the $B-L$ extension, the BLSSM, is given in chapters 3 and 4. Subsequently, a brief study of the free parameter space is performed and after deriving the Z' couplings and partial decay widths, the branching ratios into the various SM and supersymmetric particles are shown. We will particularly highlight the impact of gauge kinetic mixing, an effect that naturally arises in this class of extended gauge groups. We will then concentrate on the on-shell production of the Z' at a proton-proton collider and derive the lower bounds on the mass of the particle, followed by an analysis of its most interesting supersymmetric decay modes. At the end, in chapter 6, we show the results of a Monte Carlo analysis searching for smuons at the LHC driven by a Z' resonance. Finally, we will summarize. In the appendix we show the relevant Z' vertices, branching ratios at distinct parameter points as well as some mass matrices.

Chapter 2

Z' physics

It is a common belief among particle physicists that the symmetry group of the Standard Model, which is $\mathcal{G}_{SM} = SU(3)_c \times SU(2)_L \times U(1)_Y$, is not all there is. One instead often assumes that it arises from a higher symmetry group which unifies the gauge couplings at some high energy scale and gets broken down to the Standard Model group at lower energies. The simplest gauge group which fully contains $\mathcal{G}_{SM}$ and thus is a candidate for a Grand Unified Theory (GUT) is $SU(5)$ [6, 7]. As the rank of $SU(5)$ is 4, which is the same for $\mathcal{G}_{SM}$, no additional gauge groups appear with the breakdown to the SM group. However, non-supersymmetric $SU(5)$-GUT has been ruled out by experimental data[1]. Moreover, a global $B - L$ symmetry is present in $SU(5)$, which is why there is no Majorana mass term available for neutrinos. Thus, a mechanism to explain neutrino masses is absent in these models [10, 11]. As a consequence, larger GUT-groups like $SO(10)$ or E_6 are considered. As those have ranks higher than $\mathcal{G}_{SM}$, breaking them at a high scale can lead to $\mathcal{G}_{SM} \times U(1)'^n$. Thus, additional $U(1)$ gauge groups appear quite naturally if one tries to extend the Standard Model towards higher energies. As gauge symmetries are always accompanied by gauge bosons, a new local $U(1)$ involves a new electrically neutral spin-1 boson, which we will call Z'. In what follows, we will consider $n = 1$, *i.e.* we add one Z' to the gauge sector of the Standard Model.

2.1 Implications of a new gauged $U(1)$

Extending the SM gauge group by a $U(1)'$, the group structure reads

$$\mathcal{G}' = SU(3)_c \times SU(2)_L \times U(1)_Y \times U(1)' \,. \tag{2.1}$$

Besides the arising Z', an additional $U(1)$ symmetry also has implications on the matter content. The cancellation of both gauge and mixed gauge-gravity anomalies

[1] SU(5) GUTs predict proton decay as they involve bosons which carry both lepton and baryon number and thus mediate L and B breaking interactions. In minimal $SU(5)$, the proton lifetime is at most $\mathcal{O}(10^{-31})$ years [8]. This limit has been exceeded experimentally decades ago (see, *e.g.*, [9]).

is in general not possible if one assumes SM particles alone, but additional fermions, so-called exotics, are needed [12–14]. Depending on the particular model, these may carry some SM quantum numbers or be singlets under $\mathcal{G}_{SM}$.

Looking at the Lagrangian of our model, we see a special feature arising in the presence of two $U(1)$ groups in eq. (2.1) known as gauge kinetic mixing. As the corresponding field strength tensors $F_i^{\mu\nu}$ are Abelian and thus gauge invariant by themselves [15], this allows for a mixing term between the hypercharge and the additional field tensor in the kinetic part of the Lagrangian [16]:

$$\mathscr{L}_{\text{mix}} = -\chi \hat{F}_Y^{\mu\nu} \hat{F}'_{\mu\nu} \,. \tag{2.2}$$

This in turn gives rise to a mixing between the two $U(1)$s as the physical fields need to be diagonal. Diagonalization can be done by a rotation in the $U(1)$ fields B^μ and B'^μ, which leads new, mixed linear combinations [15]. These fields consequently couple to both hypercharge and the new $U(1)'$ charge.

An equivalent and technically more manageable approach [17] is to consider a general covariant derivative of the form [16]

$$D_\mu = \partial_\mu - iQ^i G^{ij} A^j \,, \tag{2.3}$$

where Q^i and A^j are 2-vectors containing the charges and $U(1)$ fields, respectively and G is a 2×2 coupling matrix that allows for off-diagonal couplings. This approach has been chosen to work with in our model (see chapter 4).

As there are no additional gauge bosons observed yet, the Z', if it exists, needs to be a massive particle. Thus, the corresponding $U(1)'$ has to be broken by some scalar field Φ which couples to the Z' and, by acquiring a vacuum expectation value (VEV), generates a mass term for the Z'. Allowing for a kinetic mixing between the fields then implies mass mixing terms between the Standard Model Z and the Z'. Additional mixing terms can arise if the Higgs field responsible for the $U(1)$ breaking is gauged under the SM gauge group or vice versa [15, 18]. The mass mixing can be parametrized by a mixing angle θ'_W so that the rotation between the gauge and mass eigenstates reads [19]

$$\begin{pmatrix} B^\mu \\ W^{3\mu} \\ B'^\mu \end{pmatrix} = \begin{pmatrix} \cos\theta_W & -\sin\theta_W \cos\theta'_W & \sin\theta_W \sin\theta'_W \\ \sin\theta_W & \cos\theta_W \cos\theta'_W & -\cos\theta_W \sin\theta'_W \\ 0 & \sin\theta'_W & \cos\theta'_W \end{pmatrix} \begin{pmatrix} \gamma^\mu \\ Z^\mu \\ Z'^\mu \end{pmatrix} . \tag{2.4}$$

Electroweak precision measurements at the Z pole have the power to strongly constrain the mixing with a Z' because its influence will alter precision observables like asymmetries, decay ratios and the Z lineshape. Thus, limits of the order $|\theta'_W| < \mathcal{O}(10^{-3})$ could be set [13].

2.2 Different models

There is a huge number of distinct Z' models which all have different features. We do not name all of them here but give a brief overview over some frequently discussed classes of models.

The sequential model

In the sequential model, the Z' is assumed to be a copy of the Standard Model Z boson, but only with a higher mass. Thus, all the couplings remain the same.

E_6-derived models: $U(1)_\chi$ and $U(1)_\psi$

When decomposing E_6 into effective subgroups, several different $U(1)$s can arise, *e.g.* $E_6 \to SO(10) \times U(1)_\psi \to SU(5) \times U(1)_\chi \times U(1)_\psi$ [14, 18] where linear combinations $\psi \cos\beta + \chi \sin\beta$ can give a light Z'. The charges of the matter fields associated with these $U(1)$s are [14]

$$-Q_\chi^{q_L} = \frac{1}{3} Q_\chi^{l_L} = \frac{1}{\sqrt{40}},\ Q_\psi^{q_L} = Q_\psi^{l_L} = \frac{1}{\sqrt{24}},\ g_1' = g_1 \sqrt{\frac{5}{3}} \sin\theta_W. \tag{2.5}$$

Often discussed Z' scenarios (see, *e.g.* [13, 14]) are the pure Z'_χ and Z'_ψ and also the Z'_η where $\beta = -\arctan\sqrt{5/3}$.

Z'_{B-L}: charged baryon and lepton number

In a large variety of models a $U(1)_{B-L}$ occurs after the decomposition of some higher GUT group, *i.e.* the matter fields carry charges proportional to their baryon number minus lepton number.

As $U(1)_{B-L}$ is a subgroup of $SO(10)$, gauged $B-L$ often appears associated with an $SO(10)$-GUT over an intermediate left-right-symmetric stage $SU(3)_c \times SU(2)_L \times SU(2)_R \times U(1)_{B-L}$ (see *e.g.* [20]). However, in this work we focus on the minimal (supersymmetric) $B-L$ model, *i.e.* we consider the gauge group $\mathcal{G}_{SM} \times U(1)_{B-L}$ in a so to speak bottom-up approach. Beginning from a GUT, this structure can, for instance, arise from an $E_8 \times E_8$ heterotic string and M-theory [21].

Gauged $B-L$ is a very appealing extension of the Standard Model as it explains the (in the SM accidental) conservation of baryon minus lepton number. Additionally, to cancel anomalies, at least one SM-singlet fermion per generation has to be introduced [19]. The $B-L$ charge these singlets have to carry can be interpreted as a lepton number of -1 which, in turn, points directly towards right-handed neutrinos. Hence the theory incorporates right-handed neutrinos by default and neutrino masses can be generated in a natural way.

2.3 Current bounds

LEP-II limits

No non-SM resonances have been observed over the full energy range of LEP-II, implying that either the $U(1)'$ coupling g_1' is at most of the order 10^{-2}, or that the mass of the Z' is above 209 GeV [22]. We will study the latter case.

In order to get information about a possible Z' intermediate state, 4-fermion contact interactions of the form [12, 23]

$$\mathscr{L}_{eff} = \frac{\pm 4\pi}{(1+\delta_{ef})\left(\Lambda_{AB}^{f\pm}\right)^2}\left(\bar{e}\gamma_\mu P_A e\right)\left(\bar{f}\gamma^\mu P_B f\right) \tag{2.6}$$

have been considered where $A, B = L, R$ and thus $P_{A/B}$ are the left/right projection operators. Also vector-like (V) and axial-vector-like (A) coupling structures have been taken into account, such that for instance $P_V = P_R + P_L$. Λ is the mass dimension observable. The contact interaction for an s-channel Z' up to the order $s/M_{Z'}$ then reads [12, 22]

$$\mathcal{M} \approx \frac{g_1'^2}{M_{Z'}^2 - s}\left(\bar{e}\gamma_\mu\left(Q_{e_L}P_L + Q_{e_R}P_R\right)e\right)\left(\bar{f}\gamma^\mu\left(Q_{f_L}P_L + Q_{f_R}P_R\right)f\right)\,, \tag{2.7}$$

where Q_{e_L}/Q_{f_L} and Q_{e_R}/Q_{f_R} denote the $U(1)'$ charges of the left- and right-handed components of the electron/final-state fermion. The impact of kinetic and mass mixing has been neglected for these derivations.

Since the LEP data agrees with the Standard Model expectations, bounds on $M_{Z'}/g_1'$ can be set. According to ref. [12], the bounds on a non-supersymmetric Z'_{B-L} with its $B-L$ coupling $g_{\mathrm{BL}} \equiv g_1'$ read

$$\frac{M_{Z'}}{g_{\mathrm{BL}}Q_e^{B-L}} > 6\ \mathrm{TeV}\,. \tag{2.8}$$

However, ref. [24] claims to be able to set even stronger bounds of $M_{Z'}/(g_{\mathrm{BL}}Q_e^{\mathrm{B\text{-}L}}) > 6.7$ TeV by the combination of all the 4-fermion operators measured in [23]. In what follows, we will refer to this bound as it is the more conservative one. We will see later on that this formula has to be modified if we do not neglect gauge kinetic mixing since then the Z' vertex with fermions is altered by means of the off-diagonal coupling.

LHC limits

The results on the searches for dilepton resonances have recently been published by the LHC-collaborations ATLAS [25] and CMS [26] for an integrated luminosity of 5 fb^{-1} at $\sqrt{s} = 7$ TeV. The theoretical calculation has been done for the on-shell production of a Z' assuming the factorisation

$$\sigma(pp \to Z' + X \to l^+l^- + X) \approx \sigma(Z') \times BR(Z' \to l^+l^-)\,, \tag{2.9}$$

where the convolution of the proton PDFs is understood to be included in $\sigma(Z')$. Interference between the Z' and Z/γ exchange has been neglected. The experimental limits have been compared to the expectations of Z's originating from E_6 models and

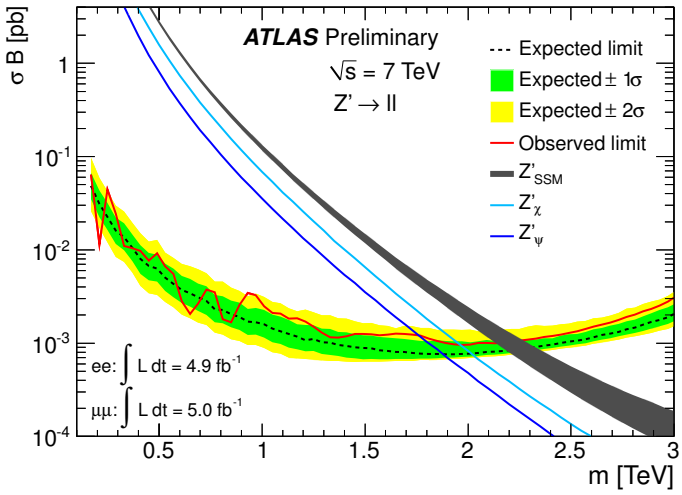

Figure 2.1: ATLAS results for the upper bound on $M_{Z'}$ in the search for dilepton resonances. The red curve shows the experimental limits using data with 5 fb^{-1} of integrated luminosity. Image taken from [25].

for the sequential model. Fig. 2.1 shows the related ATLAS plot of the experimental constraints.

Bounds on the Z'_{B-L} have not been given but will be derived in section 5.5 for the minimal supersymmetric $B-L$ model whereby we explicitly take care of the influence of $U(1)$-mixing.

Chapter 3

Supersymmetry

3.1 Motivation

When constructing a theory from scratch, one needs to know which symmetries should be fulfilled by the S-Matrix. The theorem of Coleman and Mandula [27] states that the only conserved charges transforming as tensors under the Lorentz group – and thus the only spacetime symmetries – are the generators of translations P_μ and of Lorentz transformations $M_{\mu\nu}$. All other symmetries ought to be Lorentz scalars [28]. This is, however, not true in its entirety. What Coleman and Mandula assumed for their no-go theorem were exclusively commutation relations between the charges and thus bosonic symmetries. Haag, Łopuszański and Sohnius [29], however, showed that Fermi-type generators, obeying anticommutation relations and transforming as spinors under the Lorentz group, may be added as a third nontrivial spacetime symmetry. As these generators Q carry spinor charge, they will turn fermionic degrees of freedom into bosonic ones and vice versa. Thus, they create a symmetry which connects bosons and fermions:

$$Q|\text{fermion}\rangle = |\text{boson}\rangle, \quad Q|\text{boson}\rangle = |\text{fermion}\rangle\,. \tag{3.1}$$

This type of symmetry is called supersymmetry (SUSY). But why should we make the effort to consider this type of additional symmetry?

It is well known that the Standard Model has some severe problems to face which are assumed to be solved by introducing new physics at some high scale. A simple example of a phenomenon where the description of nature fails is the missing dark matter candidate in the SM[1]. The probably most popular theoretical issue is the so-called hierarchy problem [30, 31], which is a problem of quadratic divergencies appearing in loop corrections to scalar fields: the masses in the SM are generated by the couplings to the Higgs field, which has the scalar potential

$$V = m_H^2 \phi^\dagger \phi + \lambda (\phi^\dagger \phi)^2\,. \tag{3.2}$$

[1]Such candidates can be found in supersymmetry, as we will see later on, *e.g.* in the fermionic counterpart of the neutral SM bosons.

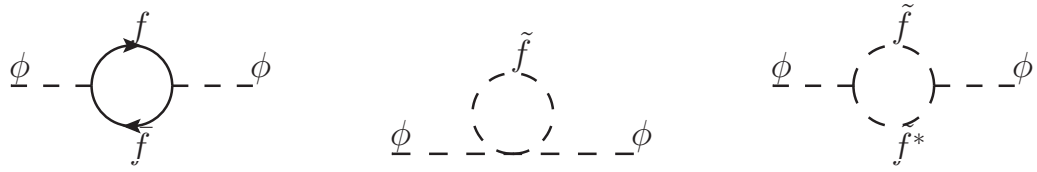

Figure 3.1: Loop corrections to a scalar line coming from a fermion loop (left) and from scalar loops (middle, right).

The mass scale of the SM is set by the Higgs VEV $v/\sqrt{2} = \langle\phi\rangle = \sqrt{-m_H^2/2\lambda}$ which is experimentally determined by the mass of the W boson to $\langle\phi\rangle = 174$ GeV [30]. Hence, all masses range up to $\mathcal{O}(100\text{ GeV})$, depending on the distinct couplings to the Higgs field.

By calculating the quantum corrections to the scalar field, it turns out that m_H^2 receives large loop contributions from all the particles that couple to the Higgs. If we do the regularization by a cut-off Λ, this has to be set for logical reasons to the scale of new physics or, if no new physics does occur, at least the Planck scale $M_P \sim \sqrt{G_{\text{Newton}}}^{-1} \sim 10^{-19}$ GeV, since quantum gravitational effects should become sizeable here[2]. Consider *e.g.* the coupling to fermions: the interaction term in the Lagrangian reads $-\lambda_f \phi \bar{f} f$, which results in loop contributions of the form [30]

$$\Delta m_H^2 = -\frac{|\lambda_f|^2}{8\pi^2}\Lambda^2 + \dots , \tag{3.3}$$

i.e., the loop corrections are orders of magnitude higher (up to 30 orders if $\Lambda = M_P$) than the actual value of m_H^2. This in turn has to be around $-(100\text{ GeV})^2$ if we take λ as a small quantity in order to preserve perturbativity. This behaviour needs enormous fine-tuning and thus spoils the desirable principle of naturalness, which in plain terms says that physical observables should be stable under small variations of the bare (unrenormalized) quantities [28].

A way to elegantly avoid this problem is provided by SUSY: assume a scalar counterpart $\tilde{f}$ for each Standard Model fermion. Then, for each fermion loop diagram, there exist two loops containing the scalar which together give positive contributions to Δm_H^2 (recall that the minus sign in eq. (3.3) is due to the fermion loop and does not appear in scalar loops). The additional quantum correction quadratic in Λ reads[3]

$$\Delta m_H^2 = \frac{\lambda_S}{16\pi^2}\Lambda^2 - \dots , \tag{3.4}$$

with λ_S being the quadrilinear coupling related to the interaction term $-\lambda_S |\phi|^2 |\tilde{f}|^2$. Since supersymmetry not only adds a scalar to each fermion but relates them by a

[2]The renormalizability of the Standard Model ensures that the theory is well-defined and just receives finite loop contributions even in the limit of infinite energies, *i.e.* for $\Lambda \to \infty$ [31]. This would, however, imply that the SM is all there is. Hence, a finite cut-off scale seems natural.

[3]To be exact, only the quadrilinear coupling in fig. 3.1 gives a term quadratic in Λ which may cancel the contribution in eq. (3.3).

symmetry transformation, the coupling parameters $|\lambda_f|^2$ and λ_S are equal. With a fermion getting a scalar counterpart for each chirality state, for each SM fermion, there are two scalars running in the second loop of fig. 3.1. Thus, the leading terms in Δm_H^2 cancel exactly and the hierarchy problem is solved.

3.2 Superalgebra and Superfields

As stated in the last section, the generators of supersymmetry transformations carry spinorial charges. They can be expressed by the two-component Weyl spinors Q_α and $\bar{Q}^{\dot{\alpha}} = (Q^\alpha)^*$ [32]. In general, N different generators Q_α^A are allowed, where A labels a possible internal symmetry[4]. We will restrict ourselves to the case $N = 1$ in this work. As they perform spacetime operations, the generators have to form a closed algebra [32, 33]:

$$\{Q_\alpha, Q_\beta\} = \{\bar{Q}_{\dot{\alpha}}, \bar{Q}_{\dot{\beta}}\} = 0 \tag{3.5}$$

$$\{Q_\alpha, \bar{Q}_{\dot{\beta}}\} = 2\sigma^\mu_{\alpha\dot{\beta}} P_\mu \tag{3.6}$$

$$[P^\mu, Q_\alpha] = 0\,, \tag{3.7}$$

where $\sigma^\mu = (\mathbb{1}_2, \boldsymbol{\sigma})$.

The irreducible representations of the SUSY algebra contain both fermionic and bosonic states with the same quantum numbers, the so-called superpartners. These representations are known as supermultiplets. The bosonic superpartners of the SM fermions are commonly labelled by an additional "s" in front of the name, while the fermionic superpartners receive an extra "ino" at the end, so we are talking about sfermions and gauginos. For this reason, supersymmetric particles are sometimes called "sparticles". One can show that, in a supersymmetric theory, the number of fermionic degrees of freedom n_F equals the number of bosonic ones n_B [30, 32].

The corresponding matter supermultiplets can be realized by chiral supermultiplets containing one Weyl fermion ψ_i and one complex scalar (or two real scalars) ϕ_j. In order to close the SUSY algebra off-shell[5], we require an auxiliary complex scalar field F with mass dimension 2. The supersymmetric free-field Lagrangian may be written as [30, 32]

$$\mathscr{L}_{\text{free}} = (\partial_\mu \phi^*)(\partial^\mu \phi) + i\bar{\psi}\bar{\sigma}^\mu \partial_\mu \psi + F^* F\,. \tag{3.8}$$

The Euler-Lagrange equation of motion accordingly gives $F = 0$ on-shell, which means that F is a non-propagating (unphysical) field which is just needed to formulate an interacting theory.

[4] Only the cases $N \leq 4$ allow for renormalizable theories while for $N > 8$, gravity can not included consistently into the theory [28].

[5] A Weyl spinor field has one complex component in the on-shell case while it has two components off-shell. This would imply a mismatch of n_F and n_B that has to be absorbed.

In order to write an interaction term, we define the (left) chiral superfield

$$\begin{aligned}\Phi(x,\theta,\bar{\theta}) =&\phi(x) + \sqrt{2}\theta\psi(x) + \theta\theta F(x) - i\partial_\mu\phi(x)\theta\sigma^\mu\bar{\theta} \\ &+ \frac{i}{\sqrt{2}}\theta\theta\partial_\mu\psi(x)\sigma^\mu\bar{\theta} - \frac{1}{4}\partial_\mu\partial^\mu\phi(x)\theta\theta\bar{\theta}\bar{\theta}\,,\end{aligned} \tag{3.9}$$

with the two-component Grassmann variables θ and $\bar{\theta}$. Particularly interesting for the kinetic part of the Lagrangian are the coefficients of the $\theta\theta\bar{\theta}\bar{\theta}$ terms in the products of superfields, the so-called D-terms. The F-terms, in contrast, are the coefficients of $\theta\theta$. They are especially useful for supersymmetric model construction [33].

Now, we are ready to write down an interacting Lagrangian. In the Wess-Zumino Model, it is given by [32]

$$\mathscr{L} = \sum_i [\Phi_i^\dagger \Phi_i]_D + ([W(\Phi)]_F + \text{h.c.})\ , \tag{3.10}$$

where we have made use of the superpotential

$$W(\Phi) = \frac{1}{2}m_{ij}\Phi_i\Phi_j + \frac{1}{3}\lambda_{ijk}\Phi_i\Phi_j\Phi_k\,, \tag{3.11}$$

m_{ij} and λ_{ijk} being totally symmetric. A special feature of the superpotential is that it has to be analytic in the fields such that terms like $\Phi^*\Phi$ are forbidden [30]. The derivatives due to the scalar fields are commonly written as

$$W^i = \frac{\partial}{\partial\phi_i}W(\phi), \qquad W^{ij} = \frac{\partial^2}{\partial\phi_i\partial\phi_j}W(\phi)\,. \tag{3.12}$$

The auxiliary fields in the chiral Lagrangian can be eliminated by its equations of motion [30]:

$$F_i = -W_i^*, \qquad F^{*i} = -W^i\,, \tag{3.13}$$

so that we arrive at the chiral Lagrangian

$$\mathscr{L}_{\text{chiral}} = \partial_\mu\phi_i^*\partial^\mu\phi_i + i\bar{\psi}_i\bar{\sigma}^\mu\partial_\mu\psi_i - \frac{1}{2}(W^{ij}\psi_i\psi_j + W_{ij}^*\bar{\psi}^i\bar{\psi}^j) - W^iW_i^*\,, \tag{3.14}$$

whereas $W^iW_i^*$ is the scalar potential V[6].

The gauge fields are included in gauge supermultiplets containing one vector boson A_μ^a and a Weyl fermion λ^a. The Lagrangian for that reads [30]

$$\mathscr{L}_{\text{gauge}} = -\frac{1}{4}F_{\mu\nu}^a F^{a,\mu\nu} + i\bar{\lambda}^a\bar{\sigma}^\mu D_\mu\lambda^a + \frac{1}{2}D^aD^a\,, \tag{3.15}$$

[6]Therefore, if we replace the superfields Φ by scalar fields ϕ in the superpotential, m_{ij} corresponds to a fermion mass matrix and λ_{ijk} to the Yukawa couplings.

with the covariant derivative D_μ. Here again, auxiliary fields D^a are needed to close the algebra off-shell. The interaction terms between the gauge and chiral multiplets read

$$\mathscr{L}_{\text{int}} = -\sqrt{2}g(\phi^* T^a \psi)\lambda^a - \sqrt{2}g\bar{\lambda}^a(\bar{\psi}T^a\phi) + g(\phi^* T^a \phi)D^a \,. \tag{3.16}$$

whereas the last term together with $\frac{1}{2}D^a D^a$ in $\mathscr{L}_{\text{gauge}}$ induces the equations of motion for the auxiliary fields [30]

$$D^a = -g(\phi^* T^a \phi)\,. \tag{3.17}$$

Altogether, one arrives at the full supersymmetric Lagrangian

$$\mathscr{L} = \mathscr{L}_{\text{chiral}} + \mathscr{L}_{\text{gauge}} + \mathscr{L}_{\text{int}}\,, \tag{3.18}$$

where we imply the substitution $\partial_\mu \to D_\mu$ in $\mathscr{L}_{\text{chiral}}$.

3.3 Soft SUSY-breaking

Eq. (3.7) implies that the masses of the superpartners are identical. This, however, would have been measured long time ago and thus is not the case. Hence, if SUSY is realized in nature, it has to be broken spontaneously, *i.e.* while the Lagrangian is invariant under supersymmetry transformations, the vacuum state is not. The mechanism of how this should occur is an open question. Thus, it is useful to parametrize the breaking by adding explicit SUSY-breaking terms to the Lagrangian.

We introduced (unbroken) supersymmetry as a solution of the hierarchy problem. This is still possible if the mass difference $m_{\tilde{f}} - m_f$ is not too big as the leading contribution to Δm_H^2 is proportional to $(m_{\tilde{f}}^2 - m_f^2)\log(m_{\tilde{f}}^2/m_f^2)$ [33]. These contributions are small enough if the breaking occurs at most at the TeV scale. One then speaks about softly broken supersymmetry. A generic soft breaking Lagrangian can be written as [30]

$$\mathscr{L}_{\text{soft}} = -M_{ij}^2\phi_i^*\phi_j - \left(\frac{1}{2}M_a\lambda^a\lambda^a + \frac{1}{6}a_{ijk}\phi_i\phi_j\phi_k + \frac{1}{2}b_{ij}\phi_i\phi_j + t_i\phi_i\right) + \text{h.c.}\,, \tag{3.19}$$

with the explicit gaugino mass parameters M_a as well as additional scalar-only mass terms and couplings which shift the sfermion masses to higher values.

3.4 The MSSM

In its minimal supersymmetric realization, the Standard Model particle content is just doubled by the respective superpartners and additional fields or symmetries are only included if necessary. We label it the Minimal Supersymmetric Model (MSSM). Detailed overviews can be found in [28, 30, 31, 34].

superfield		spin-0	spin-$\frac{1}{2}$	$SU(3)_c \times SU(2)_L \times U(1)_Y$
quarks	$\hat{Q}$	$\tilde{Q} = (\tilde{u}, \tilde{d})$	$Q = (u, d)$	$(\mathbf{3}, \mathbf{2}, \frac{1}{6})$
and squarks	$\hat{U}$	$\tilde{u}^c$	u^c	$(\bar{\mathbf{3}}, \mathbf{1}, -\frac{2}{3})$
	$\hat{D}$	$\tilde{d}^c$	d^c	$(\bar{\mathbf{3}}, \mathbf{1}, \frac{1}{3})$
sleptons	$\hat{L}$	$\tilde{L} = (\tilde{\nu}, \tilde{e})$	$L = (\nu, e)$	$(\mathbf{1}, \mathbf{2}, -\frac{1}{2})$
and leptons	$\hat{E}$	$\tilde{e}^c$	e^c	$(\mathbf{1}, \mathbf{1}, 1)$
Higgses	$\hat{H}_u$	(H_u^+, H_u^0)	$(\tilde{H}_u^+, \tilde{H}_u^0)$	$(\mathbf{1}, \mathbf{2}, \frac{1}{2})$
and Higgsinos	$\hat{H}_d$	(H_d^0, H_d^-)	$(\tilde{H}_d^0, \tilde{H}_d^-)$	$(\mathbf{1}, \mathbf{2}, -\frac{1}{2})$

Table 3.1: Matter content of the MSSM.

There is, however, one peculiarity that arises when extending the SM towards the MSSM: while it is sufficient in the SM to have just one scalar $SU(2)_L$ doublet field H that generates the masses of all matter fields, this is not possible within the MSSM: invariance under supersymmetry imposes a superpotential that has to be analytic in the chiral superfields [34]. Hence, the adjoint of a chiral superfield, $\hat{H}^\dagger$, may not appear together with $\hat{H}$ in the superpotential and thus a term proportional to $\hat{H}^\dagger \hat{H}$ is not allowed. So, in order to write a gauge and supersymmetry invariant Lagrangian but also break $SU(2)_L \times U(1)_Y$ by Higgs VEV(s), two complex Higgs doublets H_u and H_d are needed such that the superpotential of the MSSM reads

$$W_{MSSM} = Y_u^{ij}\, \hat{U}_i\, \hat{Q}_j\, \hat{H}_u - Y_d^{ij}\, \hat{D}_i\, \hat{Q}_j\, \hat{H}_d - Y_e^{ij}\, \hat{E}_i\, \hat{L}_j\, \hat{H}_d + \mu\, \hat{H}_u\, \hat{H}_d\,. \tag{3.20}$$

$\hat{U}, \hat{D}, \hat{Q}, \hat{E}$ and $\hat{L}$ denote the chiral superfields and Y are the corresponding Yukawa couplings. Generation indices have been suppressed. A summary over the chiral and gauge supermultiplets is given in tables 3.1 and 3.2.

The soft SUSY-breaking terms of the MSSM, which follow from eq. (3.19), are

$$\begin{aligned}\mathscr{L}_{\text{soft,MSSM}} = &-\frac{1}{2}\left(M_1\, \tilde{B}\tilde{B} + M_2\, \tilde{W}_i \tilde{W}_i + M_3\, \tilde{g}^a \tilde{g}^a + \text{h.c.}\right) - m_{H_u}^2\, |H_u|^2 - m_{H_d}^2\, |H_d|^2 \\ &- M_{\tilde{Q}}^2\, (\tilde{u}^* \tilde{u} + \tilde{d}^* \tilde{d}) - M_{\tilde{u}}^2\, (\tilde{u}^c)^* \tilde{u}^c - M_{\tilde{d}}^2\, (\tilde{d}^c)^* \tilde{d}^c - M_{\tilde{L}}^2\, (\tilde{\nu}^* \tilde{\nu} + \tilde{e}^* \tilde{e}) \\ &- M_{\tilde{e}}^2\, (\tilde{e}^c)^* \tilde{e}^c + B\mu\, (H_u H_d + \text{h.c.}) - \left(T_u\, H_u \tilde{Q} \tilde{u}^c + T_d\, H_d \tilde{Q} \tilde{d}^c + T_e\, H_d \tilde{L} \tilde{e}^c\right)\,.\end{aligned} \tag{3.21}$$

The mass dimension 1 parameters M_i and B are in general complex parameters. $M_{\tilde{Q}}^2, M_{\tilde{u}}^2, M_{\tilde{d}}^2, M_{\tilde{L}}^2$ and $M_{\tilde{e}}^2$ are hermitian, while T_u, T_d and T_e are complex 3×3 matrices. $m_{H_i}^2$ are real quantities [33].

3.5 R-parity

So far, we have not written down the most generic superpotential. In general, we can also allow for terms which explicitly violate baryon number B or lepton number L as

superfield	spin-$\frac{1}{2}$	spin-1	$SU(3)_c \times SU(2)_L \times U(1)_Y$
winos and Ws	$\tilde{W}^{\pm}, \tilde{W}^0$	$W^{\pm}, W^0$	$(\mathbf{1}, \mathbf{3}, 0)$
bino and B	$\tilde{B}$	B	$(\mathbf{1}, \mathbf{1}, 0)$
gluino and gluon	$\tilde{g}$	g	$(\mathbf{3}, \mathbf{1}, 0)$

Table 3.2: Gauge content of the MSSM.

they are not protected by any symmetry in the MSSM. Yet this would immediately lead to the possibility of proton decay, which has not been observed to date, despite huge efforts[7].

Thus, in order to protect the theory from that issue, an additional symmetry is imposed, expressed by the multiplicative quantum number called R-parity. It is defined by [30]

$$R = (-1)^{3(B-L)+2s}\,, \tag{3.22}$$

with s being the spin of the particle. Now, one can easily check that all SM particles have $R = 1$ while the superpartners have $R = -1$. Hence, if R-parity is conserved, SUSY particles can only be pair-produced from collisions of SM particles. Additionally, a sparticle can not decay into SM particles only. The consequences are apparent: supersymmetric decay chains are forced to end up with the lightest supersymmetric particle (LSP), which is compulsorily stable. If the LSP happens to be neutral and only weakly interacting, it provides an excellent candidate for dark matter.

3.6 The CMSSM

The MSSM as we introduced it above has a lot of free parameters, most of them due to the soft SUSY-breaking terms, which make complete parameter studies impossible. One thus aims to reduce the parameter space. This is commonly done by imposing GUT scale conditions which connect or even unify some of the free parameters. For this purpose, however, one has to restrict oneself to a particular supersymmetry breaking pattern. A widely used scheme that we will also apply in this work considers a gravity-mediated SUSY-breaking. One introduces non-renormalizable terms to the Lagrangian which are suppressed by powers of M_P while the breaking occurs by the VEV of some auxiliary field F. The soft scale thus arises through the combination $m_{\text{soft}} \sim \langle F \rangle / M_P$ [30]. A nice feature of this breaking scheme is the flavour-blindness of gravity.

In the framework of minimal supergravity (mSUGRA), the soft SUSY-breaking

[7] Current experiments (see, *e.g.*, [35]) have set bounds on the proton lifetime of $\tau_p > \mathcal{O}(10^{33})$ yrs.

terms have a particularly simple form at the GUT scale [31]:

$$M_1 = M_2 = M_3 = M_{1/2} \tag{3.23}$$

$$m_{\tilde{Q}}^2 = m_{\tilde{u}}^2 = m_{\tilde{d}}^2 = m_{\tilde{L}}^2 = m_{\tilde{e}}^2 = m_0^2 \mathbb{1} \quad \text{and} \quad m_{H_u}^2 = m_{H_d}^2 = m_0^2 \tag{3.24}$$

($\mathbb{1}$ being the unit matrix in generation space)

$$T_u = A_0 Y_u, \; T_d = A_0 Y_d \quad \text{and} \quad T_e = A_0 Y_e \,. \tag{3.25}$$

The GUT scale is set to the energy value where the gauge couplings g_1, g_2 and g_3 unify. This is possible in supersymmetric theories due to the additional particles running in the loops and thus modifying the renormalization group equations (RGEs) for the gauge couplings (see, *e.g.*, [30]). The GUT scale is typically of the order 10^{16} GeV.

Altogether, when applying the mSUGRA-like conditions to the parameters of the MSSM, we are left with only five free parameters which give the whole spectrum of MSSM parameters with RGE evolution of the particular quantities. The free parameters at M_{GUT} are

- the soft mass of the scalars m_0,
- the soft mass of the fermions $M_{1/2}$,
- the trilinear coupling A_0,
- the ratio of the Higgs VEVs, $\tan\beta = v_u/v_d$ and
- the sign of μ in W_{MSSM}.

This model is known as the constrained MSSM, or CMSSM.

3.7 Particle content

3.7.1 Higgs sector

With the MSSM containing two complex Higgs doublets, we have four scalar and four pseudoscalar degrees of freedom in the MSSM. The particular fields in gauge eigenbasis are

$$H_u = \begin{pmatrix} \phi_u^+ \\ \frac{1}{\sqrt{2}}(v_u + \phi_u^0 + i\chi_u) \end{pmatrix}, \qquad H_d = \begin{pmatrix} \frac{1}{\sqrt{2}}(v_d + \phi_d^0 + i\chi_d) \\ \phi_d^- \end{pmatrix}, \tag{3.26}$$

with VEVs $\langle H_u^0 \rangle = v_u/\sqrt{2}$ and $\langle H_d^0 \rangle = v_d/\sqrt{2}$. They have to satisfy

$$v = \sqrt{v_u^2 + v_d^2} = 246 \text{ GeV} \tag{3.27}$$

in order to give the correct masses to the electroweak gauge bosons. The rotations into the mass eigenstates can be done by [36]

$$\begin{aligned}
\begin{pmatrix} H^0 \\ h^0 \end{pmatrix} &= \begin{pmatrix} \cos\alpha & \sin\alpha \\ -\sin\alpha & \cos\alpha \end{pmatrix} \begin{pmatrix} \phi_d^0 \\ \phi_u^0 \end{pmatrix} \\
\begin{pmatrix} G^0 \\ A^0 \end{pmatrix} &= \begin{pmatrix} \cos\beta & \sin\beta \\ -\sin\beta & \cos\beta \end{pmatrix} \begin{pmatrix} \chi_d^0 \\ \chi_u^0 \end{pmatrix} \\
\begin{pmatrix} G^+ \\ H^+ \end{pmatrix} &= \begin{pmatrix} \cos\beta & \sin\beta \\ -\sin\beta & \cos\beta \end{pmatrix} \begin{pmatrix} \phi_d^+ \\ \phi_u^+ \end{pmatrix} ,
\end{aligned} \tag{3.28}$$

so that G^0 and $G^\pm$ are (pseudo-) Goldstone bosons which, after electroweak symmetry breaking (EWSB) and gauge fixing, serve as the longitudinal components of the Z and $W^\pm$ bosons. The remaining fields are massive physical states such that there are two (CP-even) neutral Higgs bosons h^0 and H^0, one (CP-odd) pseudoscalar A^0 and two charged Higgs bosons $H^\pm$.

3.7.2 Neutralinos and charginos

The superpartners of the neutral gauge bosons, the gauginos, as well as the Higgs counterparts, the Higgsinos, are spin-$\frac{1}{2}$ fermions. All of them mix after EWSB to four neutral fermion fields, the so-called neutralinos $\tilde{\chi}_i^0$. The tree-level mass matrix in the basis $(\tilde{B}, \tilde{W}^0, \tilde{H}_d^0, \tilde{H}_u^0)$ reads

$$m_{\tilde{\chi}^0} = \begin{pmatrix} M_1 & 0 & -\frac{g_1 v_d}{2} & \frac{g_1 v_u}{2} \\ 0 & M_2 & \frac{g_2 v_d}{2} & -\frac{g_2 v_u}{2} \\ -\frac{g_1 v_d}{2} & \frac{g_2 v_d}{2} & 0 & -\mu \\ \frac{g_1 v_u}{2} & -\frac{g_2 v_u}{2} & -\mu & 0 \end{pmatrix} . \tag{3.29}$$

Diagonalization can be done by a unitary matrix.

The lightest neutralino is the LSP in a wide range of parameter space and thus serves as a dark matter candidate if R-parity is conserved.

As stated above, there are also two charged Higgs bosons in the MSSM. Thus the superpartners are two charged Weyl fermions, likewise with the charged winos. The mass eigenstates are called charginos $\tilde{\chi}_i^\pm$. The mass matrix in the basis $(\tilde{W}^+, \tilde{H}_u^+, \tilde{W}^-, \tilde{H}_d^-)$ has the form [30]

$$m_{\tilde{\chi}^\pm} = \begin{pmatrix} 0 & X^T \\ X & 0 \end{pmatrix} \quad \text{with} \quad X = \begin{pmatrix} M_2 & \frac{g_2 v_u}{\sqrt{2}} \\ \frac{g_2 v_d}{\sqrt{2}} & \mu \end{pmatrix} \tag{3.30}$$

and can be diagonalized using two unitary 2×2 matrices U and V such that

$$U^* X V^{-1} = \begin{pmatrix} m_{\tilde{\chi}_1^\pm} & 0 \\ 0 & m_{\tilde{\chi}_2^\pm} \end{pmatrix} . \tag{3.31}$$

3.7.3 Gluinos

Due to unbroken $SU(3)_c$, the superpartners of the gluons are the only SUSY particles that do not mix with others. The mass of the colour-octet fermions is determined by the soft parameter M_3 and its RGE evolution. With mSUGRA-like boundary conditions, it can be related to the other soft SUSY-breaking gaugino masses in the form [30]

$$M_3 = \frac{\alpha_s}{\alpha} \sin^2 \theta_W M_2 = \frac{3\alpha_s}{5\alpha} \cos^2 \theta_W M_1 \,. \tag{3.32}$$

Hence, at the TeV scale, the mass hierarchy is about

$$M_3 : M_2 : M_1 \approx 6 : 2 : 1 \,, \tag{3.33}$$

which predicts the gluino to be among the heaviest supersymmetric particles.

3.7.4 Sfermions

As stated above, there exists one scalar superpartner for each chirality state of a Standard Model fermion as these are two different degrees of freedom. We thus distinguish between right-handed and left-handed sfermions, which have the same quantum numbers as their respective fermionic partners. Of course, handedness is just a labelling for the scalars and does not have any physical interpretation. Due to broken $SU(2)_L \times U(1)_Y$, the left- and right-handed sfermions may mix with each other. Consequently, by means of the generic soft SUSY-breaking terms, there are in general three 6×6 matrices for the up- and down-type squarks as well as for the charged sleptons and additionally one 3×3 matrix for the sneutrinos (as right-handed neutrinos are not included in the minimal realization of SUSY). Restricting ourselves to mSUGRA-inspired boundary conditions, most of the mixing angles are small or zero due to the flavour-blindness of gravitational interactions and thus the diagonal form at the GUT scale (see eqns. (3.24) and (3.25)).

All sfermions then have the same mass at the GUT scale, m_0. The mass splitting at the electroweak scale (which is the energy observable for us) is generated by RGE evolution where a strong dependence of $M_{1/2}$ occurs due to virtual gauginos running in the loops. Usually, the squarks are heavier than the sleptons because of the additional coupling to gluinos.

The Yukawa couplings are the only couplings that differ in flavour. As they are small for the first and second family, Higgsino contributions can be neglected to a good approximation, leading to nearly mass-degenerate states of the first- and second-generation sfermions. Noticeable mass splitting and also left-right-mixing will thus only occur for the third-generation squarks and sleptons [30].

Chapter 4

The Model: BLSSM

In this work we consider an R-parity conserving $U(1)_{B-L}$ extension of the MSSM, which we will call the BLSSM. Thus, we combine the advantages of supersymmetry with those of having a local $B-L$ symmetry. As already stated in chapter 2, this will lead to some new particles as well as new mixings which we will discuss in the following sections. A detailed overview of the model with its particles and masses as well as loop-corrections can be found in ref. [16]. Studies of the non-supersymmetric version and its Z' physics are for instance provided in [37, 38].

4.1 Particle content and superpotential

Compared with the MSSM, there is one right-handed neutrino per generation plus their superpartners in addition to the chiral supermultiplets. It is known that all matter particles can be embedded in $SO(10)$ 16-plets [39]. The Higgs sector also has to be extended as $U(1)_{B-L}$ must be broken. Therefore we need two scalar fields η and $\bar{\eta}$ similar to the two MSSM Higgs doublets. A Majorana mass term of the right-handed neutrinos is generated by the VEV of η such that their mass is driven by the $B-L$ breaking scale. In order to get a gauge invariant Lagrangian, η needs to have twice the $B-L$ charge of the right-handed neutrinos. For this reason we label them bileptons. In table 4.1 we summarize the chiral supermultiplets with their distinct quantum numbers.

The superpotential of the model is given by

$$\begin{aligned} W = & Y_u^{ij}\,\hat{U}_i\,\hat{Q}_j\,\hat{H}_u - Y_d^{ij}\,\hat{D}_i\,\hat{Q}_j\,\hat{H}_d - Y_e^{ij}\,\hat{E}_i\,\hat{L}_j\,\hat{H}_d + \mu\,\hat{H}_u\,\hat{H}_d \\ & + Y_\nu^{ij}\,\hat{\nu}_i\,\hat{L}_j\,\hat{H}_u - \mu'\,\hat{\eta}\,\hat{\bar{\eta}} + Y_x^{ij}\,\hat{\nu}_i\,\hat{\eta}\,\hat{\nu}_j\,, \end{aligned} \tag{4.1}$$

where Y_ν^{ij} and Y_x^{ij} are the Dirac and Majorana Yukawa couplings of the neutrinos which generate their masses. With Y_ν being small and Y_x large, we can thus achieve light left-handed and heavy right-handed neutrinos. Due to the new supersymmetric particles in the spectrum compared to the MSSM, there are also additional soft

superfield		spin-0	spin-$\frac{1}{2}$	$SU(3)_c \times SU(2)_L \times U(1)_Y \times U(1)_{B-L}$
quarks	$\hat{Q}$	$\tilde{Q} = (\tilde{u}, \tilde{d})$	$Q = (u, d)$	$(\mathbf{3}, \mathbf{2}, \frac{1}{6}, \frac{1}{6})$
and squarks	$\hat{U}$	$\tilde{u}^c$	u^c	$(\bar{\mathbf{3}}, \mathbf{1}, -\frac{2}{3}, -\frac{1}{6})$
	$\hat{D}$	$\tilde{d}^c$	d^c	$(\bar{\mathbf{3}}, \mathbf{1}, \frac{1}{3}, -\frac{1}{6})$
leptons	$\hat{L}$	$\tilde{L} = (\tilde{\nu}, \tilde{e})$	$L = (\nu, e)$	$(\mathbf{1}, \mathbf{2}, -\frac{1}{2}, -\frac{1}{2})$
and sleptons	$\hat{E}$	$\tilde{e}^c$	e^c	$(\mathbf{1}, \mathbf{1}, 1, \frac{1}{2})$
	$\hat{\nu}$	$\tilde{\nu}^c$	ν^c	$(\mathbf{1}, \mathbf{1}, 0, \frac{1}{2})$
Higgses	$\hat{H}_u$	(H_u^+, H_u^0)	$(\tilde{H}_u^+, \tilde{H}_u^0)$	$(\mathbf{1}, \mathbf{2}, \frac{1}{2}, 0)$
and Higgsinos,	$\hat{H}_d$	(H_d^0, H_d^-)	$(\tilde{H}_d^0, \tilde{H}_d^-)$	$(\mathbf{1}, \mathbf{2}, -\frac{1}{2}, 0)$
bileptons	$\hat{\eta}$	η	$\tilde{\eta}$	$(\mathbf{1}, \mathbf{1}, 0, -1)$
and bileptinos	$\hat{\bar{\eta}}$	$\bar{\eta}$	$\tilde{\bar{\eta}}$	$(\mathbf{1}, \mathbf{1}, 0, 1)$

Table 4.1: Matter content of the BLSSM.

SUSY-breaking terms such that the soft Lagrangian reads

$$\begin{aligned}\mathscr{L}_{\text{soft}} =& \mathscr{L}_{\text{soft,MSSM}} - \tilde{B}\tilde{B}' M_{BB'} - \frac{1}{2}\tilde{B}'\tilde{B}' M_{B'} - m_\eta^2|\eta|^2 - m_{\bar{\eta}}^2|\bar{\eta}|^2 - M_{\tilde{\nu},ij}^2(\tilde{\nu}_i^c)^*\tilde{\nu}_j^c \\ & - \eta\bar{\eta}B_{\mu'} + T_\nu^{ij} H_u \tilde{\nu}_i^c \tilde{L}_j + T_x^{ij}\eta\tilde{\nu}_i^c\tilde{\nu}_j^c \,. \end{aligned} \tag{4.2}$$

We have the freedom to choose B'_μ as well as B_μ to be real quantities [40].

4.2 Gauge kinetic mixing

We have already introduced the possibility of gauge kinetic mixing due to the two Abelian gauge groups in chapter 2. Here we study this effect in some more detail in terms of the BLSSM as it has been neglected in most phenomenological studies so far (see, *e.g.*, [41, 42]). Actually, we will show the necessity of taking into account the kinetic mixing in the next sections since it leads to tree level particle mixing and mass shifts that would be absent otherwise. Moreover, even if we force the mixing term to vanish at a particular scale, it will be inevitably induced with RGE evaluation. One can illustrate this behaviour by the consideration of the anomalous dimension γ_{ab} (with a and b labelling the different $U(1)$ groups). At 1-loop, it is given by [16]

$$\gamma_{ab} = \frac{1}{16\pi^2}\text{Tr}\{Q_a Q_b\}\,, \tag{4.3}$$

the trace running over all $U(1)$ charges Q. Regarding the BLSSM, in the basis $(U(1)_Y\,, U(1)_{B-L})^T$ the anomalous dimension can be written as [16]

$$\gamma = \frac{1}{16\pi^2}\begin{pmatrix} \frac{33}{5} & 6\sqrt{\frac{2}{5}} \\ 6\sqrt{\frac{2}{5}} & 9 \end{pmatrix}\,. \tag{4.4}$$

Accordingly, off-diagonal elements and thus mixing between the two Abelian groups will always be generated by RGE running. As pointed out in chapter 2, we can handle the kinetic mixing in terms of off-diagonal couplings in the coupling matrix G of eq. (2.3). We define this coupling matrix in the basis (A^Y, A^{B-L}) as

$$G = \begin{pmatrix} g_{\mathrm{YY}} & g_{\mathrm{YB}} \\ g_{\mathrm{BY}} & g_{\mathrm{BB}} \end{pmatrix} . \tag{4.5}$$

As both couplings and mass of the Z boson are severely constrained by electroweak precision data, explicit coupling terms to $B-L$ are disfavoured at the associated scale. Therefore, we perform an orthogonal rotation in the fields and the coupling matrix that fixes the corresponding off-diagonal coupling to zero. Such a rotation may always be executed in the still-unbroken fields. Hence, at the scale of EWSB, we are left with

$$g_1 = g'_{\mathrm{YY}} = \frac{g_{\mathrm{YY}} g_{\mathrm{BB}} - g_{\mathrm{YB}} g_{\mathrm{BY}}}{\sqrt{g_{\mathrm{BB}}^2 + g_{\mathrm{BY}}^2}} \tag{4.6}$$

$$g_{\mathrm{BL}} = g'_{\mathrm{BB}} = \sqrt{g_{\mathrm{BB}}^2 + g_{\mathrm{BY}}^2} \tag{4.7}$$

$$\bar{g} = g'_{\mathrm{YB}} = \frac{g_{\mathrm{YB}} g_{\mathrm{BB}} + g_{\mathrm{BY}} g_{\mathrm{YY}}}{\sqrt{g_{\mathrm{BB}}^2 + g_{\mathrm{BY}}^2}} \tag{4.8}$$

$$g'_{\mathrm{BY}} = 0 . \tag{4.9}$$

In the following discussion of the model we will make use of these definitions and explicitly direct our attention to points where kinetic mixing affects the phenomenology of the model.

4.3 Neutral gauge sector

As stated in chapter 2, the gauge kinetic mixing also gives rise to a tree level mass mixing between the neutral gauge bosons. In the basis (B, W^3, B'), it reads

$$M_V^2 = \begin{pmatrix} \frac{1}{4} g_1^2 v^2 & -\frac{1}{4} g_1 g_2 v^2 & \frac{1}{4} \bar{g} g_1 v^2 \\ -\frac{1}{4} g_1 g_2 v^2 & \frac{1}{4} g_2^2 v^2 & -\frac{1}{4} \bar{g} g_2 v^2 \\ \frac{1}{4} \bar{g} g_1 v^2 & -\frac{1}{4} \bar{g} g_2 v^2 & \frac{1}{4} \bar{g}^2 v^2 + g_{\mathrm{BL}}^2 x^2 \end{pmatrix} , \tag{4.10}$$

whereas v and x are defined in analogy to eq. (3.27): $v^2 = v_d^2 + v_u^2$ as well as $x^2 = v_\eta^2 + v_{\bar{\eta}}^2$, v_η and $v_{\bar{\eta}}$ being the bilepton VEVs.

The neglection of gauge kinetic mixing would lead to a decoupling of the upper-left block, restoring the same relations between the gauge bosons as in the SM and leaving an isolated Z' with the simple mass formula $M_{Z'} = x g_{\mathrm{BL}}$. By applying eq. (2.4), the

mass matrix can be diagonalized. The eigenvalues after the rotation are given by

$$M_\gamma^2 = 0 \tag{4.11}$$

$$M_{Z/Z'}^2 = \frac{1}{8}\Big((g_1^2+g_2^2+\bar{g}^2)v^2 + 4g_{\mathrm{BL}}^2x^2 \mp \sqrt{(g_1^2+g_2^2+\bar{g}^2)^2v^4 - 8(g_1^2+g_2^2-\bar{g}^2)g_{\mathrm{BL}}^2v^2x^2 + 16g_{\mathrm{BL}}^4x^4}\Big)\,. \tag{4.12}$$

The mixing angle θ'_W that characterizes the mixing of the gauge eigenstate B' with B and W^3 to the mass eigenstates Z', γ and Z can be calculated as [43]

$$\tan 2\theta'_W = \frac{2\bar{g}\sqrt{g_1^2+g_2^2}}{\bar{g}^2 + 16\frac{x^2}{v^2}g_{\mathrm{BL}}^2 - g_1^2 - g_2^2}\,. \tag{4.13}$$

Obviously, $\tan 2\theta'_W$ and thus θ'_W has to be very small with Z' masses in the TeV range since it is suppressed by powers of v^2/x^2.

4.4 Higgs sector

Here we review the masses and mixing of the neutral Higgs fields. In the same manner as in eq. (3.26) for the MSSM Higgs bosons, we decompose the bileptons η and $\bar{\eta}$ into CP-even and CP-odd components:

$$\eta = \frac{1}{\sqrt{2}}\Big(v_\eta + \phi_\eta + i\chi_\eta\Big), \qquad \bar{\eta} = \frac{1}{\sqrt{2}}\Big(v_{\bar{\eta}} + \phi_{\bar{\eta}} + i\chi_{\bar{\eta}}\Big)\,. \tag{4.14}$$

4.4.1 CP-even states

A mixing between the MSSM Higgs bosons and the bileptons already exists at tree level through the off-diagonal coupling $\bar{g}$. The mass matrix in the basis $(\phi_d^0, \phi_u^0, \phi_\eta, \phi_{\bar{\eta}})$ reads at tree level

$$m_h^2 = \begin{pmatrix} m_{h,11}^2 & -\frac{(g_1^2+g_2^2+\bar{g}^2)v_dv_u}{4} - B_\mu & \frac{1}{2}\bar{g}g_{\mathrm{BL}}v_dv_\eta & -\frac{1}{2}\bar{g}g_{\mathrm{BL}}v_dv_{\bar{\eta}} \\ -\frac{(g_1^2+g_2^2+\bar{g}^2)v_dv_u}{4} - B_\mu & m_{h,22}^2 & -\frac{1}{2}\bar{g}g_{\mathrm{BL}}v_uv_\eta & \frac{1}{2}\bar{g}g_{\mathrm{BL}}v_uv_{\bar{\eta}} \\ \frac{1}{2}\bar{g}g_{\mathrm{BL}}v_dv_\eta & -\frac{1}{2}\bar{g}g_{\mathrm{BL}}v_uv_\eta & m_{h,33}^2 & -g_{\mathrm{BL}}^2v_\eta v_{\bar{\eta}} - B_\mu \\ -\frac{1}{2}\bar{g}g_{\mathrm{BL}}v_dv_{\bar{\eta}} & \frac{1}{2}\bar{g}g_{\mathrm{BL}}v_uv_{\bar{\eta}} & -g_{\mathrm{BL}}^2v_\eta v_{\bar{\eta}} - B_\mu & m_{h,44}^2 \end{pmatrix} \tag{4.15}$$

and the diagonal elements are

$$m^2_{h,11} = m^2_{H_d} + \frac{1}{8}(g_1^2 + g_2^2 + \bar{g}^2)(3v_d^2 - v_u^2) + \frac{1}{4}\bar{g}g_{\mathrm{BL}}(v_\eta^2 - v_{\bar{\eta}}^2) + |\mu|^2 \tag{4.16}$$

$$m^2_{h,22} = m^2_{H_u} - \frac{1}{8}(g_1^2 + g_2^2 + \bar{g}^2)(v_d^2 - 3v_u^2) - \frac{1}{4}\bar{g}g_{\mathrm{BL}}(v_\eta^2 - v_{\bar{\eta}}^2) + |\mu|^2 \tag{4.17}$$

$$m^2_{h,33} = m^2_{\eta} + \frac{1}{4}\bar{g}g_{\mathrm{BL}}(v_d^2 - v_u^2) + \frac{1}{2}g_{\mathrm{BL}}^2(3v_\eta^2 - v_{\bar{\eta}}^2) + |\mu'|^2 \tag{4.18}$$

$$m^2_{h,44} = m^2_{\bar{\eta}} - \frac{1}{4}\bar{g}g_{\mathrm{BL}}(v_d^2 - v_u^2) - \frac{1}{2}g_{\mathrm{BL}}^2(v_\eta^2 - 3v_{\bar{\eta}}^2) + |\mu'|^2\,. \tag{4.19}$$

The soft SUSY-breaking Higgsino and bileptino masses can be eliminated by applying the tadpole equations (see sec. 4.7).

4.4.2 CP-odd states

Analogously to the scalar Higgs sector, there exist four pseudoscalar states that can in principle mix with each other. After the rotation into the mass eigenbasis, two of the states must be physical particles A^0 and A^0_η while the other two form the Goldstone bosons G^0_1 and G^0_2 which become the longitudinal parts of the neutral gauge bosons after electroweak and $B-L$ symmetry breaking. The masses of these bosons are adjusted by gauge fixing. We choose to work in the Feynman-'t Hooft gauge, *i.e.* the values are shifted to the masses of the Z and Z' boson, respectively.

It was claimed in ref. [16] that in contrast to the CP-even Higgses, the pseudoscalar mass matrix had a block-diagonal form at tree level. This is true for the part of the mass matrix that emerges from the kinetic terms of the Lagrangian. At tree level, it reads

$$m^2_{A,\mathrm{kin}} = \begin{pmatrix} B_\mu \tan\beta & B_\mu & 0 & 0 \\ B_\mu & B_\mu \cot\beta & 0 & 0 \\ 0 & 0 & B_{\mu'} \tan\beta' & B_{\mu'} \\ 0 & 0 & B_{\mu'} & B_{\mu'} \cot\beta' \end{pmatrix}. \tag{4.20}$$

The other part which influences the pseudoscalar masses is the gauge fixing Lagrangian. A simple choice would be the gauge fixing terms of the MSSM in mass eigenbasis, just appended by a term that connects the Z' and its corresponding Goldstone boson. The resulting gauge fixing Lagrangian for the massive neutral gauge bosons can be written as

$$\mathscr{L}_{\mathrm{GF},Z/Z'} = -\frac{1}{2\xi_Z}\left|\partial_\mu Z^\mu - G^0_1 M_Z \xi_Z\right|^2 - \frac{1}{2\xi_{Z'}}\left|\partial_\mu Z'^\mu - G^0_2 M_{Z'} \xi_{Z'}\right|^2. \tag{4.21}$$

Such terms imply that the rotation of the pseudoscalar fields into the mass eigenstates has to be done before gauge fixing, simply using the mass matrix in eq. (4.20). This in turn means that the Goldstone bosons would be purely MSSM- or $B-L$-like as the upper-left and the lower-right block decouple. Hence, despite the

fact that Z and Z' already mix at tree level, their longitudinal components would decouple completely.

The gauge fixing procedure described above works correctly if $U(1)$ mixing is turned off. However, as soon as we consider a non-zero $\bar{g}$, we have to be more careful. In the loop corrections to the pseudoscalar Higgs masses we find that with gauge kinetic mixing, the correct Goldstone boson masses cannot be restored with the respective values for ξ_i in eq. (4.21) which, of course, must not be and thus is unsustainable.

The issue can be traced back to the kind of gauge fixing applied. While it is fine in the MSSM to use a gauge fixing Lagrangian like eq. (4.21), this is not the case if a second $U(1)$ can mix with the initial $U(1)_Y$. With a diagonal gauge fixing term, the ghost fields associated with the Z and Z' bosons also decouple and thus cannot cancel all the related terms in the loops. In a consistent approach we thus consider a gauge fixing Lagrangian in the gauge eigenbasis of the pseudoscalars and allow for explicit mixing terms, as has been done in [44]. Hence, we use

$$\mathscr{L}_{\mathrm{GF},Z/Z'} = \frac{1}{2\xi_Z}\left|\partial_\mu Z^\mu + \sum_i c_i \chi_i \xi_Z\right|^2 + \frac{1}{2\xi_{Z'}}\left|\partial_\mu Z'^\mu + \sum_i d_i \chi_i \xi_{Z'}\right|^2, \qquad i = u, d, \eta, \bar{\eta}\,. \tag{4.22}$$

The mass-dimension coefficients c_i and d_i correspond to those occurring in the kinetic Lagrangian after the rotation of the gauge bosons into the mass eigenstates:

$$\sum_i c_i Z^\mu \partial_\mu \chi_i + \sum_j d_i Z'^\mu \partial_\mu \chi_j\,. \tag{4.23}$$

They may depend on the Higgs VEVs, gauge couplings, and the gauge boson mixing angles θ_W and θ'_W. The gauge fixing defined above automatically contains off-diagonal mass terms that have to be added to the mass matrix of eq. (4.20) before diagonalization. Thus, a tree level mixing of the Goldstone bosons is induced which vanishes in the limit $\bar{g} \to 0$. The physical states cannot depend on the gauge fixing, so they still decouple at tree level and gain the masses already stated in ref. [16]:

$$m^2_{A^0} = \frac{2B_\mu}{\sin 2\beta}\,, \qquad m^2_{A^0_\eta} = \frac{2B'_\mu}{\sin 2\beta'}\,. \tag{4.24}$$

4.5 Neutralinos

The neutralino sector contains three more states in the BLSSM, which are the superpartner of the B' – the BLino $\tilde{B}'$ – and the two bileptinos $\tilde{\eta}$ and $\tilde{\bar{\eta}}$. All of them mix at tree level with the MSSM submatrix (see eq. (3.29)) proportional to $\bar{g}$. The

mass matrix reads in the basis $(\tilde{B}^0, \tilde{W}^0, \tilde{H}_d^0, \tilde{H}_u^0, \tilde{B}', \tilde{\eta}, \tilde{\bar{\eta}})$

$$m_{\tilde{\chi}^0} = \begin{pmatrix} M_1 & 0 & -\frac{g_1 v_d}{2} & \frac{g_1 v_u}{2} & \frac{M_{BB'}}{2} & 0 & 0 \\ 0 & M_2 & \frac{g_2 v_d}{2} & -\frac{g_2 v_u}{2} & 0 & 0 & 0 \\ -\frac{g_1 v_d}{2} & \frac{g_2 v_d}{2} & 0 & -\mu & -\frac{\bar{g} v_d}{2} & 0 & 0 \\ \frac{g_1 v_u}{2} & -\frac{g_2 v_u}{2} & -\mu & 0 & \frac{\bar{g} v_u}{2} & 0 & 0 \\ \frac{M_{BB'}}{2} & 0 & -\frac{\bar{g} v_d}{2} & \frac{\bar{g} v_u}{2} & M_{B'} & -g_{\mathrm{BL}} v_\eta & g_{\mathrm{BL}} v_{\bar{\eta}} \\ 0 & 0 & 0 & 0 & -g_{\mathrm{BL}} v_\eta & 0 & -\mu' \\ 0 & 0 & 0 & 0 & g_{\mathrm{BL}} v_{\bar{\eta}} & -\mu' & 0 \end{pmatrix} . \tag{4.25}$$

Depending on the soft gaugino masses M_i as well as the parameters μ and μ', the lightest neutralino can have a different nature. Hence, in comparison to the MSSM, two more dark matter scenarios are conceivable: BLino-like LSP and bileptino-like LSP. A detailed discussion of this matrix as well as various dark matter scenarios due to different admixtures of the lightest neutralino is provided by ref. [45].

4.6 Sleptons

There are a few changes in the slepton sector in comparison to the MSSM that we briefly discuss in this section. The most obvious change in this sector of course is the presence of right-handed sneutrinos. Moreover, due to the Majorana mass term in the superpotential (eq. (4.1)) a splitting of the sneutrino states into real and imaginary parts occurs such that we end up with one 6×6 mixing matrix for the real (scalar) part $\tilde{\nu}^S$ and one for the imaginary (pseudoscalar) part $\tilde{\nu}^P$. The respective terms in the mass matrix are shown in appendix C.1 whereas as a discussion about possible sneutrino LSPs and thus dark matter scenarios can be found in ref. [45]. In general, the masses of the scalar and pseudoscalar sneutrinos differ.

The most important change one gets in the charged slepton sector due to the $U(1)_{B-L}$ is the existence of new D-terms in the mass matrix. Furthermore, the MSSM-like D-term is modified by means of gauge kinetic mixing. The slepton mass matrix in the basis $(\tilde{e}_L, \tilde{e}_R)$ is given by

$$m_{\tilde{e}}^2 = \begin{pmatrix} m_{LL} & \frac{1}{\sqrt{2}}\Big(v_d T_e - v_u \mu^* Y_e\Big) \\ \frac{1}{\sqrt{2}}\Big(v_d T_e^\dagger - v_u \mu Y_e^\dagger\Big) & m_{RR} \end{pmatrix} \tag{4.26}$$

$$m_{LL} = M_{\tilde{L}}^2 + \frac{v_d^2}{2} Y_e^\dagger Y_e + \frac{1}{8}\Big((g_1^2 - g_2^2 + \bar{g}^2 + \bar{g} g_{\mathrm{BL}})(v_d^2 - v_u^2) + 2(\bar{g} g_{\mathrm{BL}} + g_{\mathrm{BL}}^2)(v_\eta^2 - v_{\bar{\eta}}^2)\Big)\mathbb{1} \tag{4.27}$$

$$m_{RR} = M_{\tilde{e}}^2 + \frac{v_d^2}{2} Y_e Y_e^\dagger + \frac{1}{8}\Big((2g_1^2 + 2\bar{g}^2 + \bar{g} g_{\mathrm{BL}})(v_u^2 - v_d^2) - 2\Big(2\bar{g} g_{\mathrm{BL}} + g_{\mathrm{BL}}^2\Big)(v_\eta^2 - v_{\bar{\eta}}^2)\Big)\mathbb{1} , \tag{4.28}$$

where $\mathbb{1}$ is the unit matrix in flavour space. With large bilepton VEVs – and thus large $M_{Z'}$ – the mass splitting between left- and right-handed sleptons gets even more

enhanced than in the MSSM since in mSUGRA-inspired models $M_{\tilde{e}}$ is usually smaller than $M_{\tilde{L}}$ and we conventionally take $\tan\beta' > 1$. We will refer to the respective left- and right-handed slepton eigenstates as L-sleptons and R-sleptons.

4.7 Tadpole equations

The minimalization conditions for the scalar potential stemming from the electroweak and $B-L$ symmetry breaking are provided by the tadpole equations. There are four of them in the BLSSM due to the new scalar fields η and $\bar{\eta}$. At tree level, these are given by

$$\begin{aligned}|\mu|^2 =&\frac{1}{8}\Big(\Big(2\bar{g}g_{\rm BL}x^2\cos(2\beta') + 4m_{H_u}^2 - 4m_{H_d}^2\Big)\sec(2\beta) - 4\Big(m_{H_u}^2 + m_{H_d}^2\Big)\\ &- \Big(g_1^2 + \bar{g}^2 + g_2^2\Big)v^2\Big)\end{aligned} \tag{4.29}$$

$$B_\mu = -\frac{1}{8}\Big(-2\bar{g}g_{\rm BL}x^2\cos(2\beta') - 4m_{H_u}^2 + 4m_{H_d}^2 + \Big(g_1^2 + \bar{g}^2 + g_2^2\Big)v^2\cos(2\beta)\Big)\tan(2\beta) \tag{4.30}$$

$$|\mu'|^2 =\frac{1}{4}\Big(-2\Big(g_{\rm BL}^2x^2 + m_\eta^2 + m_{\bar{\eta}}^2\Big) + \Big(2m_\eta^2 - 2m_{\bar{\eta}}^2 + \bar{g}g_{\rm BL}v^2\cos(2\beta)\Big)\sec(2\beta')\Big) \tag{4.31}$$

$$B_{\mu'} =\frac{1}{4}\Big(-2g_{\rm BL}^2x^2\cos(2\beta') + 2m_\eta^2 - 2m_{\bar{\eta}}^2 + \bar{g}g_{\rm BL}v^2\cos(2\beta)\Big)\tan(2\beta')\,. \tag{4.32}$$

Omitting kinetic mixing in eq. (4.12), the Z' mass would, as stated above, have the simple form $M_{Z'} = g_{\rm BL}x$. Using this approximate equality, we can roughly relate the Z' mass to the soft breaking parameter μ' [16]:

$$M_{Z'}^2 \approx -2|\mu'|^2 + \frac{4(m_{\bar{\eta}}^2 - m_\eta^2\tan^2\beta') - v^2\bar{g}g_{\rm BL}\cos\beta(1+\tan\beta')}{2(\tan^2\beta' - 1)}\,. \tag{4.33}$$

Obviously, $\tan\beta'$ needs to be close to 1 in order to obtain high Z' masses. Apparently, the tadpole equations have the power to restrict the allowed parameter space severely.

4.8 GUT scale boundary conditions

Similar to the CMSSM, we assume GUT scale boundary conditions for our model. Thus, we force all new soft SUSY-breaking masses to unify to either m_0 or $M_{1/2}$ and the trilinear couplings to A_0Y. Analogously to the CMSSM, we impose the additional conditions

$$M_{B'} = M_{1/2} \tag{4.34}$$

$$M_{\tilde{\nu}}^2 = m_0^2\mathbb{1} \quad \text{and} \quad m_\eta^2 = m_{\bar{\eta}}^2 = m_0^2 \tag{4.35}$$

$$T_x = A_0Y_x \quad \text{and} \quad T_\nu = A_0Y_\nu\,. \tag{4.36}$$

The energy value for the GUT scale is found by the assumption that the gauge couplings unify at this point. So, according to eq. (4.6), this is where

$$g_2 = \frac{g_{\mathrm{YY}} g_{\mathrm{BB}} - g_{\mathrm{YB}} g_{\mathrm{BY}}}{\sqrt{g_{\mathrm{BB}}^2 + g_{\mathrm{BY}}^2}} \,. \tag{4.37}$$

Since the BLSSM gauge group can be accommodated in the intermediate breaking scenario of a product group like $E_8 \times E_8$, the $U(1)_{B-L}$ should be orthogonal to the SM gauge group at the GUT scale. Hence, we further assume that all off-diagonal couplings and soft masses to vanish at this scale:

$$g_{\mathrm{YB}} = g_{\mathrm{BY}} = 0 \tag{4.38}$$

$$M_{BB'} = 0 \,. \tag{4.39}$$

This in turn means that the $U(1)$ coupling matrix is diagonal, such that $g_{\mathrm{YY}} = g_1$ and $g_{\mathrm{BB}} = g_{\mathrm{BL}}$ which, of course, also has to unify with g_1 and g_2.

Note that $\bar{g}$ will always be driven negative with RGE running if it is zero at the GUT scale. This is a consequence of the fact that the β-functions of g_{YB} and g_{BY} are always positive [16].

The parameters μ, μ', B_μ and $B_{\mu'}$ can be evaluated from the tadpole equations such that the free parameters of the model are:

$$m_0,\, M_{1/2},\, A_0,\, \tan\beta,\, \tan\beta',\, \text{sign}\ \mu,\, \text{sign}\ \mu',\, M_{Z'},\, Y_x \text{ and } Y_\nu \,. \tag{4.40}$$

We always have the freedom to choose a basis where one of the neutrino Yukawa coupling matrices is diagonal. Consequently, we take Y_x diagonal. Thus, there are altogether two signs and eighteen parameters that determine the whole spectrum. Nine of them, namely Y_ν^{ij}, are heavily constrained by neutrino data: the numbers have to be very small (at most $|Y_\nu^{ij}| \lesssim 10^{-5}$ [40]) in order to explain the light neutrino masses. Thus, they do not affect our numerical calculations and the spectrum is effectively provided by only nine parameters and two signs.

Chapter 5

Production and supersymmetric decays of the Z'_{B-L}

In our analysis, we have focussed on the additional neutral gauge boson arising from the $B - L$ symmetry and in especially on its production at the LHC and its supersymmetric decay modes. For this purpose, parameter points with large branching fractions into supersymmetric particles are preferred.

5.1 Calculation chain

In order to do numerical calculations starting from the Lagrangian of chapter 4, a chain of tools was used. The basis for all calculations is provided by the *Mathematica* package `SARAH` [46–48], in which the model is implemented and which is able to derive the vertices, mass matrices, RGEs and loop corrections as well as the model output for various other tools out of a given particle content and Lagrangian. As a second step, the complete mass spectrum with mixing matrices and branching ratios has to be generated, which is done by `SPheno` [49, 50]. We further used `WHIZARD` [51] for the calculation of cross sections and event generation, whereas `CalcHep` [52] and `MadGraph` [53] served for numerical cross-checks with `SPheno` and `WHIZARD`. The scans in parameter space were done by `SSP`, which combines these tools to work together. All the mentioned tools have recently been combined to form the `SUSY Toolbox` for supersymmetric studies [54].

5.2 Study of the parameter space

In order to find parameter points which potentially give interesting and measurable signatures at the LHC and are allowed by both experiment and theory, the parameter space had to be scanned in the quantities which determine the Z' properties and decays. The Z' mass as well as the GUT scale masses m_0 and $M_{1/2}$ have the biggest impact to the decays as the couplings to the Z' are mostly fixed by baryon and

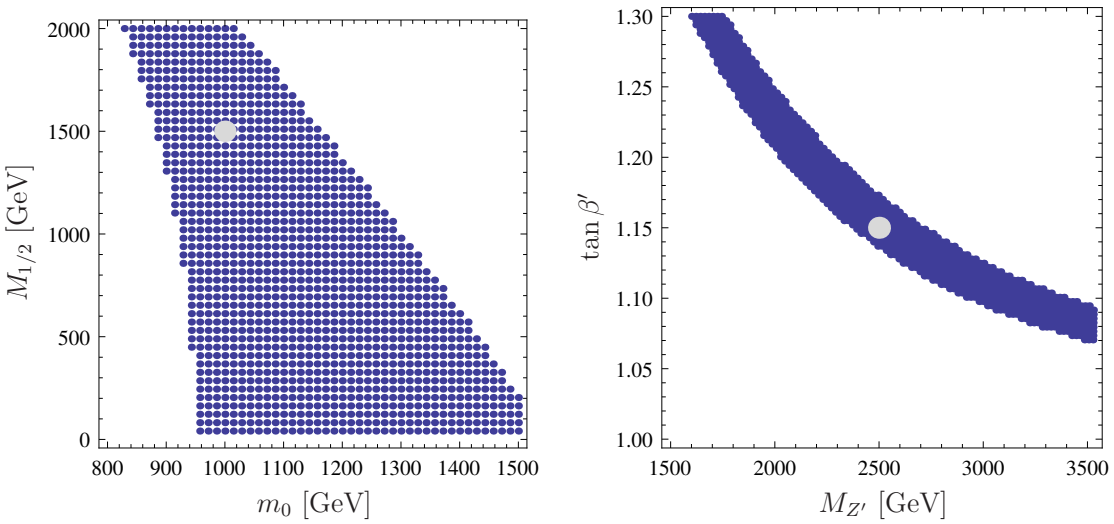

Figure 5.1: Study of the allowed (= calculable) GUT scale input parameter space in the $m_0 - M_{1/2}$ plane for $M_{Z'} = 2.5$ TeV, $\tan\beta' = 1.15$ (left) and in the $M_{Z'} - \tan\beta'$ plane for $m_0 = 1$ TeV and $M_{1/2} = 1.5$ TeV (right). The other parameters have been fixed to $\tan\beta = 20$, $A_0 = -1.5$ TeV, sign $\mu =$ sign $\mu' = +$. The grey dot indicates the selected benchmark point (BLV).

lepton number, *i.e.* the allowed phase space and thus the sparticle masses are the quantities which are the most interesting and which can be addressed by GUT scale input. The trilinear coupling parameter, A_0, is found to play a negligible role and is simply fixed to values which give a calculable spectrum.

Selected parameter scans are shown in figs. 5.2 - 5.1. White space is where no valid spectrum could be calculated due to scalar masses squared which ran negative with RGE evolution or non-existent solutions to the tadpole equations. As can be seen from eq. (4.33), $\tan\beta'$ has to be small (close to 1) in order to get high Z' masses, thus the parameter space in the $M_{Z'} - \tan\beta'$ plane is very restricted (see right plots in figs. 5.2 and 5.1). For a closer look on how $\tan\beta'$ affects especially the Z' and Higgs masses, we refer to [16].

By exploring the allowed parameter space of the neutrino mass coefficients Y_X of the superpotential (see fig. 5.3), one can see that these have to be approximately equal and bigger than around 0.4 to obtain a calculable spectrum. Note that the size of Y_X is crucial for the question of whether R-parity is conserved or not if one allows for sneutrino VEVs. Only if the entries of Y_X and thus also the masses of the right-handed neutrinos are nearly degenerate, an R-parity conserving vacuum can occur [42], otherwise R-parity will be broken by the RGE running of the sneutrino masses. Hence, the constrained parameter space in fig. 5.3, which is in accordance with ref. [42], is a consequence of demanding an unbroken R-symmetry and thus in most cases of the parameter space a stable lightest neutralino or, in some scenarios, a stable sneutrino.

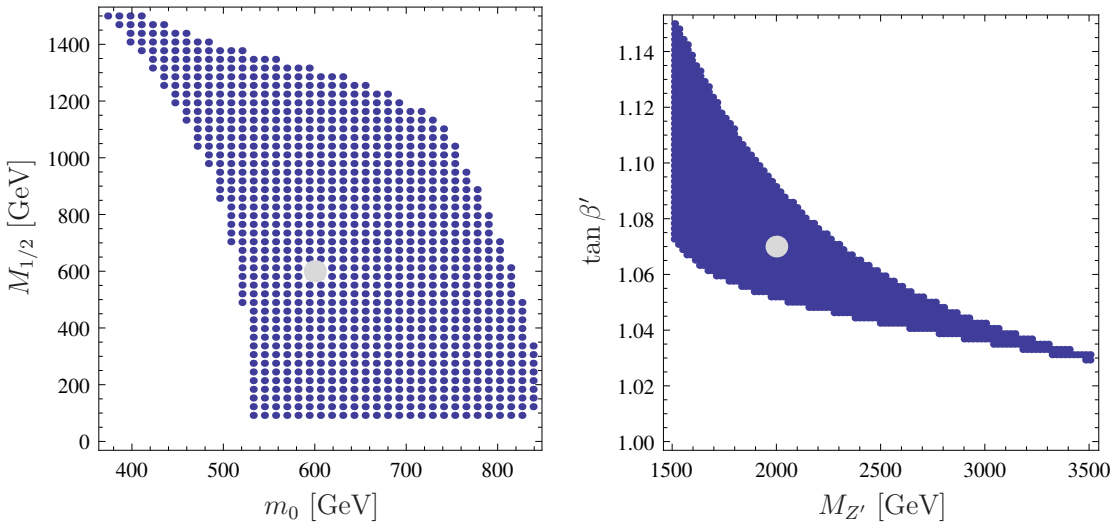

Figure 5.2: Study of the allowed GUT scale input parameter space in the $m_0 - M_{1/2}$ plane for $M_{Z'} = 2$ TeV, $\tan\beta' = 1.07$ (left) and in the $M_{Z'} - \tan\beta'$ plane for $m_0 = 0.6$ TeV and $M_{1/2} = 0.6$ TeV (right). The other parameters have been fixed to $\tan\beta = 10$, $A_0 = 0$, sign $\mu =$ sign $\mu' = +$. The grey dot indicates the selected benchmark point (BLVI).

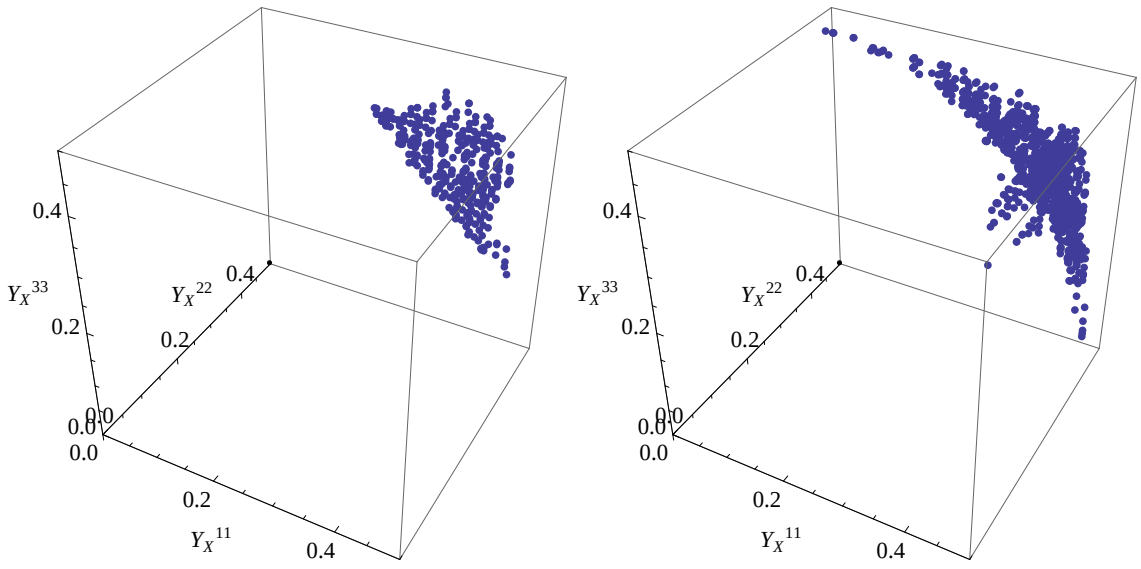

Figure 5.3: Study of the available parameter space in Y_x^{ii} for the parameter choices (left) $m_0 = 1$ TeV, $M_{1/2} = 1.5$ TeV, $\tan\beta = 20$, $A_0 = -1.5$ TeV, $\tan\beta' = 1.15$, $M_{Z'} = 2.5$ TeV and (right) $m_0 = 0.6$ TeV, $M_{1/2} = 0.6$ TeV, $\tan\beta = 10$, $A_0 = 0$, $\tan\beta' = 1.07$, $M_{Z'} = 2$ TeV. The signs of the μ parameters were chosen equally in both cases: sign $\mu =$ sign $\mu' = +$.

We chose two representative benchmark points out of the parameter study: the first of which was selected due to the nature of the LSP, which is bileptino-like with this parameter set and thus allows for enhanced branching fractions of $Z' \to \tilde{\chi}_1^0 \tilde{\chi}_1^0$. The dark matter aspects of this possible LSP nature are discussed in [45]. The second benchmark point has as light as possible GUT scale masses (still consistent with the recent LHC bounds on the CMSSM-parameters [55, 56]) in order to achieve as light as possible sfermions for large partial decay widths $\Gamma(Z' \to \tilde{f}\tilde{f}^*)$. The LSP in this case is a bino-like neutralino. In accordance with [16] and [40], we label the points BLV and BLVI, respectively. A summary with the total GUT scale input of the two benchmark points as well as the neutralino and sfermion masses is given in table 5.1. As stated above, the neutrino Yukawa couplings Y_ν are negligible for our purposes. Hence, we chose some arbitrary values that qualitatively respect the hierarchy obtained from solar and atmospheric neutrino experiments: $Y_\nu^{11} = 10^{-7},\ Y_\nu^{22} = 10^{-6},\ Y_\nu^{33} = 10^{-5}$.

5.3 Z' decay modes on tree level

A vector boson can, at tree level, in general decay in four different ways: into a pair of fermions, scalars and vector bosons, or into one vector boson and one scalar. The partial widths may depend on the masses, coupling constants and mixing angles of the particles involved. The tree level partial width is given by

$$\Gamma_{Z'} = \frac{\overline{|\mathcal{M}|^2}}{16\pi M_{Z'}} \frac{\sqrt{\Big((m_i - m_j)^2 - M_{Z'}^2\Big)\Big((m_i + m_j)^2 - M_{Z'}^2\Big)}}{M_{Z'}^2}\,, \tag{5.1}$$

where $\mathcal{M}$ is the matrix element of the underlying process and $m_{i/j}$ are the masses of the particles the Z' decays into. We list here the partial decay widths into the four different final states as well as distinct vertex factors. A summary of all relevant Z' vertices can be found in appendix A.

5.3.1 Decay into a pair of scalars

The most interesting case for our purposes, as it leads to the production of sfermions, is the decay into a pair of scalars. The general vertex structure is simply given by $ic(p-q)^\mu$ with the momenta q and p of the decay products and the vertex factor c, which is, *e.g.* for two sleptons i and j

$$\begin{aligned} c_{\tilde{\mu}\tilde{\mu}} = -\frac{1}{2}\Big(\Big((\bar{g} + g_{\mathrm{BL}})c'_W - \Big(g_2 c_W - g_1 s_W\Big)s'_W\Big)\sum_{a=1}^{3} Z_{i,a}^{E*} Z_{j,a}^{E} + \\ + \Big(\Big(g_{\mathrm{BL}} + 2\bar{g}\Big)c'_W + 2g_1 s_W s'_W\Big)\sum_{a=1}^{3} Z_{i,3+a}^{E*} Z_{j,3+a}^{E}\Big)\,. \end{aligned} \tag{5.2}$$

	BLV	BLVI
GUT scale input		
m_0 [TeV]	1	0.6
$M_{1/2}$ [TeV]	1.5	0.6
A_0 [TeV]	-1.5	0
$\tan\beta$	20	10
sign μ	+	+
$\tan\beta'$	1.15	1.07
sign μ'	+	+
$M_{Z'}$ [TeV]	2.5	2
Y_X^{11}	0.37	0.42
Y_X^{22}	0.4	0.43
Y_X^{33}	0.4	0.44
Masses [GeV]		
$m_{\tilde{\chi}_1^0}$	678.0	280.7
$m_{\tilde{\chi}_2^0}$	735.2	475.4
$m_{\tilde{\chi}_3^0}$	1241.9	719.1
$m_{\tilde{\chi}_4^0}$	1827.0	733.9
$m_{\tilde{\chi}_5^0}$	1867.5	798.2
$m_{\tilde{\chi}_6^0}$	1871.5	1488.7
$m_{\tilde{\chi}_7^0}$	3131.4	2530.6
$m_{\tilde{\chi}_1^\pm}$	1242.0	475.4
$m_{\tilde{\chi}_2^\pm}$	1872.0	733.9
$m_{\tilde{\tau}_1}$	1002.0	603.7
$m_{\tilde{\tau}_2}$	1446.5	759.9
$m_{\tilde{\mu}_R}$	1094.2	610.8
$m_{\tilde{\mu}_L}$	1477.4	761.9
$m_{\tilde{e}_R}$	1094.5	610.8
$m_{\tilde{e}_L}$	1477.5	761.9

	BLV	BLVI
$m_{\tilde{\nu}_1^S}$	811.3	754.9
$m_{\tilde{\nu}_1^P}$	1442.4	754.9
$m_{\tilde{\nu}_2^S}$	1027.0	757.5
$m_{\tilde{\nu}_2^P}$	1474.9	757.5
$m_{\tilde{\nu}_3^S}$	1027.0	757.5
$m_{\tilde{\nu}_3^P}$	1475.0	757.5
$m_{\tilde{\nu}_4^S}$	1442.4	1105.5
$m_{\tilde{\nu}_4^P}$	2439.9	1969.3
$m_{\tilde{\nu}_5^S}$	1474.9	1141.2
$m_{\tilde{\nu}_5^P}$	2532.3	2003.5
$m_{\tilde{\nu}_6^S}$	1475.0	1177.0
$m_{\tilde{\nu}_6^P}$	2532.3	2037.8
$m_{\tilde{t}_1}$	2180.8	1020.5
$m_{\tilde{t}_2}$	2664.0	1257.5
$m_{\tilde{s}_R}$	2892.4	1324.0
$m_{\tilde{s}_L}$	2998.0	1357.1
$m_{\tilde{u}_R}$	2892.4	1324.0
$m_{\tilde{u}_L}$	2998.0	1357.1
$m_{\tilde{b}_1}$	2642.8	1224.0
$m_{\tilde{b}_2}$	2830.0	1326.4
$m_{\tilde{c}_R}$	2900.7	1332.8
$m_{\tilde{c}_L}$	2999.0	1359.3
$m_{\tilde{d}_R}$	2900.7	1332.8
$m_{\tilde{d}_L}$	2999.1	1359.3
$m_{\tilde{g}}$	3181.5	1378.8

Table 5.1: Parameters of the study points and corresponding masses.

$Z^E_{k,l}$ indicates the slepton mixing matrix and we use the notation $s_W = \sin\theta_W$ as well as $c_W = \cos\theta_W$, same with θ'_W. A special feature which can be seen in all $Z'-$(s)fermion couplings is the impact of gauge kinetic mixing. As highlighted in chapter 4, the off-diagonal coupling $\bar{g}$ will be negative from running down from the GUT to the SUSY scale. It is of the order ($\mathcal{O}(10^{-1})$) and thus definitely non-negligible. Hence, it will have effect on the couplings and thus the signatures of the Z', depending on what relative sign with respect to g_{BL} it receives in the vertex. The coupling to charged sleptons in eq. (5.2) thus is weakened.

The matrix element squared is given by

$$\overline{|\mathcal{M}|^2}_{ss} = \frac{1}{3}|c|^2 \left(M_{Z'}^2 - 2(m_i^2 + m_j^2) + \frac{(m_i^2 - m_j^2)^2}{M_{Z'}^2} \right) . \tag{5.3}$$

5.3.2 Decay into a pair of fermions

The second most interesting decay mode is the one resulting in a pair of fermions, *e.g.* two electrons. The vertex structure is of the form $i\gamma^\mu \left(aP_L + bP_R\right)$ where P_L and P_R are the left- and right projection operators. In case of a decay $Z' \to e^+e^-/\nu_i\bar{\nu}_j$, the coefficients read

$$\begin{aligned}
a_{ee} &= \frac{1}{2}\Big(\left(\bar{g} + g_{\mathrm{BL}}\right) c'_W - \left(g_2 c_W - g_1 s_W\right) s'_W \Big) \\
b_{ee} &= \frac{1}{2}\Big(\left(2\bar{g} + g_{\mathrm{BL}}\right) c'_W + 2 g_1 s_W s'_W \Big) \qquad (5.4) \\
a_{\nu_i\nu_j} &= \frac{1}{2}\Big(\Big(\Big(\bar{g} + g_{\mathrm{BL}}\Big) c'_W + \Big(g_1 s_W + g_2 c_W\Big) s'_W \Big) \sum_{a=1}^{3} U^{V,*}_{i,a} U^{V}_{j,a} \\
&\quad - g_{\mathrm{BL}} c'_W \sum_{a=1}^{3} U^{V,*}_{i,3+a} U^{V}_{j,3+a} \Big) \\
b_{\nu_i\nu_j} &= -\frac{1}{2}\Big(\Big(\Big(\bar{g} + g_{\mathrm{BL}}\Big) c'_W + \Big(g_1 s_W + g_2 c_W\Big) s'_W \Big) \sum_{a=1}^{3} U^{V,*}_{j,a} U^{V}_{i,a} \\
&\quad - g_{\mathrm{BL}} c'_W \sum_{a=1}^{3} U^{V,*}_{j,3+a} U^{V}_{i,3+a} \Big) , \qquad (5.5)
\end{aligned}$$

where $U^V_{k,l}$ is the 6×6 neutrino mixing matrix.

One can again see from the structure above that gauge kinetic mixing plays an important role in the process $p, p \to Z' + X \to e^+e^- + X$, which is used to set bounds on $M_{Z'}$. Since θ'_W is a small quantity, the main Z' discovery channel may thus be reduced sizeably.

We also list here the couplings to quarks as they will influence the Z' production in Drell-Yan processes and can also be used as indicators for the Z' nature.

$$\begin{aligned}
a_{uu} &= -\frac{1}{6}\Big((\bar{g} + g_{\mathrm{BL}}) c'_W - (3 g_2 c_W - g_1 s_W) s'_W \Big) \\
b_{uu} &= -\frac{1}{6}\Big((4\bar{g} + g_{\mathrm{BL}}) c'_W + 4 g_1 s_W s'_W \Big) \qquad (5.6) \\
a_{dd} &= -\frac{1}{6}\Big((\bar{g} + g_{\mathrm{BL}}) c'_W + (3 g_2 c_W + g_1 s_W) s'_W \Big) \\
b_{dd} &= \frac{1}{6}\Big((2\bar{g} - g_{\mathrm{BL}}) c'_W + 2 g_1 s_W s'_W \Big) . \qquad (5.7)
\end{aligned}$$

Obviously, the coupling to up-type quarks will be reduced when taking into account $U(1)$ mixing, while it will be enhanced in the case of down-type quarks. One may thus already expect a small reduction of Z' production in a proton machine.

The matrix element squared reads

$$\overline{|\mathcal{M}|^2}_{ff} = \frac{2}{3}\left(\frac{|a|^2+|b|^2}{2}\left(2M_{Z'}^2 - m_i^2 - m_j^2 - \frac{(m_i^2-m_j^2)^2}{M_{Z'}^2}\right) + 3(a^*b+b^*a)m_i m_j\right). \tag{5.8}$$

5.3.3 Decay into a scalar and a vector boson

The vertex structure for the third possibility is of the form $icg^{\mu\nu}$ with, *e.g.* in the case of $Z' \to Zh$,

$$\begin{aligned} c_{Zh} = -\frac{1}{8}\Big(\Big(&4\bar{g}g_2 c_W c'_{2W} + 4\bar{g}g_1 s_W c'_{2W} + (g_2^2-g_1^2)c_{2W}s'_{2W} + 2g_1 g_2 s_{2W}s'_{2W} \\ &+ (g_1^2+g_2^2-2\bar{g}^2)s'_{2W}\Big)\Big(v_d Z^H_{1,1} + v_u Z^H_{1,2}\Big) - 8g_{\mathrm{BL}}^2 s'_{2W}\Big(v_\eta Z^H_{1,3} + v_{\bar{\eta}} Z^H_{1,4}\Big)\Big), \end{aligned} \tag{5.9}$$

where $Z^H_{i,j}$ is the neutral Higgs mixing matrix and

$$\overline{|\mathcal{M}|^2}_{Vs} = \frac{1}{3}|c|^2\left(2 + \frac{(m_S^2 - M_{Z'}^2 - M_V^2)^2}{4M_{Z'}^2 M_V^2}\right). \tag{5.10}$$

5.3.4 Decay into a pair of vector bosons

In this case, the interaction is of the form $ic\,(g^{\rho\sigma}(q-p)^\mu + g^{\mu\sigma}(k-q)^\rho + g^{\mu\rho}(p-k)^\sigma)$ while for two final state W bosons, which embodies the only three-vector coupling including a Z', the coefficient reads

$$c_{WW} = g_2 c_W s'_W \tag{5.11}$$

and

$$\begin{aligned} \overline{|\mathcal{M}|^2}_{VV} =& \frac{1}{3}|c|^2\Big[\left(M_{Z'}^2 - (m_i-m_j)^2\right)\left(M_{Z'}^2 - (m_i+m_j)^2\right)\times \\ &\times \frac{M_{Z'}^4 + 10m_j^2m_i^2 + m_i^4 + 10M_{Z'}^2m_i^2 + m_j^4 + 10M_{Z'}^2m_j^2}{4m_i^2m_j^2M_{Z'}^2}\Big]. \end{aligned} \tag{5.12}$$

5.4 Branching ratios

We have calculated the branching ratios of the Z' decaying into various final states for the two selected benchmark points while taking care of the influence of kinetic mixing.

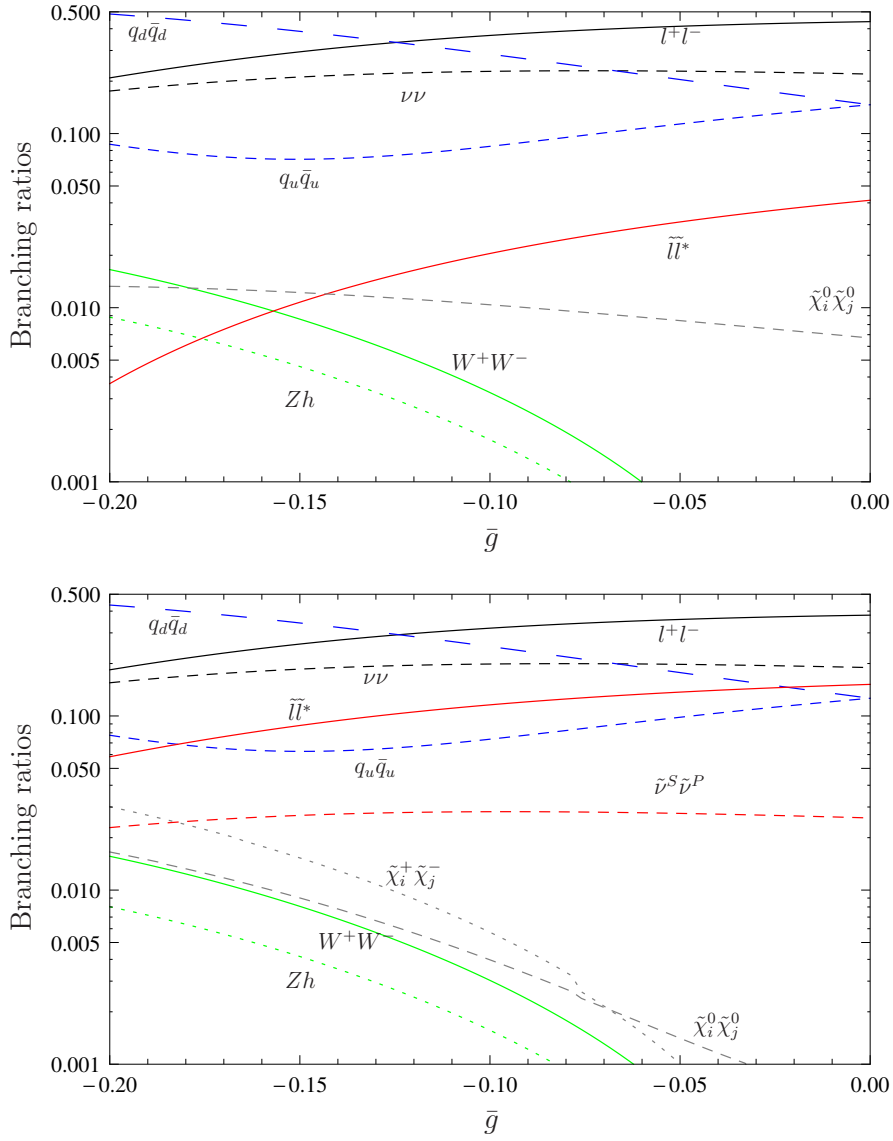

Figure 5.4: Branching ratios of the Z' at the considered parameter points BLV (above) and BLVI (below) as a function of the off-diagonal coupling parameter.

In fig. 5.4 we show the branching ratios of the Z' as a response to the variation of the off-diagonal gauge coupling for both benchmark points. It can be seen that the impact of $\bar{g}$ can be quite drastic. The strongest dependence on $\bar{g}$ arises in the quark sector where up-type and down-type quarks split with $\bar{g}$ growing negative. This influences the Z' production at a hadron collider, which we will see in sec. 5.6. Moreover, as already seen in the vertex structure for the Z' decay into charged (s)leptons (see eqns. (5.2), (5.4)), these channels get reduced by the impact of kinetic mixing, which has some phenomenological consequences. So, gauge kinetic mixing largely influences the Z' decay properties as it changes the magnitude of distinct

channels at the per-cent level while *e.g.* decays into charginos or W pairs are only possible due to a non-zero $\bar{g}$.

We will now have a closer look at the different decay channels as a function of the Z' mass with their respective features. As fig. 5.2 as well as eq. 4.33 show, a scan over the mass range can not be done by just varying the input parameter $M_{Z'}$ since only a very restricted parameter space is available. Thus, other parameters also have to be adjusted to be in the right range in order to be able to solve the tadpole equations and to be in a true minimum of the scalar potential. For that reason, all mass scans imply a variation of $\tan\beta'$ along the allowed range of fig. 5.2.

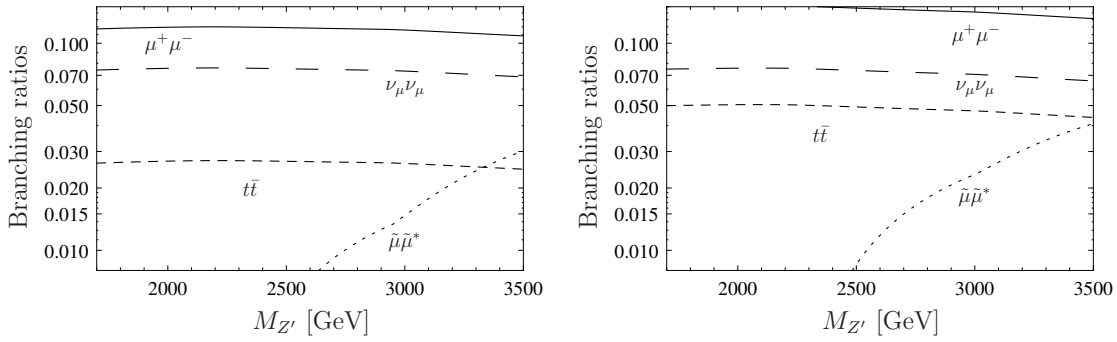

Figure 5.5: Branching ratios of the Z' to selected final states for BLV with consideration of gauge kinetic mixing (left) and without (right).

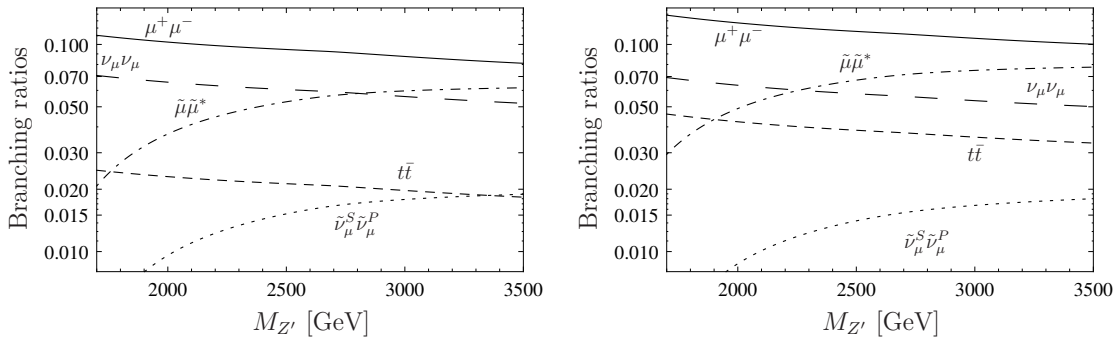

Figure 5.6: Branching ratios of the Z' to selected final states for BLVI with consideration of gauge kinetic mixing (left) and without (right).

An overview of different decay channels as a function of $M_{Z'}$ is given in figs. 5.5 and 5.6. Here again we distinguish between cases with and without gauge kinetic mixing but taking the value for $\bar{g}$ we obtain from our GUT-inspired approach ($\bar{g} \approx -0.11$). In the following, we discuss the decay channels into the various final states as a function of the Z' mass, leaving the other parameters as obtained from the two benchmark points.

5.4.1 Leptons

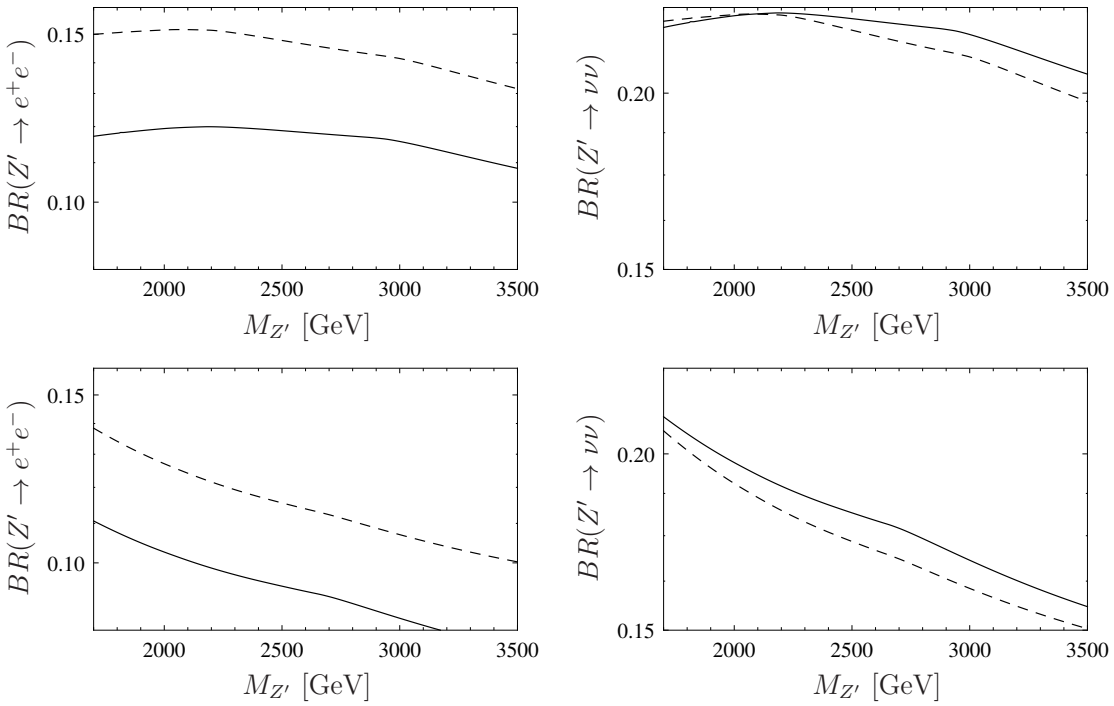

Figure 5.7: Branching ratios of $Z' \to e^+e^-$ (left) and $Z' \to \nu\nu$ (right) at benchmark points BLV (above) and BLVI (below). We summed over all neutrino generations for the plots on the right-hand side. The dotted curves represent the case neglecting $U(1)$ mixing.

The charged lepton and neutrino branching ratios are shown in fig. 5.7 for the considered parameter points. The kinks in the curves are obviously the mass values where decays into heavier particles become kinematically allowed and so lower the other branching fractions. As already discussed above, the off-diagonal coupling $\bar{g}$ in eq. (5.4) reduces the Z' coupling to charged leptons if it is taken into account correctly. In contrast, the neutrino decays are slightly pushed up by $\bar{g}$ due to the relative minus sign between the two vertex contributions in eq. (5.5).

5.4.2 Quarks

In fig. 5.8 we show the decay modes $Z' \to t\bar{t}/b\bar{b}$ for both benchmark points. Since the third-generation quarks are the only ones that can be distinguished from the other jets in a detector, these channels may be tested in order to gain information about the couplings and thus the nature of a Z'. It is quite obvious that the off-diagonal coupling $\bar{g}$ will have sizeable effect on the signatures of the Z'. The hypercharge doublet would be produced equally (with slight deviations because of the mass differences), if the Z' would solely couple to $B - L$ (compare the values at $\bar{g} = 0$ in

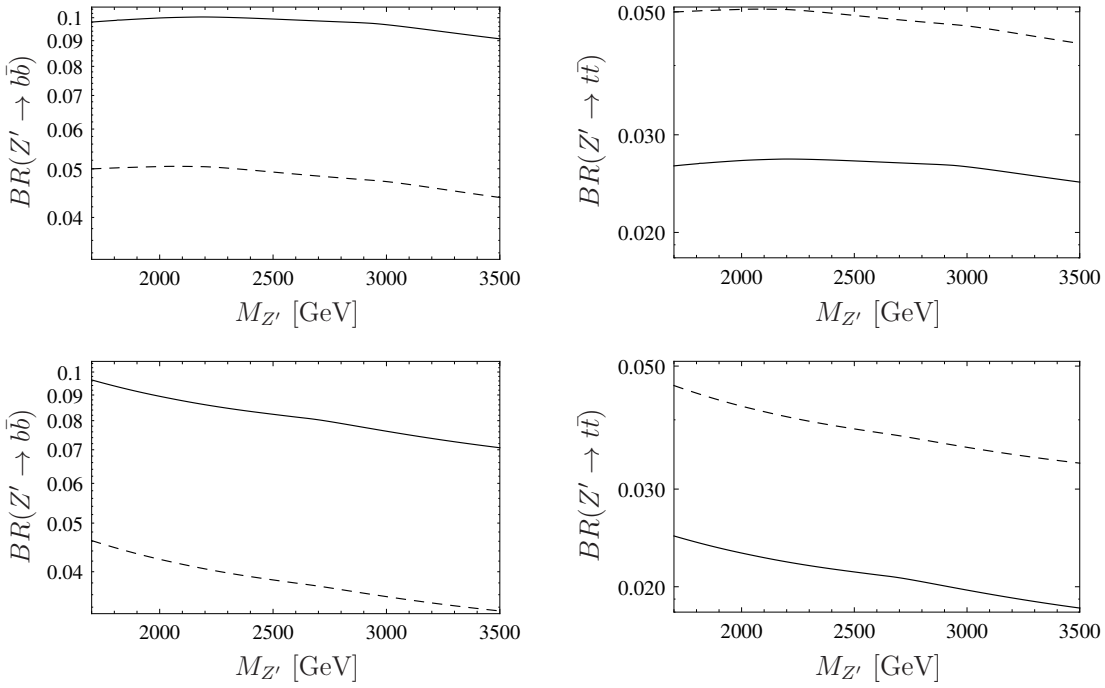

Figure 5.8: Branching ratios of $Z' \to b\bar{b}$ (left plots) and $Z' \to t\bar{t}$ (right plots) for the parameter choices BLV (above) and BLVI (below). The dotted curve stands for $\bar{g} = 0$.

fig. 5.4). Yet, they get split enormously as the hypercharge information plays a role at the Z' vertices where a mixture of right- and left-handed quarks are produced. The hypercharge of right-handed quarks differs in both sign and value. Thus there are huge differences between the branching ratios into up-type and down-type quarks which disappear with $\bar{g} \to 0$.

5.4.3 Gauge and Higgs bosons

Let us now consider the decays into gauge and Higgs bosons. These are possible through the mixing of the gauge eigenstates to the physical states, by which the Z' gets some amount of the W^3 and B boson proportional to $\sin\theta'_W$. Thus, *e.g.* the vertex $Z' - W^+ - W^-$ exists, but is small compared to vertices which include baryon or lepton charge. The decay into a pair of charged Higgs bosons (see fig. 5.9) is only observed at BLVI, which is just due to the high masses at BLV ($m_{H^\pm} = 2.2$ TeV). The reason for the incidence that the decay into Z plus Higgs is different at the two benchmark points ($h_2 Z$ for BLVI and $h_1 Z$ for BLV) can be found in the admixture of the Higgs bosons. While at point BLVI the lightest Higgs is bilepton-like, which does not couple at all to the (pure) Z, the second-lightest Higgs, h_2, is MSSM-like and so corresponds to h_1 at BLV.

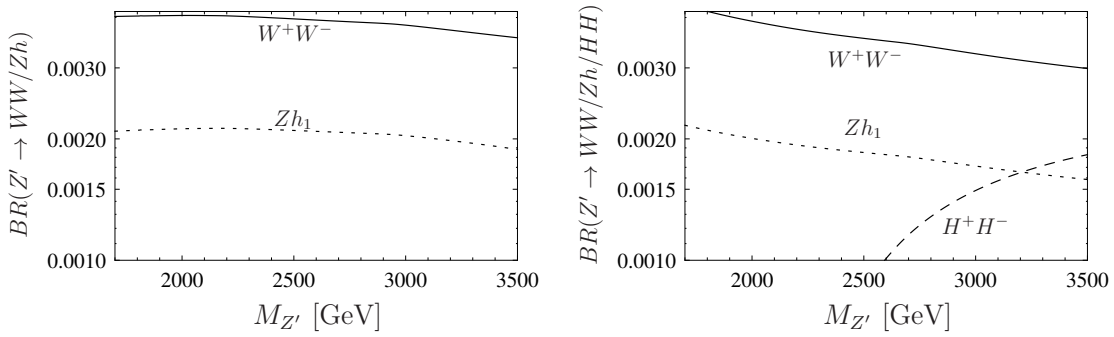

Figure 5.9: Branching ratios of the Z' to gauge and Higgs bosons for BLV (left) and BLVI (right). For $\bar{g} \to 0$ these decays do not exist.

5.4.4 Neutralinos and charginos

As expected, this sector is where the Z' decays in the two benchmark points differ the most. Recall that the lightest neutralino is bileptino-like at BLV and bino-like at BLVI. While the Z' can only couple to electroweak gauginos and Higgsinos through the off-diagonal coupling $\bar{g}$, it couples directly to bileptinos with the strength of g_{BL}, which is about four times the value of $\bar{g}$. The decay rate into neutralinos is thus at the percent level at BLV, while it ranges about a per mille at BLVI (see fig. 5.10). This is also the reason why there are neutralino final states for the case $\bar{g} = 0$ at BLV while they only occur as a small bump at the right-hand side of fig. 5.10. This is the mass range where the decay into a pair of $\tilde{\chi}^0_5$, which is bileptino-like at point BLVI, becomes kinematically accessible.

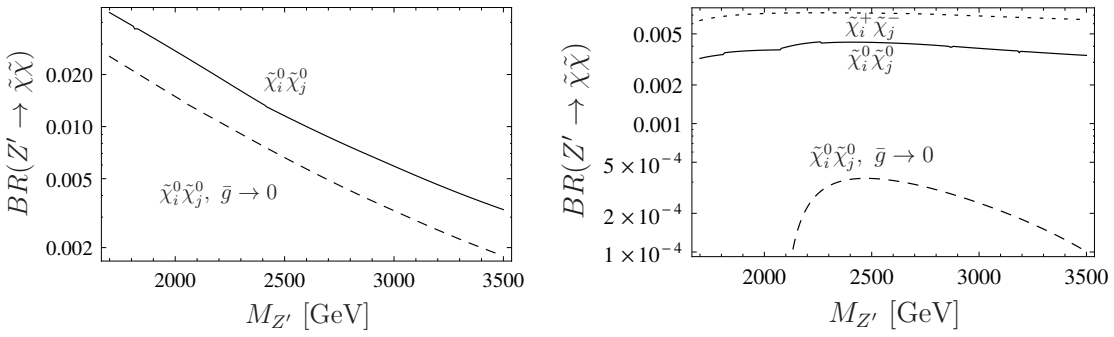

Figure 5.10: Branching ratios of $Z' \to \tilde{\chi}^\pm_i\tilde{\chi}^\pm_j$ and $Z' \to \tilde{\chi}^0_i\tilde{\chi}^0_j$ for BLV (left) and BLVI (right). The dashed curves are the neutralino BRs for $\bar{g} = 0$, while decays into charginos cannot occur in that case.

The channel $Z' \to \tilde{\chi}^\pm\tilde{\chi}^\pm$ is not available for BLV just due to the heavy charginos: they have masses of 1.2 TeV and 1.9 TeV.

5.4.5 Squarks

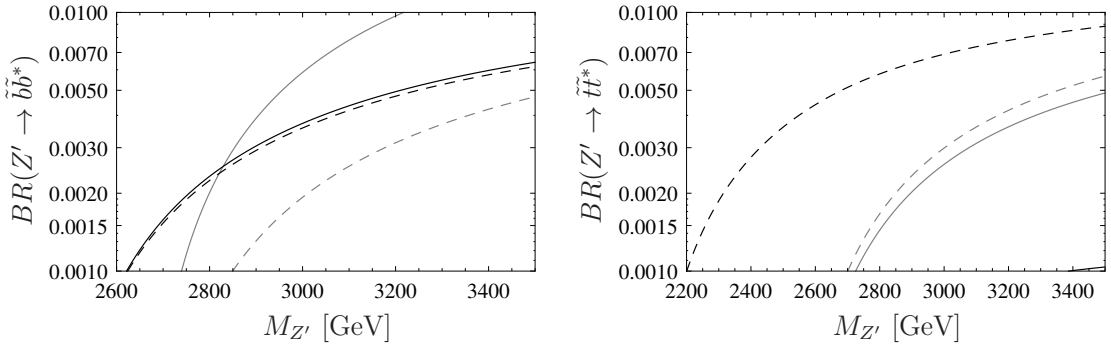

Figure 5.11: Branching ratios of $Z' \to \tilde{b}\tilde{b}^*$ (left) and $Z' \to \tilde{t}\tilde{t}^*$ (right) at benchmark point BLVI. The dotted curve represents the case neglecting $U(1)$ mixing. Black lines are the lighter squark mass eigenstates, grey curves are the heavy states.

The squark masses are around 1 TeV at BLVI, which is why the decays into them are disfavoured kinematically at low Z' masses. At benchmark point BLV, due to the high input values for m_0 and $M_{1/2}$, the lightest squark is the stop with 2.2 TeV, so squark decays are not possible in the considered mass range.

Fig. 5.11 summarizes the decays into the lightest, *i.e.* the third-generation squarks. The black lines are the light stops/sbottoms while the grey ones are the heavier states. By comparison with the case $\bar{g} = 0$ (dashed lines), one can already get an idea of the admixture of the light and heavy states: the lightest top squark is mainly a right stop, so it has a high hypercharge of $Y = 2/3$ and thus also a huge discrepancy between the cases with and without kinetic mixing (the stop line in the case of $\bar{g} \neq 0$ can only be seen as a small extract at around 3.4 TeV in the right plot of fig. 5.11). The orders of magnitude of difference are the result of a nearly exact cancellation in the $Z' - \tilde{t}_R - \tilde{t}_R^*$ vertex. The light sbottom, however, is mainly left-handed, thus big differences occur only in the decay into the heavy sbottoms.

5.4.6 Sleptons

The Z' decay into charged sleptons is potentially the most interesting channel as it contains charged particles which are produced at the percent level (each; the summed-up channels receive about 10% of the total decay width) and decay mostly to clean detector signals. Of course, as parameter point BLVI was chosen to give light sfermions and in especially light sleptons, the decays have a more important fraction there than in BLV, which can be seen in fig. 5.12.

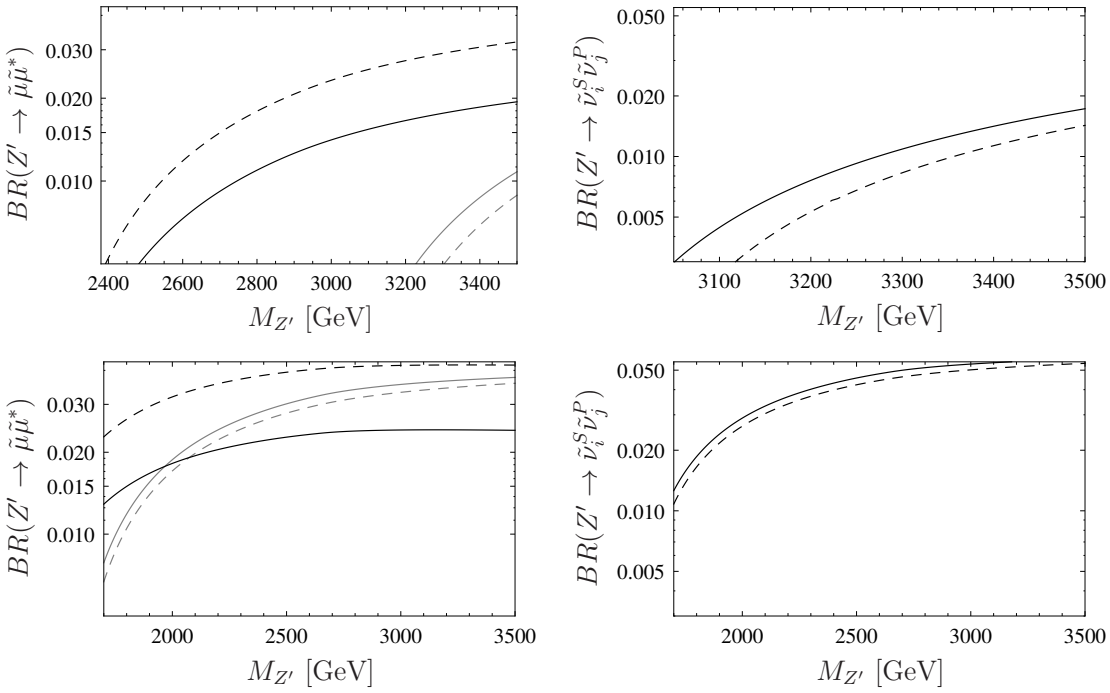

Figure 5.12: Branching ratios of $Z' \to \tilde{\mu}\tilde{\mu}^*$ (left) where the black curve is the light (R-) and the grey one the heavy (L-) smuon and $\sum_{i,j=1}^{6} Z' \to \tilde{\nu}_i^S \tilde{\nu}_j^P$ (right) at the parameter points BLV (above) and BLVI (below). The dotted curve represents the case where $\bar{g} = 0$.

5.5 LHC limits on the Z'_{B-L} production

The current bounds on the mass of a Z' are reviewed in section 2.3. As the LEP-II limits read $M_{Z'}/(g_{\mathrm{BL}} Q_e^{\mathrm{B\text{-}L}}) > 6.7$ TeV and $g_{\mathrm{BL}} \approx 0.55$ in our CMSSM-like calculations, these results would imply lower limits to our model of $M_{Z'} \gtrsim 1.84$ TeV. This, however, is only true in the limit of no gauge kinetic mixing and no mass mixing. As outlined before, mass mixing can indeed be neglected, whereas kinetic mixing can not. Thus, we have to take into account the form of the $Z' - l^+ - l^-$ vertex, which reads in the limit $\sin\theta'_W \to 0$ (see eq. (5.4))

$$\frac{i}{2}\gamma^\mu \left((g_{\mathrm{BL}} + \bar{g})P_L + (g_{\mathrm{BL}} + 2\bar{g})P_R\right) \tag{5.13}$$

instead of simply $\frac{i}{2}\gamma^\mu g_{\mathrm{BL}}$. Thus, we have to redefine the formula of the LEP limits. The vertex structure with $\bar{g} \neq 0$ is more complicated due to the different coefficients of the left and right projection operators. A derivation of the exact LEP II bounds on our model would require a full re-analysis of the electroweak observables, which we will not do here. Instead, we take the more conservative coefficient and thus make the substitution

$$g_{\mathrm{BL}} \to g_{\mathrm{BL}} + \bar{g}\,, \tag{5.14}$$

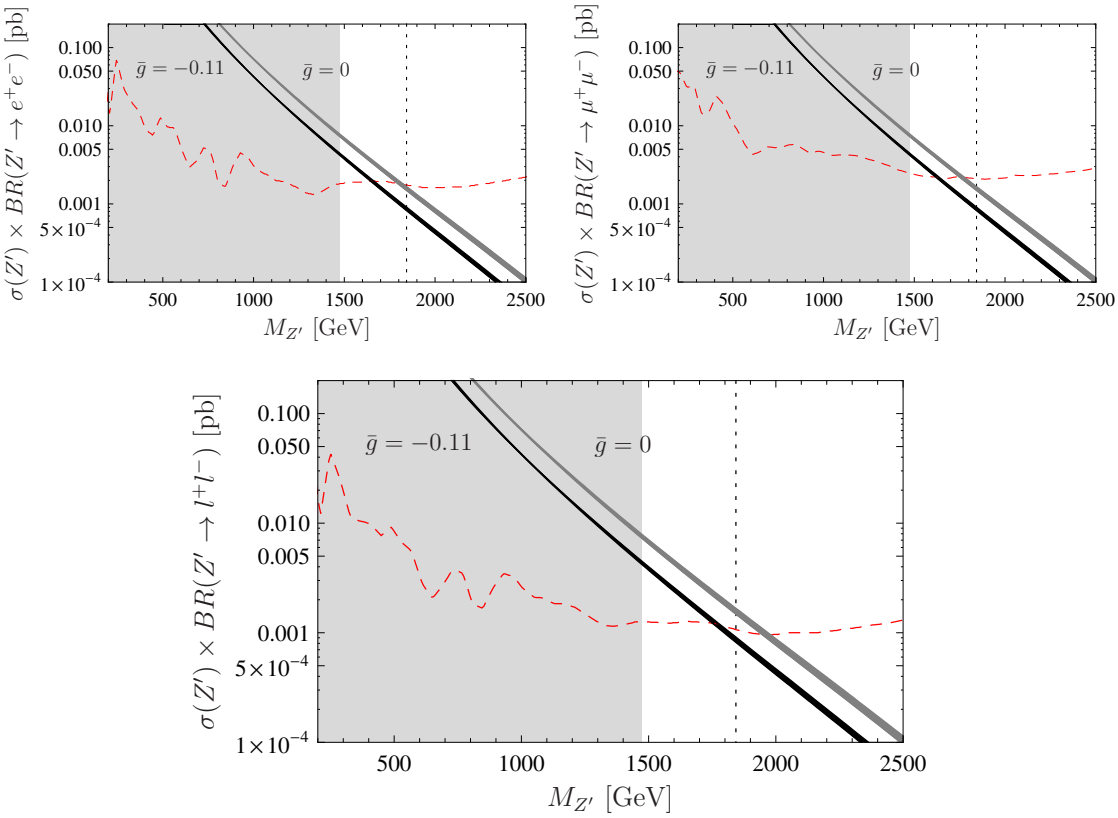

Figure 5.13: Current limits on $M_{Z'}$ for benchmark point BLV: the red curve shows the recent experimental ATLAS limits. The black and grey bands are the dilepton production cross sections on the Z' peak for the case of $U(1)$ mixing, $\bar{g} = -0.11$ (black) and without (grey). The grey shaded area shows the mass range forbidden by LEP II, while the black dotted line shows the LEP limits without taking into account gauge kinetic mixing. Upper-left: limits on electron production, upper-right: limits on muon production. Below: combined limits on lepton production.

so that the LEP II limits read

$$\frac{M_{Z'}}{(g_{\mathrm{BL}} + \bar{g})Q_e^{\mathrm{B\text{-}L}}} > 6.7 \text{ TeV}\,. \tag{5.15}$$

With $\bar{g} = -0.11$, this results in upper limits of $M_{Z'} > 1.47$ TeV.

The mass limits from LHC data [25, 26] range in the same order of magnitude (see fig. 2.1). However, the bounds derived there for selected models do not apply to ours for three reasons: First, the supersymmetric decay modes broaden the Z' width and so push down the dilepton cross section as the branching fraction into leptons gets lowered. Second, the coupling structure is different to the models considered there due to different $U(1)$ charges and third, as it has been shown in section 5.4, the possibility of gauge kinetic mixing reduces the dilepton production rate.

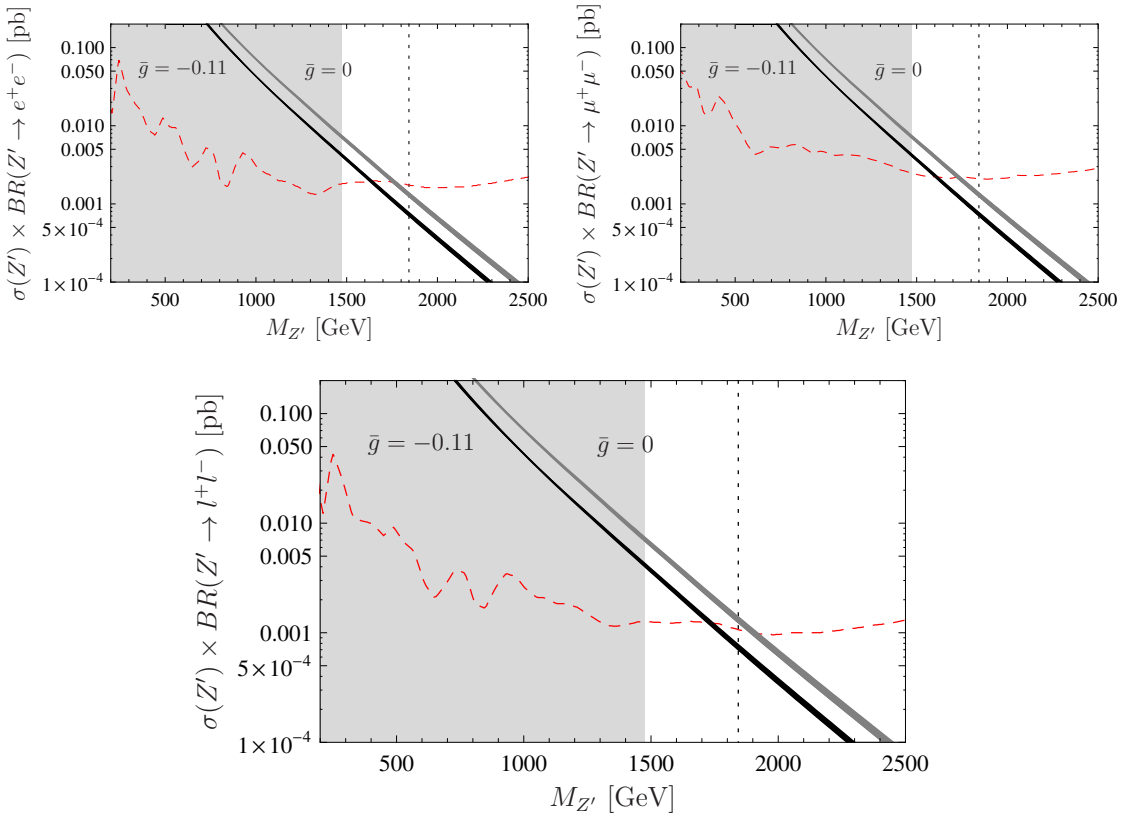

Figure 5.14: Current limits on $M_{Z'}$ for BLVI: the red curve shows the recent experimental ATLAS limits. The black and grey bands are the dilepton production cross sections on the Z' peak for the case of $U(1)$ mixing, $\bar{g} = -0.11$ (black) and without (grey). The grey shaded area shows the mass range forbidden by LEP II, while the black dotted line shows the LEP limits without taking into account gauge kinetic mixing. Upper-left: limits on electron production, upper-right: limits on muon production. Down: combined limits on lepton production.

For our calculation of the up-to-date bounds on the Z'_{B-L}, we derived the lepton production cross section at $\sqrt{s} = 7$ TeV using `WHIZARD`. For this purpose we collected electrons and muons with an invariant mass of ± 50 GeV around the Z' peak. The experimental limit was extracted from the ATLAS data. The minimal theoretical uncertainty was estimated using different sets of parton distribution functions as the main theoretical error sources are due to QCD effects, in particular in the value of α_s. Loop effects and thus K-factors have not been included here, although we are aware of the fact that they may change the results by a non-negligible amount. K-factors of around 1.3 are used in most non-supersymmetric Z' models [37, 57, 58] for the Z' production, whereas the ATLAS collaboration used a considerably smaller factor of 0.91 (at $M_{Z'} = 2$ TeV) [25] for their derivations. Accordingly, since there is no obvious choice and also the modification due to the inclusion of supersymmetric

	$\bar{g} = -0.11$	$\bar{g} = 0$
BLV	1770 GeV	1965 GeV
BLVI	1730 GeV	1900 GeV

Table 5.2: Current bounds on $M_{Z'}$ in the supersymmetric $B - L$ model derived from 5 fb^{-1} of ATLAS data [25] for both benchmark points.

particles is uncertain, we will use tree level results here and also in what follows.

Fig. 5.13 shows the exclusion curves for benchmark point BLV. The shaded area shows the region already excluded by LEP II, taking into account gauge kinetic mixing and thus applying eq. (5.15). The bound obtained by the negligence of $\bar{g}$ is shown as a black dashed line.

Fig. 5.14 shows for comparison the limits for benchmark point BLVI. As the sparticles are lighter in this scenario, there are more Z' decays into supersymmetric particles in the low $M_{Z'}$ regime and thus the diboson production is reduced with respect to the first case.

For a case where the Z' decays into only SM particles, we find as a lower limit $M_{Z'} < 1970$ GeV if we set $\bar{g}$ to zero, or $M_{Z'} < 1790$ GeV for $\bar{g} = -0.1$. The limits for the two considered benchmark points are even less severe due to the open SUSY channels. The current bounds from the ATLAS data for both points are summarized in table 5.2. Accordingly, we restrict ourselves to cases with $M_{Z'} > 1.7$ TeV in the further analysis.

While for $\bar{g} = 0$ the ATLAS limits give approximately the same value as for LEP II, this isn't the case anymore for $\bar{g} \neq 0$ where the ATLAS bounds are already more restrictive by an amount of about 200 GeV. The experimental bounds from the CMS collaboration, which are very new at that moment, are somewhat stronger than the ATLAS limits (see ref. [26]). Since they have only recently been made available as a preprint, they have not been included in this work. A combined analysis of course would be preferable.

5.6 Z' production and SUSY cascade decays

We saw in the last section that the production of a Z' is reduced by taking into account a non-zero $\bar{g}$. We now explore this behaviour in some more detail by varying the off-diagonal coupling on the analogy of fig. 5.4. In fig. 5.15, we show the response of the Z' production cross section by such a variation. The minimum in the plots at around $\bar{g} \approx -0.14$ corresponds to the one seen in the decays into up-type quarks in fig. 5.4. It can be identified with the term proportional to $(4\bar{g} + g_{\mathrm{BL}})$ in the Z' vertex with up-quarks, which in that case vanishes (see eq. 5.6). Hence, σ decreases at a proton-proton collider. In our GUT-inspired approach which results in $\bar{g} \approx -0.11$, we happen to be close to that production minimum. As expected, the qualitative behaviour does not depend on the center-of mass energy $\sqrt{s}$.

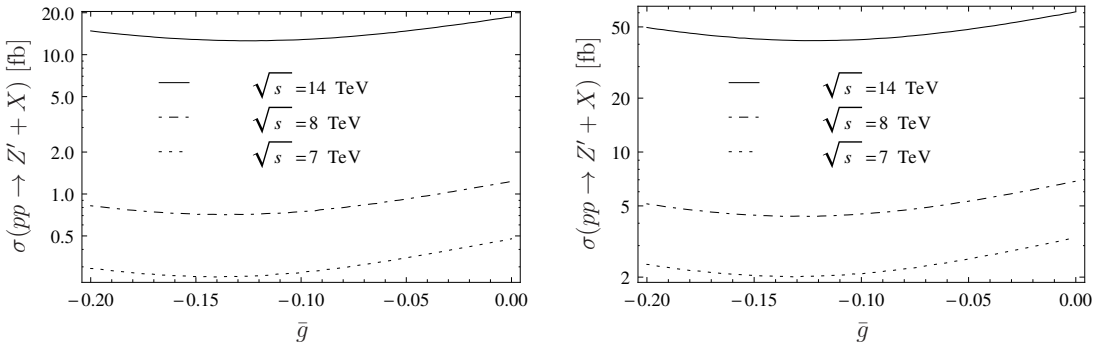

Figure 5.15: LHC production cross sections of the Z' at the considered parameter points BLV (left) and BLVI (right) and three different center-of-mass energies as a function of the off-diagonal coupling parameter.

Since we are interested in the LHC phenomenology of the supersymmetric Z' decays, which have relatively low branching ratios and, as it was shown before, the cross section in the multi-TeV range is low, we decided to do our calculations assuming a center-of-mass energy of $\sqrt{s} = 14$ TeV. For this purpose we used `WHIZARD` with the parton distribution set `CTEQ6L1` [59] and scanned over the interesting Z' mass range. Fig. 5.16 shows the evolution of the production cross section with growing $M_{Z'}$ and the corresponding fraction of supersymmetric particles that will be produced by subsequent Z' decays. With the Z' cross section being reduced by gauge kinetic mixing, the production of sparticles on the Z' resonance is also reduced in most cases. This, however, depends on the chosen SUSY parameter point. At BLV, for instance, the production of supersymmetric particles is enhanced at low $M_{Z'}$. This can be identified with the decay into neutralinos which dominates in this mass region and receives positive contributions from kinetic mixing (see fig. 5.4).

In order to work out which supersymmetric decay channels are the most interesting, we calculated all possible decay channels of the on-shell Z' into SM particles plus the LSP using narrow width approximation [60, 61]; *i.e.*, the decay cascade was regarded as a chain of on-shell particles decaying into lighter ones (with $m_a > m_b + m_c$) while neglecting all off-shell and interference effects. Thus, we simplified

$$\sigma(i, j \to Z' \to k, l \to ...) \approx \sigma(i, j \to Z') \times BR(Z' \to k, l) \times BR(k \to ...) \times BR(l \to ...)\,. \tag{5.16}$$

The inaccuracy we produce by approximating the propagator of a particle by an on-shell leg times its branching ratio into the particular final state is of the order Γ/M [60], *i.e.* about 1 % in case of the Z'.

All SUSY particles (except the LSP) were regarded as unstable as well as the massive gauge bosons, scalars and the top quark. The rest of the matter particles, including the bottom quark, were treated as a stable (*i.e.* detectable) final state.

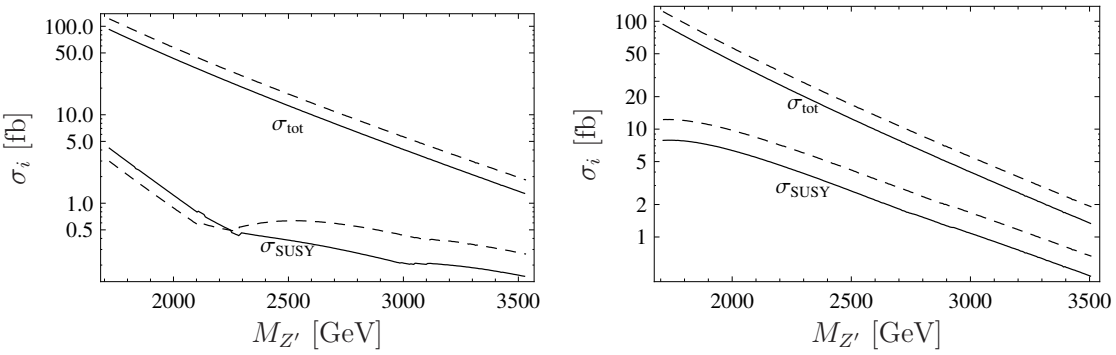

Figure 5.16: Production cross sections of the Z' at LHC-14 as a function of $M_{Z'}$ for the benchmark points BLV (left) and BLVI (right). The upper lines show the total cross section while the lower two show the cross section of produced SUSY particles stemming from an on-shell Z'. The solid lines represent the cases where we included gauge kinetic mixing whereas the dashed lines are the results if we neglected it.

5.6.1 BLVI

With cross sections of the order of some femtobarns for supersymmetric channels (see fig. 5.16), this benchmark point could potentially give interesting signatures at the LHC. In fig. 5.17, we summarize the final states which occur the most after the decay of a Z' into two supersymmetric particles.

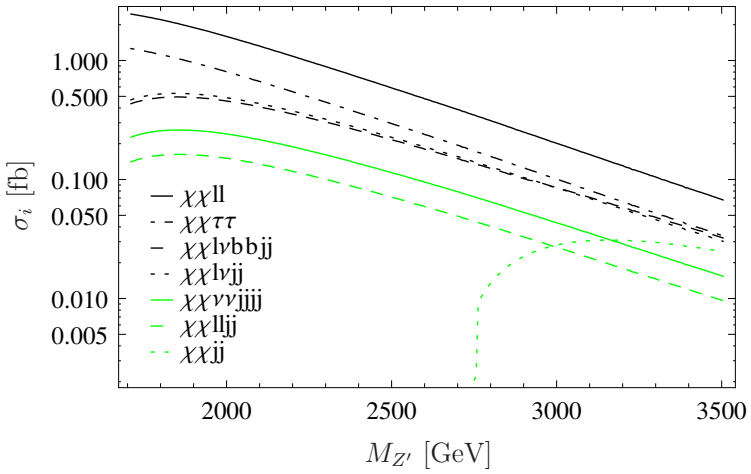

Figure 5.17: Summary of the dominant supersymmetric final states following after a Z' decay at BLVI. The abbreviations denote: $\chi \mathrel{\widehat{=}} \tilde{\chi}_1^0$, l $\mathrel{\widehat{=}}$ (anti-) lepton (e, μ), b $\mathrel{\widehat{=}}$ (anti-) bottom quark, $\nu \mathrel{\widehat{=}}$ neutrino, j $\mathrel{\widehat{=}}$ jet (up, down, strange and charm quarks)

Naturally, as R-parity is assumed to be conserved, the only remaining supersymmetric particle in the final state is the LSP, which is the lightest neutralino in all

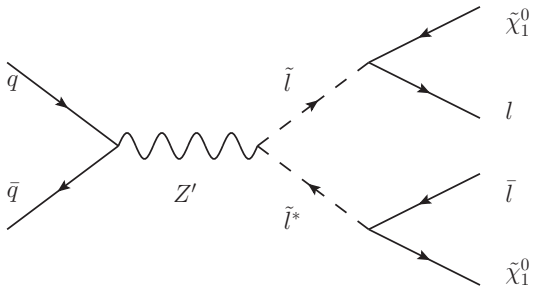

Figure 5.18: Feynman diagram for the production of $\tilde{l}\tilde{l}^*$ via an s-channel Z' exchange and the subsequent decay into $l^+l^-\tilde{\chi}_1^0\tilde{\chi}_1^0$.

considered cases. Most of the channels contain a high jet rate, which is due to the decays of squarks, Higgs and W/Z bosons which occur as intermediate states in the cascade. The final state with the highest cross section over the whole interesting mass range, however, is the one with two leptons and two neutralinos which occur at the direct decay of a slepton into lepton plus neutralino. Taus are regarded as a separate final state here since their mostly hadronic decays make them look like hadrons in a detector.

Consider smuon production: the decays of the two smuon mass eigenstates at this parameter point are, according to `SPheno`,

$$\begin{aligned} \tilde{\mu}_R &\to \mu\tilde{\chi}_1^0 && 100\ \% && (5.17)\\ \tilde{\mu}_L &\to \mu\tilde{\chi}_1^0 && 17.6\ \% && \\ &\to \mu\tilde{\chi}_2^0 && 28.7\ \% && \\ &\to \nu_\mu\tilde{\chi}_1^\pm && 53.7\ \%\,. && (5.18) \end{aligned}$$

Hence, the majority of all produced smuon pairs decay directly into two muons and two lightest neutralinos. This behaviour is displayed in fig. 5.19. Since the cross section will be high enough to be tested at the LHC and the final state gives a rather clean detector signal of two muons plus missing energy, we will study this process in more detail in chapter 6.

5.6.2 BLV

As was already clear in sec. 5.4, this parameter point will not give very rich LHC phenomenology due to the high masses of the sparticles. What could be interesting, however, are the invisible Z' decays, *i.e.* the direct production of two LSPs. This behaviour can just be seen at low enough Z' masses as the LSP nature alters from bileptino-like to bino-like with higher mass so that the channel $Z' \to \tilde{\chi}_1^0\tilde{\chi}_1^0$ changes to $Z' \to \tilde{\chi}_2^0\tilde{\chi}_2^0$.

The 2-muon, 2-neutralino final state, which is among the most interesting at BLVI, is not expected to play a big role here. It will be produced by $Z' \to \tilde{\chi}_1^0\tilde{\chi}_2^0$ with a subsequent decay of the second-lightest neutralino to $\tilde{\chi}_1^0 Z/h$ or the three-body

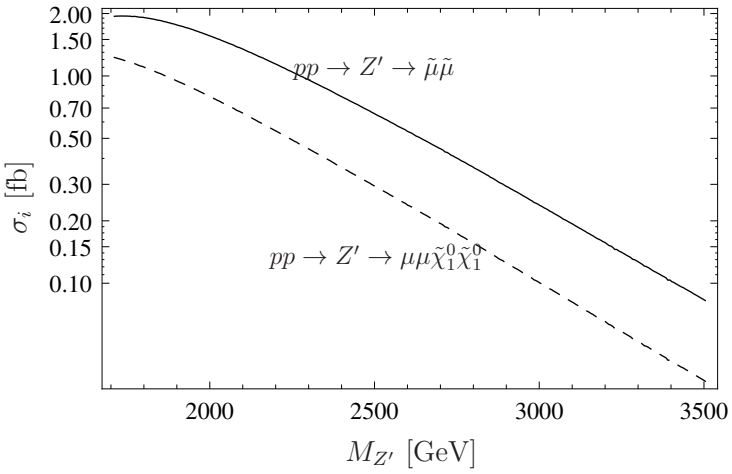

Figure 5.19: Production cross section of smuon pairs on the Z' resonance (solid line) and of the subsequent final state $\mu^+\mu^-\tilde{\chi}_1^0\tilde{\chi}_1^0$ at BLVI.

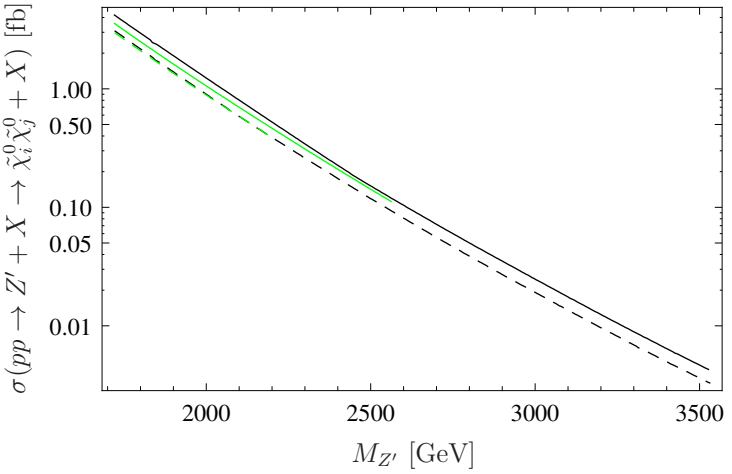

Figure 5.20: Resonant $\tilde{\chi}_i^0\tilde{\chi}_j^0$ production on the Z' peak at BLV. The solid lines represent the cases with inclusion of gauge kinetic mixing, while the dashed lines show the case neglecting $\bar{g}$. The green curves show the LSP production.

decay $\tilde{\chi}_2^0 \to \tilde{\chi}_1^0\mu^+\mu^-$ below the $\tilde{\mu}_R\tilde{\mu}_R^*$ threshold. The direct production via smuons such as at benchmark point BLVI can only occur at high enough Z' masses. This behaviour is illustrated in fig. 5.21. At about 3 TeV, the decay into $\tilde{\mu}_L\tilde{\mu}_L^*$ becomes kinematically accessible. They themselves decay into muon plus neutralino only in a small fraction, which causes the separation of the two lines in fig. 5.21. Obviously, the cross section is much too small to be tested at the LHC for this parameter point.

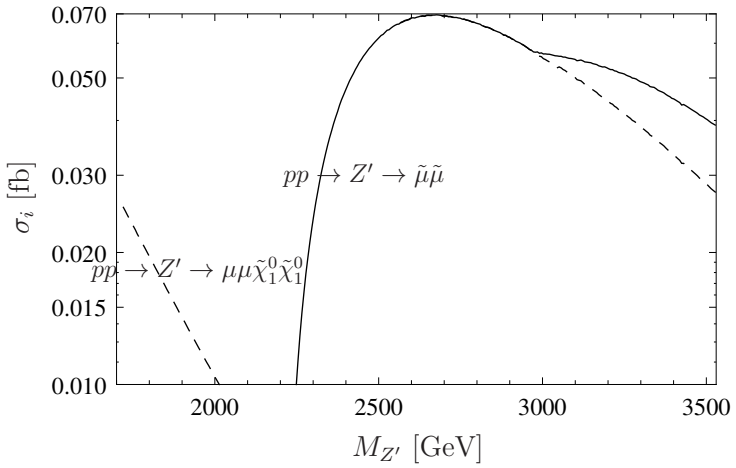

Figure 5.21: Production of the final state $\mu\mu\tilde{\chi}_1^0\tilde{\chi}_1^0$ (dashed line) as a function of the Z' mass at BLV. The solid line shows the channel $Z' \to \tilde{\mu}\tilde{\mu}^*$.

Chapter 6

Monte Carlo study: Dimuon production

The examined parameter points (as well as the experimentally allowed CMSSM-like points) all have sfermion masses of at least some hundred GeV, up to a few TeV. A direct discovery at the LHC via Drell-Yan processes and intermediate Standard Model or MSSM particles is unlikely for these high masses. Just considering particles from the MSSM, the LHC is only sensitive to sfermions with masses up to about 200 GeV. With an intermediate on-shell Z' decaying into sfermions, things look different as the production cross section peaks at the Z' mass and thus presents a smoking gun for sparticle production. In the last section we have shown that the decay $Z' \to \widetilde{ll}^* \to l\bar{l}\tilde{\chi}_1^0\tilde{\chi}_1^0$ is the most important SUSY channel for a given parameter set. In addition, we expect it to be the cleanest of all possible $Z' \to$SUSY final states since two hard leptons plus a lot of missing energy can be distinguished from the Standard Model background. In the following section we examine how the existence of a Z' could affect smuon production and discovery at the LHC via this channel.

6.1 Simulation of signal and background

The analysis has been done for benchmark point BLVI as this is the one where LHC phenomenology of a Z' decaying into sfermions seems promising. We assumed proton-proton collisions at $\sqrt{s} = 14$ TeV and 100 fb^{-1} of integrated luminosity. In order to classify the results we get for the signal process, we have to take into account all processes which give the same or similar final states in the detector. For example, the LSP can not be distinguished from a neutrino in the detector as both particles are electrically neutral and will escape the detector. Hence they both appear as missing transverse energy ($\not{E}_T$) in the detector. Furthermore, we cannot restrict ourselves to processes which result in two muons plus $\not{E}_T$ only as there will be a lot of hadronic background in a proton machine which can not be prevented. Consequently, processes which may give low-energy jets in the detector have to be regarded, too. We considered the following processes as background:

SM background:

- Diboson production, with the vector bosons decaying into two muons and two neutrinos: $q, q' \to W^+W^-/ZZ \to \mu\mu\nu\nu$
- Triple boson production, resulting in two muons, neutrinos and optionally jets: $q, q' \to WWW/ZZZ/WWZ/WZZ \to \mu\mu\nu\nu\nu\nu/\mu\mu\nu\nu jj$ ($j \,\widehat{=}$jet)
- $t\bar{t}$ production with the top quark decaying into a low-energy b-quark and a W boson, with the W then decaying into a muon and a neutrino.
- $t\bar{t}Z$ production, with the Z boson decaying invisibly or into two low-energy jets.

SUSY background:

- neutralino production: $\tilde{\chi}_i^0\tilde{\chi}_1^0 \to W^\pm\tilde{\chi}_1^\mp\chi_1^0 \to W^+W^-\chi_1^0\chi_1^0 \to \mu^+\mu^-\tilde{\chi}_1^0\tilde{\chi}_1^0\nu\nu$ or $\tilde{\chi}_i^0\tilde{\chi}_1^0 \to Z\tilde{\chi}_1^0\tilde{\chi}_1^0/h\tilde{\chi}_1^0\tilde{\chi}_1^0 \to \mu^+\mu^-\tilde{\chi}_1^0\tilde{\chi}_1^0$
- chargino production, *i.e.* $\tilde{\chi}_i^+\tilde{\chi}_j^- \to W^+W^-\tilde{\chi}_1^0\tilde{\chi}_1^0 \to \mu^+\mu^-\tilde{\chi}_1^0\tilde{\chi}_1^0\nu\nu$

Other SUSY backgrounds, such as squark and gluino production, can safely be ignored due to the high masses and the small branching fractions into neutralino plus SM fermion. Additionally, they can be distinguished from the signal quite well due to the hard jets they usually produce in their cascade decays.
As signal, we just demanded two opposite-sign muons plus two lightest neutralinos.

In order to proceed with the simulation description, we have to define some kinematical observables which are important for the analysis:

- the invariant mass of the muons: $M_{\mu\mu} = \sqrt{p^2(\mu^+) + p^2(\mu^-)}$ where p denotes the 4-vector of of the particular particle momentum.
- the transverse momentum $p_T = \sqrt{p_x^2 + p_y^2}$ if the beam points towards the z direction and p_i is the momentum component in direction i.
  The p_T of the particles which escape the detector without being measured, the missing transverse energy, can experimentally just be determined as the transverse momentum of the sum of these particles: $p_T^2(\not{E}_T) = \left(\sum_{\not{E}_T} p_x\right)^2 + \left(\sum_{\not{E}_T} p_y\right)^2$.
- the cluster transverse mass combines the transverse momentum of the lepton pair as well their invariant mass and the missing transverse energy. It is given by [62]

$$M_T = \sqrt{\left(\sqrt{p_T^2(\mu^+\mu^-) + M_{\mu\mu}^2} + p_T(\not{E}_T)\right)^2 - \left(\boldsymbol{p}_T(\mu^+\mu^-) + \boldsymbol{p}_T(\not{E}_T)\right)^2}, \quad (6.1)$$

Set of cuts	Signal	Diboson	Tripleboson	$t\bar{t}$	$t\bar{t}Z$	SUSY
no further cuts	84	18632	141	16836	6	20
cut set No. 1, no M_T cut	53	44	5	52	0	3
cut set No. 1 with M_T cut	48	25	2	16	0	2
cut set No. 2	46	20	2	12	0	2

Table 6.1: Number of generated events for $p, p \to \mu^+\mu^- + \not{E}_T + X$ from the distinct channels. The first row (no further cuts) implies $p_T(\mu^\pm) > 20$ GeV, $M_{\mu\mu} > 100$ GeV and $|\eta| < 2.7$. The other rows correspond to the two sets of cuts introduced in section 6.2.

with $\boldsymbol{p}_T$ being the 2D vector of the transverse momentum and $\boldsymbol{p}_T(\mu^+\mu^-) = \boldsymbol{p}_T(\mu^+) + \boldsymbol{p}_T(\mu^-)$. Using $\boldsymbol{p}_T(\mu^+\mu^-) = -\boldsymbol{p}_T(\not{E}_T)$, which is approximately true in case of proton collisions and the considered final state, the formula can be simplified and yields

$$M_T = p_T(\mu^+\mu^-) + \sqrt{p_T^2(\mu^+\mu^-) + M_{\mu\mu}^2}\,. \tag{6.2}$$

- the pseudorapidity $\eta = -\ln\tan(\theta/2)$ is a useful quantity to determine the angle of the particle line with respect to the beam axis. The advantage of this angle definition is the boost invariance of η in the beam direction.

The events were simulated with `WHIZARD`, where we demanded from beginning that the invariant mass of the muons is above 100 GeV and the transverse momentum of the quarks is smaller than 40 GeV. Additionally the pseudorapidity was set $|\eta| < 2.7$ to take into account the direction of the beam pipe at the LHC where detection is not possible. Fig. 6.1 shows the invariant mass, missing energy and cluster transverse mass distribution without any further cuts applied.

The total number of events that give a signal $\mu^+\mu^- + \not{E}_T$ for the distinct channels are summarized in table 6.1.

6.2 Background reduction

To reduce background, cuts on the kinematical observables were applied. The muons in the signal originate from high-energy and high-mass smuons, which themselves were mainly pair-produced by a Z' decay. Thus, the invariant muon mass is expected to be much higher than in the case of, say, a Z boson decaying into $\mu^+\mu^-$, which produces high cross sections in the invariant mass regime close to the Z, but then rapidly decreases with higher masses. This behaviour can be observed quite nicely in fig. 6.1 where an exponential decrease of the background can be observed. Additionally, the transverse mass of the missing energy is expected to be high since highly boosted massive particles with masses of a few hundred GeV escape. At least an equal reduction power can be attributed to the cluster transverse mass.

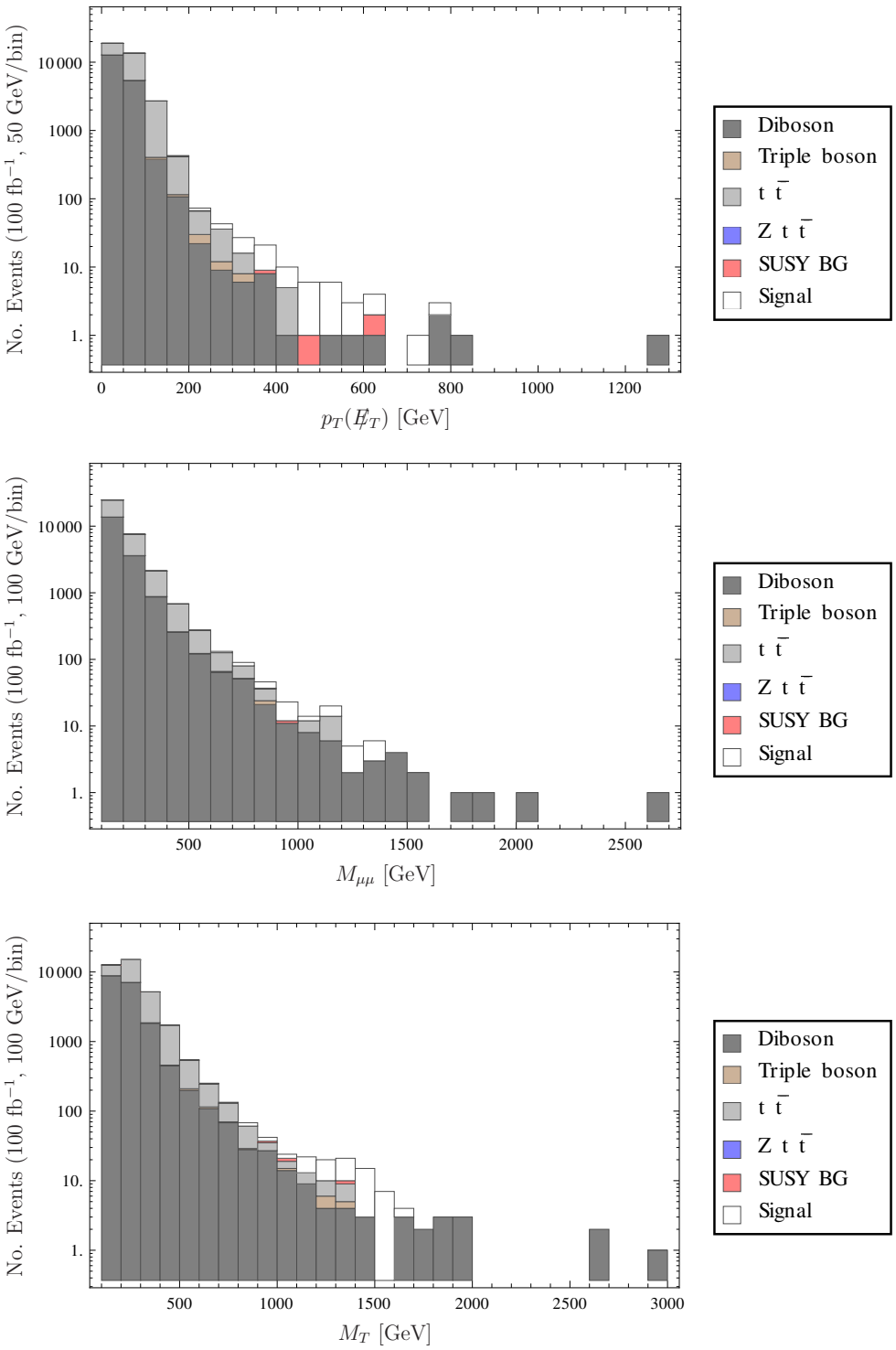

Figure 6.1: Histograms of the $\mu^+\mu^- + \not{E}_T$ production with $M_{\mu\mu} > 100$ GeV as a function of the missing transverse energy (above), the invariant mass $M_{\mu\mu}$ (middle) and the transverse cluster mass M_T (below).

The cuts have been chosen to be applicable to a wide range of Z' and $\tilde{\mu}$ masses and thus are looser than they could have been applied to the example presented exclusively. We demand (cut set No. 1)

$$\begin{aligned} p_T(\mu) &> 20 \text{ GeV} \\ p_T(\not{E}_T) &> 200 \text{ GeV} \\ M_{\mu\mu} &> 200 \text{ GeV} \end{aligned} \tag{6.3}$$

and, in addition, we add a cut on the transverse cluster mass M_T, as we see a great reduction power of this variable (see fig. 6.2)

$$M_T > 800 \text{ GeV}\,, \tag{6.4}$$

or, in a second, tighter approach, where we do not make use of the combined quantity M_T (cut set No. 2)

$$\begin{aligned} p_T(\mu) &> 20 \text{ GeV} \\ p_T(\not{E}_T) &> 250 \text{ GeV} \\ M_{\mu\mu} &> 300 \text{ GeV}\,. \end{aligned} \tag{6.5}$$

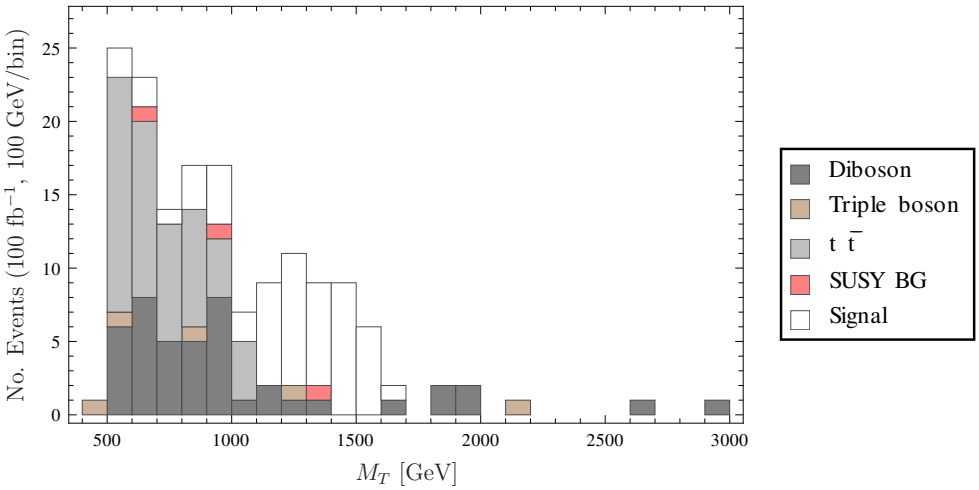

Figure 6.2: Histograms of the $\mu^+\mu^- + \not{E}_T$ production with the cuts of eq. (6.3) as a function of the transverse cluster mass.

Fig. 6.2 shows the transverse cluster mass distribution of fig. 6.1 with the first set of cuts applied, but still without the M_T cut. The irregular structure of the background is just the expected fluctuation because of the small number of events. The already small $t\bar{t}Z$ background does not survive the cuts.

A further background reduction which does not cut event by event, but that relies on statistics, could also be considered here: a large portion of the SM background

contains intermediate W^+W^- states which subsequently decay into $\mu^+\mu^-\nu\nu$. It is clear that for the final states produced by W pairs, the relation

$$\sigma(\mu^+\mu^-\nu\nu) + \sigma(e^+e^-\nu\nu) \approx \sigma(e^+\mu^-\nu\nu) + \sigma(\mu^+e^-\nu\nu) \tag{6.6}$$

must hold since the branching ratios of $W \to e\nu$ and $W \to \mu\nu$ are essentially the same. Accordingly, one can expect that for the number of produced events by these channels the equality

$$N(\mu\mu\nu\nu) \approx \frac{1}{2}N(e\mu\nu\nu) \tag{6.7}$$

is approximately fulfilled and thus most of the diboson and $t\bar{t}$ background could be erased. Naively subtracting $N(e\mu\nu\nu)$ fom the data would, however, not work since we have to account for statistical fluctuations $\Delta N = \sqrt{N}$ such that for the remaining number of background events, we would have to write

$$\begin{aligned} N_{\text{BG left}} &= N(\mu\mu\nu\nu) - \frac{1}{2}N(e\mu\nu\nu) \pm \Delta N \\ &= N(\mu\mu\nu\nu) - \frac{1}{2}N(e\mu\nu\nu) \pm \sqrt{N(\mu\mu\nu\nu) + \frac{1}{2}N(e\mu\nu\nu)}\,, \end{aligned} \tag{6.8}$$

so that effectively, we do not cut away very much background as the rates are small anyhow (see table 6.1). For this reason, we decided to only apply our event-by event cuts defined in eqns. (6.3)-(6.5) and not this method.

6.3 Significance of the signal

In order to analyse whether smuon production can be discovered at the LHC with the help of a Z' resonance, the significance level of the signal has to be determined. The significance is defined as

$$s = \frac{N_{\text{Signal}}}{\Delta N_{\text{BG}}}\,, \tag{6.9}$$

while ΔN_{BG} is the standard deviation of the number N_{BG} of the background events. From Poisson statistics,

$$\Delta N_{\text{BG}} = \sqrt{N_{\text{BG}}}\,. \tag{6.10}$$

Thus, the significance of the signal is given by

$$s = \frac{N_{\text{Signal}}}{\sqrt{N_{\text{BG}}}}\,. \tag{6.11}$$

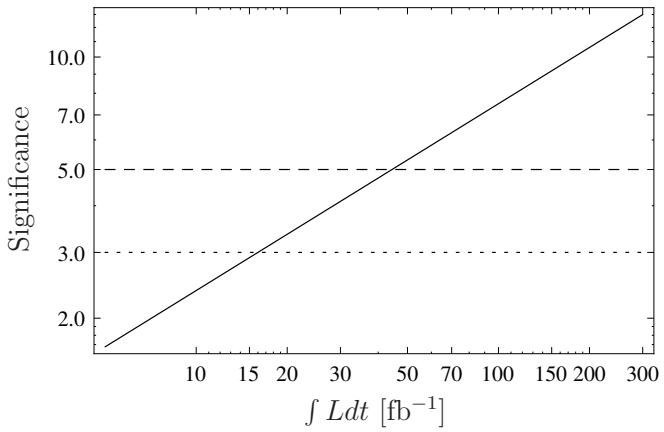

Figure 6.3: Expected evolution of the significance level with growing integrated luminosity. The discussed significance at 100 fb^{-1} fixes the curve. The borders for 3 and 5 σ are shown as dotted and dashed lines.

We have always checked that N_{Signal} is high enough in our simulations such that the formula is applicable. We can calculate the significance with these definitions and the number of events from table 6.1, resulting in

$$s = 7.5\ \sigma\,, \tag{6.12}$$

i.e., the smuon signal would be high enough to claim discovery at LHC-14 with 100 fb^{-1}. Based on eq. (6.11), an estimate of how much luminosity is needed to discover such a smuon signal is shown in fig. 6.3. Accordingly, an integrated luminosity of about 45 fb^{-1} is required to discover the signal for the simulated parameters at 5 σ.

A similar significance can be achieved with the second set of cuts such that they perform equally well at this parameter point.

6.4 Significance reach for variable Z' and $\tilde{\mu}$ masses

We showed in the last section how smuon production can be enhanced by effects of an on-shell Z' for one specific parameter point. Motivated by this fact, we repeat the analysis for variable smuon and Z' masses. Thereby we aim to determine mass regions in which discovery of smuons is possible, enabled by the Z' resonance. In particular, we want to check if sleptons with low (*i.e.* $\mathcal{O}$(few hundred GeV)) masses can be discovered with the help of the Z'. In order to perform the simulation, we did the following: we abandoned the CMSSM boundary conditions as the analysis is simply based on the Z' and $\tilde{\mu}$ properties. Hence, we took the EWSB-scale Lagrangian parameters of BLVI as a starting point and varied the masses of the smuons and the Z' freely while leaving the other parameters fixed. We distinguished three different

mass ratios between the R- and L-sleptons of 1.2, 1 and 1/1.2. These ratios can for instance be obtained by different values for $\tan\beta$ [40] or the soft SUSY-breaking masses $M_{\tilde{L}}$ and $M_{\tilde{e}}$, see eqns. (4.27) and (4.28). The latter case, $m_{\tilde{\mu}_L} = 1.2\, m_{\tilde{\mu}_R}$ is the standard hierarchy arising from mSUGRA-like boundary conditions.

Furthermore, we repeated the whole analysis with reduced neutralino masses and thus reduced mass of the LSP. For this case, we fixed $m_{\tilde{\chi}_1^0} = 140$ GeV and $m_{\tilde{\chi}_2^0} = m_{\tilde{\chi}_1^\pm} = 2\, m_{\tilde{\chi}_1^0}$ in order to guarantee that decays $\tilde{\mu} \to \mu\tilde{\chi}_1^0$ are possible even for low slepton masses and to make sure that the $\tilde{\chi}_1^0$ is the LSP.

With these conditions, we simulated the signal and SUSY background events for each parameter point, applying both sets of kinematical cuts described in section 6.2. The significance was in each case calculated using eq. (6.11). The simulations were done for both 100 fb^{-1} and 300 fb^{-1} of data.

6.4.1 $\int Ldt = 100$ fb^{-1}

The significances of the smuon signal over a mass range of 1.7 TeV $< M_{Z'} <$ 3.5 TeV and 150 GeV $< m_{\tilde{\mu}_{R/L}} <$ 850 GeV with a 140 GeV LSP are shown in fig. 6.4 for the three different L/R smuon mass relations and with the two mentioned sets of cuts.

As expected, the significance rises as the Z' mass decreases, simply because of the higher Z' cross section. Accordingly, the signal gets weaker as the smuon mass approaches a TeV due to decay kinematics. With the smuon mass going below 200 GeV, however, the signal becomes more and more SM-like, *i.e.* mainly the invariant mass of the muons drops. Thus, the cuts meant to reduce background also cut away a huge amount of signal and the significance shrinks.

Obviously, the two applied cut scenarios have a different performance. While the two sets perform equally well in the example point presented above, we see that the consideration of the variable M_T helps identifying the smuon signal in a broader area.

The regions of a potential 5 σ discovery lie in the range of about $m_{\tilde{\mu}_1} \approx$ 200 ... 800 GeV and $M_{Z'} <$ 2.8 TeV. The tail in the plots at smuon masses smaller than about 300 GeV indicates the region where the L-smuons are still light enough with respect to the lightest chargino such that their dominant decay channel is the same as for R-smuons. Hence, the discovery probability is enhanced in this area. The irregular structures in fig. 6.4 can be explained if one takes into consideration that the signal was generated by a Monte-Carlo generator using a relatively low number of events ($\mathcal{O}(100)$ at 100 fb^{-1}). Thus, fluctuations are quite normal and appear as somewhat strange contours in the plots.

In the case of heavier neutralino masses, where we fixed $m_{\tilde{\chi}_1^0}$ to the value it has at BLVI ($m_{\tilde{\chi}_1^0} \approx 280$ GeV), no qualitative change with respect to the cases with reduced $\tilde{\chi}_1^0$ mass occurs. In fig. 6.5 we show the resulting significance plot for the smuon mass relations $m_{\tilde{\mu}_L} = 1.2\, m_{\tilde{\mu}_R}$. Obviously, the region of 5 σ discovery shrinks compared to the cases above since the mass difference between the smuons and the LSP is smaller. Hence, kinematics just allow for smaller $M_{\mu\mu}$ and thus a sizeable

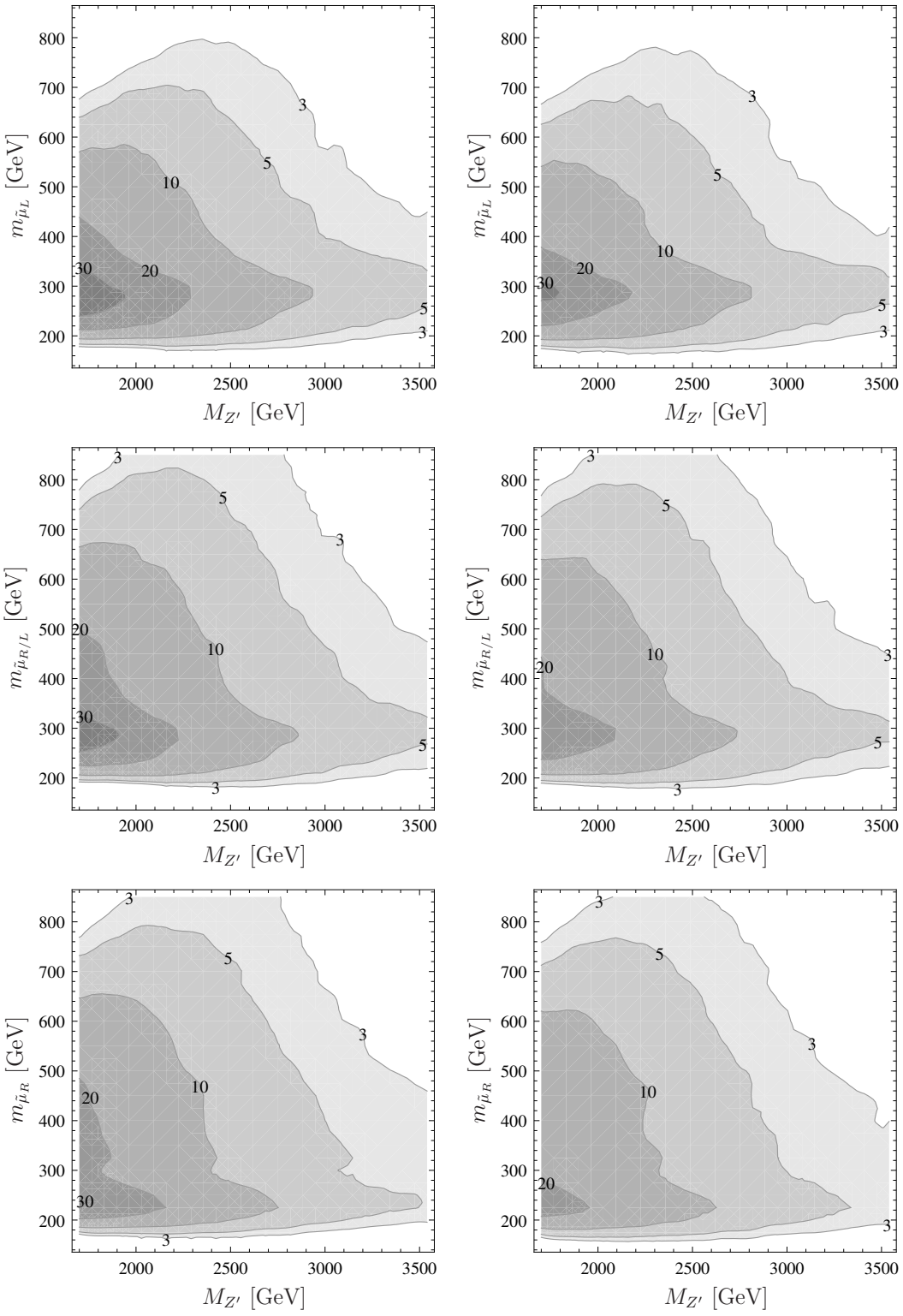

Figure 6.4: Significance of the smuon production at 100 fb^{-1} for two different sets of cuts and three different ratios of the slepton masses: (left column) first set of cuts, see eqns. (6.3), (6.4) and (right column) second cut set, see eq. (6.5). The smuon mass relations are (first row) $m_{\tilde{\mu}_R} = 1.2\, m_{\tilde{\mu}_L}$, (second row) $m_{\tilde{\mu}_L} = m_{\tilde{\mu}_R}$ and (last row) $m_{\tilde{\mu}_L} = 1.2\, m_{\tilde{\mu}_R}$.

part of the signal events do not survive the applied cuts. Similar results are obtained for the other smuon mass ratios.

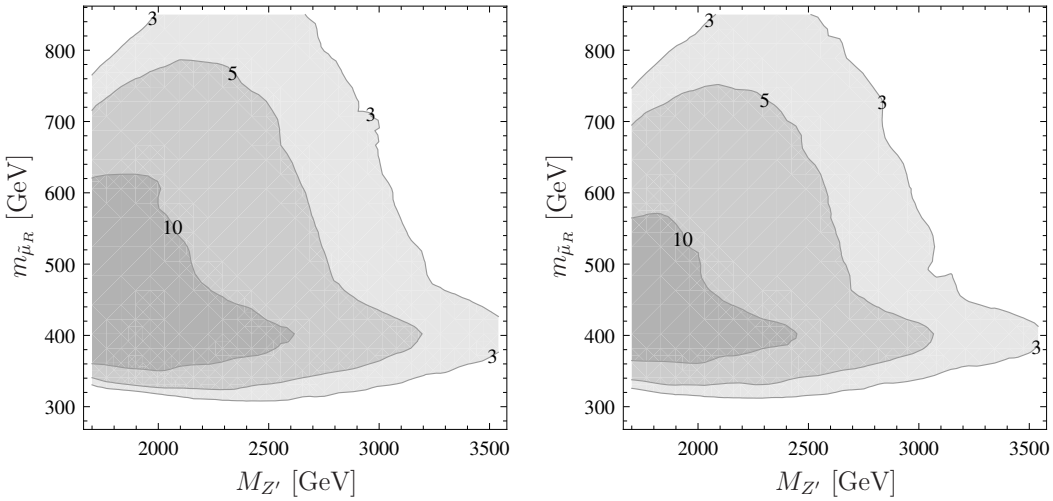

Figure 6.5: Significance level of the smuon production at 100 fb^{-1} for (left column) cut set 1, see eqns. (6.3), (6.4) and (right column) cut set 2, see eq. (6.5). The mass of the LSP is about 280 GeV and the smuon mass ratio is $m_{\tilde{\mu}_L} = 1.2\, m_{\tilde{\mu}_R}$.

6.4.2 $\int Ldt = 300$ fb^{-1}

The same as in 6.4.1 has been done here for an integrated luminosity of 300 fb^{-1}. Naturally, the area of (at least) 5 σ significance broadens, while even significances of considerably more than 10 σ could potentially be achieved. Exemplary plots are shown in fig. 6.6 for the case $m_{\tilde{\mu}_L} = 1.2\, m_{\tilde{\mu}_R}$.

Summarizing, if a Z'_{B-L} exists in the considered mass range, its resonant production and decays will make the detection of light sleptons possible in the mass range of some hundred GeV. Thus, the Z' could provide the first signals of supersymmetric particles at the LHC.

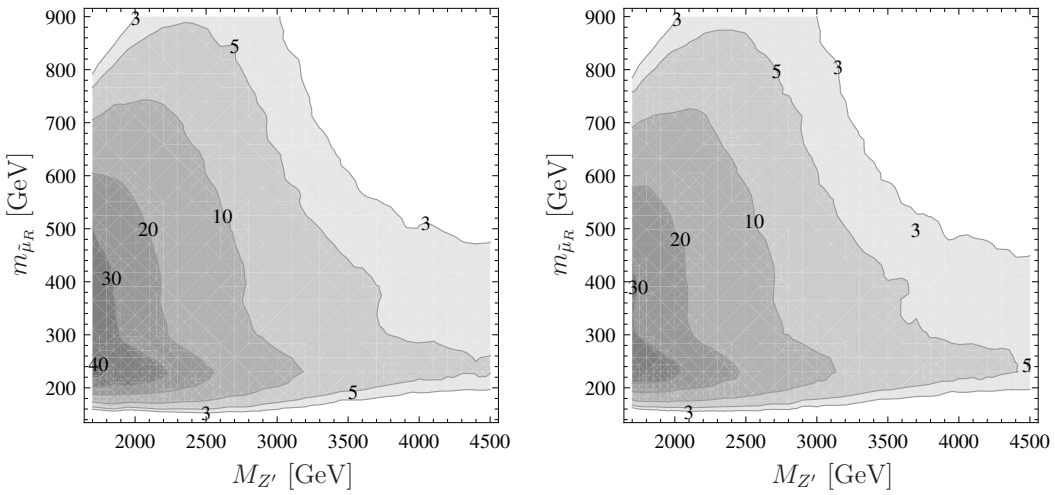

Figure 6.6: Significance level of the smuon production at 300 fb^{-1} for (left column) cut set 1, see eqns. (6.3), (6.4) and (right column) cut set 2, see eq. (6.5. The mass of the LSP is about 140 GeV and the smuon mass ratio was fixed to $m_{\tilde{\mu}_L} = 1.2\, m_{\tilde{\mu}_R}$.

Chapter 7

Summary

In this work we studied the R-parity conserving minimal supersymmetric model, extended by a local $U(1)_{B-L}$ symmetry, where $B-L$ stands for baryon number minus lepton number. We embedded the model in mSUGRA-inspired boundary conditions similar to the CMSSM, unifying the gauge couplings as well as the soft SUSY breaking parameters at the GUT scale.

Due to the extra $U(1)$ group there are new fields present in the model. First, in order to avoid anomalies, right-handed neutrinos have to be introduced which are singlets under the Standard Model gauge group. Secondly, due to gauged $B-L$, an extra neutral vector boson – the Z' – as well as fields responsible for the spontaneous breaking of the $B-L$ symmetry appear. A peculiarity here is the possibility of gauge kinetic mixing which is a mixing term between the field strength tensors of the two Abelian symmetry groups. This results in an off-diagonal coupling $\bar{g}$ connecting the Z' vertices with hypercharge and leading to various tree level mixings between the new fields and the ones already present in the MSSM.

We have calculated the partial decay widths and branching ratios of the Z' while taking care of gauge kinetic mixing. We found that $\bar{g}$ can have sizeable effect on the couplings and thus on the production and decay properties of the Z'. In particular, the couplings to leptons and up-type quarks are found to be reduced by gauge kinetic mixing which both has the effect that the lower bounds on the Z' mass get reduced considerably. Using the latest ATLAS results on dilepton production, we demonstrated that taking into account $\bar{g}$ results in a reduction of the limits by around 200 GeV.

For analysing decays of the Z' into supersymmetric particles, we have calculated the respective cross sections via an on-shell Z' at $\sqrt{s} = 14$ TeV as well as the subsequent SUSY cascade decays. Despite a suppression by means of $\bar{g}$, the channel $Z' \to \widetilde{l}\widetilde{l}^*$ can have cross sections of a few fb. Depending on the underlying SUSY parameters, also sneutrino, chargino and neutralino production may be amplified by a Z' resonance. We found that a likely final state after the decays of the sparticles down to the LSP, as well as probably one of the most accessible, is the one containing two leptons and two lightest neutralinos stemming from Z' decays into slepton pairs.

Moreover, we have performed a Monte Carlo study searching for a final state

containing two muons plus missing transverse energy in order to discuss the impact of a Z' peak on the production and discovery of smuons. We found that smuons up to masses of 800 GeV (900 GeV) can be detected at LHC-14 for an integrated luminosity of 100 fb^{-1} (300 fb^{-1}) with Z' masses up to 2.8 TeV (3.1 TeV). Thus, the Z' could possibly provide the first hints to supersymmetry.

Appendix A

Z' couplings

In this chapter we show the Z' vertices responsible for the various two-body decays discussed in this work.

A.1 Couplings to fermions

The vertex structure is given by

$$i\bar{f}_i\gamma^\mu(c_{Lf,ij}P_L + c_{Rf,ij}P_R)f_j Z'_\mu\,. \tag{A.1}$$

- charged leptons: $Z' - \bar{e}_i - e_j$

$$c_{Le,ij} = \frac{1}{2}\delta_{ij}\Big(\Big(g_1 \sin\Theta_W - g_2\cos\Theta_W\Big)\sin\Theta'_W + \Big(\bar{g} + g_{\mathrm{BL}}\Big)\cos\Theta'_W\Big) \tag{A.2}$$

$$c_{Re,ij} = \frac{1}{2}\delta_{ij}\Big(2g_1\sin\Theta_W\sin\Theta'_W + \Big(2\bar{g} + g_{\mathrm{BL}}\Big)\cos\Theta'_W\Big)\,. \tag{A.3}$$

- neutrinos: $Z' - \nu_i - \nu_j$

$$\begin{aligned} c_{L\nu,ij} =& \frac{1}{2}\Big(\Big(\Big(g_1\sin\theta_W + g_2\cos\theta_W\Big)\sin\theta'_W + \Big(\bar{g} + g_{\mathrm{BL}}\Big)\cos\theta'_W\Big)\sum_{a=1}^{3} U^{V,*}_{ja}U^V_{ia} \\ & - g_{\mathrm{BL}}\cos\theta'_W\sum_{a=1}^{3} U^{V,*}_{j3+a}U^V_{i3+a}\Big) \end{aligned} \tag{A.4}$$

$$\begin{aligned} c_{R\nu,ij} =& -\frac{1}{2}\Big(\Big(\Big(g_1\sin\theta_W + g_2\cos\theta_W\Big)\sin\theta'_W + \Big(\bar{g} + g_{\mathrm{BL}}\Big)\cos\theta'_W\Big)\sum_{a=1}^{3} U^{V,*}_{ia}U^V_{ja} \\ & - g_{\mathrm{BL}}\cos\theta'_W\sum_{a=1}^{3} U^{V,*}_{i3+a}U^V_{j3+a}\Big)\,. \end{aligned} \tag{A.5}$$

U^V_{kl} is the unitary 6×6 matrix that diagonalizes the neutrino mass matrix.

- up-type quarks: $Z' - \bar{u}_{i\alpha} - u_{j\beta}$

$$c_{Lu,ij} = -\frac{1}{6}\delta_{\alpha\beta}\delta_{ij}\Big(\Big(-3g_2\cos\theta_W + g_1\sin\theta_W\Big)\sin\theta'_W + \Big(\bar{g} + g_{\mathrm{BL}}\Big)\cos\theta'_W\Big) \tag{A.6}$$

$$c_{Ru,ij} = -\frac{1}{6}\delta_{\alpha\beta}\delta_{ij}\Big(4g_1\sin\theta_W\sin\theta'_W + \Big(4\bar{g} + g_{\mathrm{BL}}\Big)\cos\theta'_W\Big)\,. \tag{A.7}$$

- down-type quarks: $Z' - \bar{d}_{i\alpha} - d_{j\beta}$

$$c_{Ld,ij} = -\frac{1}{6}\delta_{\alpha\beta}\delta_{ij}\Big(\Big(3g_2\cos\theta_W + g_1\sin\theta_W\Big)\sin\theta'_W + \Big(\bar{g} + g_{\mathrm{BL}}\Big)\cos\theta'_W\Big) \tag{A.8}$$

$$c_{Rd,ij} = \frac{1}{6}\delta_{\alpha\beta}\delta_{ij}\Big(2g_1\sin\theta_W\sin\theta'_W + \Big(2\bar{g} - g_{\mathrm{BL}}\Big)\cos\theta'_W\Big)\,. \tag{A.9}$$

- neutralinos: $Z' - \tilde{\chi}^0_i - \tilde{\chi}^0_j$

$$\begin{aligned} c_{L\tilde{\chi}^0,ij} =& \frac{1}{2}\Big(N^*_{j3}\Big(\Big(g_1\sin\theta_W + g_2\cos\theta_W\Big)\sin\theta'_W + \bar{g}\cos\theta'_W\Big)N_{i3} \\ &- N^*_{j4}\Big(g_1\sin\theta_W\sin\theta'_W + g_2\cos\theta_W\sin\theta'_W + \bar{g}\cos\theta'_W\Big)N_{i4} \\ &+ 2g_{\mathrm{BL}}\cos\theta'_W\Big(N^*_{j6}N_{i6} - N^*_{j7}N_{i7}\Big)\Big) \end{aligned} \tag{A.10}$$

$$\begin{aligned} c_{R\tilde{\chi}^0,ij} =& -\frac{1}{2}\Big(N^*_{i3}\Big(\Big(g_1\sin\theta_W + g_2\cos\theta_W\Big)\sin\theta'_W + \bar{g}\cos\theta'_W\Big)N_{j3} \\ &- N^*_{i4}\Big(g_1\sin\theta_W\sin\theta'_W + g_2\cos\theta_W\sin\theta'_W + \bar{g}\cos\theta'_W\Big)N_{j4} \\ &+ 2g_{\mathrm{BL}}\cos\theta'_W\Big(N^*_{i6}N_{j6} - N^*_{i7}N_{j7}\Big)\Big)\,. \end{aligned} \tag{A.11}$$

  N_{kl} is the unitary 7×7 matrix that diagonalizes the neutralino mass matrix.

- charginos: $Z' - \tilde{\chi}^+_i - \tilde{\chi}^-_j$

$$\begin{aligned} c_{L\tilde{\chi}^\pm,ij} =& -\frac{1}{2}\Big(2g_2U^*_{j1}\cos\theta_W\sin\theta'_W U_{i1} \\ &- U^*_{j2}\Big(\Big(g_1\sin\theta_W - g_2\cos\theta_W\Big)\sin\theta'_W + \bar{g}\cos\theta'_W\Big)U_{i2}\Big) \end{aligned} \tag{A.12}$$

$$\begin{aligned} c_{R\tilde{\chi}^\pm,ij} =& -\frac{1}{2}\Big(2g_2V^*_{i1}\cos\theta_W\sin\theta'_W V_{j1} \\ &- V^*_{i2}\Big(\Big(g_1\sin\theta_W - g_2\cos\theta_W\Big)\sin\theta'_W + \bar{g}\cos\theta'_W\Big)V_{j2}\Big)\,. \end{aligned} \tag{A.13}$$

  U_{kl} and V_{kl} are the unitary 2×2 matrices needed to diagonalize chargino mass matrix.

A.2 Couplings to scalars

The vertex structure is given by

$$c_{s,ij}\tilde{s}_i\tilde{s}_j^*\left(p_{s_i}^\mu - p_{s_j^*}^\mu\right)Z'_\mu\,, \tag{A.14}$$

where p_{s_i} and $p_{s_j^*}$ are the four-momenta of the scalars. In the following, Z^p_{kl} denote the matrices needed to diagonalize the respective underlying mass matrix of the particles p.

- charged sleptons: $Z' - \tilde{e}_i - \tilde{e}_j^*$

$$\begin{aligned} c_{e,ij} =& -\frac{i}{2}\Big(\Big(\Big(g_1\sin\theta_W - g_2\cos\theta_W\Big)\sin\theta'_W + \Big(\bar{g}+g_{\mathrm{BL}}\Big)\cos\theta'_W\Big)\sum_{a=1}^{3} Z^{E,*}_{ia}Z^E_{ja} \\ &+ \Big(2g_1\sin\theta_W\sin\theta'_W + \Big(2\bar{g}+g_{\mathrm{BL}}\Big)\cos\theta'_W\Big)\sum_{a=1}^{3} Z^{E,*}_{i3+a}Z^E_{j3+a}\Big)\,. \end{aligned} \tag{A.15}$$

- sneutrinos: $Z' - \tilde{\nu}_i^P - \tilde{\nu}_j^S$

$$\begin{aligned} c_{\nu,ij} =& -\frac{1}{2}\Big(-\Big(\Big(g_1\sin\theta_W + g_2\cos\theta_W\Big)\sin\theta'_W + \Big(\bar{g}+g_{\mathrm{BL}}\Big)\cos\theta'_W\Big)\sum_{a=1}^{3} Z^{P,*}_{ia}Z^{S,*}_{ja} \\ &- g_{\mathrm{BL}}\cos\theta'_W\sum_{a=1}^{3} Z^{P,*}_{i3+a}Z^{S,*}_{j3+a}\Big)\,. \end{aligned} \tag{A.16}$$

- up-type squarks: $Z' - \tilde{u}_{i\alpha} - \tilde{u}^*_{j\beta}$

$$\begin{aligned} c_{q_u,ij} =& \frac{i}{6}\delta_{\alpha\beta}\Big(\Big(\Big(-3g_2\cos\theta_W + g_1\sin\theta_W\Big)\sin\theta'_W + \Big(\bar{g}+g_{\mathrm{BL}}\Big)\cos\theta'_W\Big)\sum_{a=1}^{3} Z^{U,*}_{ia}Z^U_{ja} \\ &+ \Big(4g_1\sin\theta_W\sin\theta'_W + \Big(4\bar{g}+g_{\mathrm{BL}}\Big)\cos\theta'_W\Big)\sum_{a=1}^{3} Z^{U,*}_{i3+a}Z^U_{j3+a}\Big)\,. \end{aligned} \tag{A.17}$$

- down-type squarks: $Z' - \tilde{d}_{i\alpha} - \tilde{d}^*_{j\beta}$

$$\begin{aligned} c_{q_d,ij} =& \frac{i}{6}\delta_{\alpha\beta}\Big(\Big(\Big(3g_2\cos\theta_W + g_1\sin\theta_W\Big)\sin\theta'_W + \Big(\bar{g}+g_{\mathrm{BL}}\Big)\cos\theta'_W\Big)\sum_{a=1}^{3} Z^{D,*}_{ia}Z^D_{ja} \\ &+ \Big(-2g_1\sin\theta_W\sin\theta'_W + \Big(-2\bar{g}+g_{\mathrm{BL}}\Big)\cos\theta'_W\Big)\sum_{a=1}^{3} Z^{D,*}_{i3+a}Z^D_{j3+a}\Big)\,. \end{aligned} \tag{A.18}$$

- charged Higgs: $Z' - H_i^- - H_j^+$

$$c_{H^\pm,ij} = \frac{i}{2}\delta_{ij}\Big(\Big(g_1 \sin\theta_W - g_2 \cos\theta_W\Big)\sin\theta'_W + \bar{g}\cos\theta'_W\Big)\,. \tag{A.19}$$

- CP-odd and CP-even Higgs: $Z' - A_i^0 - h_j$

$$\begin{aligned} c_{Ah,ij} =& \frac{1}{2}\Big(- \Big(\Big(g_1 \sin\theta_W + g_2 \cos\theta_W\Big)\sin\theta'_W + \bar{g}\cos\theta'_W\Big) Z^A_{i1} Z^H_{j1} \\ &+ \Big(\Big(g_1 \sin\theta_W + g_2 \cos\theta_W\Big)\sin\theta'_W + \bar{g}\cos\theta'_W\Big) Z^A_{i2} Z^H_{j2} \\ &- 2 g_{\mathrm{BL}} \cos\theta'_W \Big(Z^A_{i3} Z^H_{j3} - Z^A_{i4} Z^H_{j4}\Big)\Big)\,. \end{aligned} \tag{A.20}$$

A.3 Coupling to vector bosons

The only three-vector-boson vertex containing a Z' is the coupling $Z'_\mu - W^+_\rho - W^-_\sigma$. It is parametrized as follows:

$$i c_{V_i V_j}\Big(g_{\rho\mu}\Big(- p_\sigma^{Z'_\mu} + p_\sigma^{W^+_\rho}\Big) + g_{\rho\sigma}\Big(- p_\mu^{W^+_\rho} + p_\mu^{W^-_\sigma}\Big) + g_{\sigma\mu}\Big(- p_\rho^{W^-_\sigma} + p_\rho^{Z'_\mu}\Big)\Big) Z'^\mu V_i^\rho V_j^\sigma\,, \tag{A.21}$$

with

$$c_{WW} = g_2 \cos\theta_W \sin\theta'_W\,. \tag{A.22}$$

A.4 Coupling to one vector boson and one scalar

The vertices are parametrized as follows

$$i c_{Vs,i} s_i g_{\sigma\mu} Z'^\mu V^\sigma\,. \tag{A.23}$$

- Z and Higgs: $Z'_\mu - Z_\sigma - h_i$

$$\begin{aligned} c_{Zh,i} = \frac{1}{2}\Big(& - v_d\Big(g_1 \bar{g} \cos\theta'^2_W \sin\theta_W + g_2^2 \cos\theta_W^2 \cos\theta'_W \sin\theta'_W \\ & + \cos\theta'_W\Big(g_1^2 \sin\theta_W^2 - \bar{g}^2\Big)\sin\theta'_W - g_1 \bar{g} \sin\theta_W \sin\theta'^2_W \\ & + g_2 \cos\theta_W\Big(g_1 \sin\theta_W \sin 2\theta'_W + \bar{g}\cos\theta'^2_W - \bar{g}\sin\theta'^2_W\Big)\Big) Z^H_{i1} \\ & - v_u\Big(g_1 \bar{g} \cos\theta'^2_W \sin\theta_W + g_2^2 \cos\theta_W^2 \cos\theta'_W \sin\theta'_W \\ & + \cos\theta'_W\Big(g_1^2 \sin\theta_W^2 - \bar{g}^2\Big)\sin\theta'_W - g_1 \bar{g} \sin\theta_W \sin\theta'^2_W \\ & + g_2 \cos\theta_W\Big(g_1 \sin\theta_W \sin 2\theta'_W + \bar{g}\cos\theta'^2_W - \bar{g}\sin\theta'^2_W\Big)\Big) Z^H_{i2} \\ & + 2 g_{\mathrm{BL}} \sin 2\theta'_W \Big(v_\eta Z^H_{i3} + v_{\bar{\eta}} Z^H_{i4}\Big)\Big)\,. \end{aligned} \tag{A.24}$$

- W and charged Higgs: $Z'_\mu - W^\pm_\sigma - H^\mp_i$

$$c_{W^+H^-,i} = -\frac{1}{2}g_2\Big(v_d Z^{+,*}_{i1} - v_u Z^{+,*}_{i2}\Big)\Big(g_1 \sin\theta_W \sin\theta'_W + \bar{g}\cos\theta'_W\Big)\,. \quad \text{(A.25)}$$

$$c_{W^-H^+,i} = -\frac{1}{2}g_2\Big(v_d Z^{+}_{i1} - v_u Z^{+}_{i2}\Big)\Big(g_1 \sin\theta_W \sin\theta'_W + \bar{g}\cos\theta'_W\Big)\,. \quad \text{(A.26)}$$

Appendix B

Z' decays at BLV and BLVI

B.1 BLV

Width of the Z': $\Gamma_{Z'} = 22.1$ GeV

$$BR(Z' \to e^+e^-) = 11.87\ \% \quad \text{(B.1)}$$
$$BR(Z' \to \mu^+\mu^-) = 11.87\ \% \quad \text{(B.2)}$$
$$BR(Z' \to \tau^+\tau^-) = 11.87\ \% \quad \text{(B.3)}$$
$$BR(Z' \to d\bar{d}) = 9.93\ \% \quad \text{(B.4)}$$
$$BR(Z' \to s\bar{s}) = 9.93\ \% \quad \text{(B.5)}$$
$$BR(Z' \to b\bar{b}) = 9.93\ \% \quad \text{(B.6)}$$
$$BR(Z' \to \nu_e\nu_e) = 7.52\ \% \quad \text{(B.7)}$$
$$BR(Z' \to \nu_\mu\nu_\mu) = 7.52\ \% \quad \text{(B.8)}$$
$$BR(Z' \to \nu_\tau\nu_\tau) = 7.52\ \% \quad \text{(B.9)}$$
$$BR(Z' \to u\bar{u}) = 2.71\ \% \quad \text{(B.10)}$$
$$BR(Z' \to c\bar{c}) = 2.71\ \% \quad \text{(B.11)}$$
$$BR(Z' \to t\bar{t}) = 2.69\ \% \quad \text{(B.12)}$$
$$BR(Z' \to \tilde{\chi}_1^0\tilde{\chi}_1^0) = 1.11\ \% \quad \text{(B.13)}$$
$$BR(Z' \to \tilde{\tau}_1\tilde{\tau}_1^*) = 0.98\ \% \quad \text{(B.14)}$$
$$BR(Z' \to \tilde{\mu}_R\tilde{\mu}_R^*) = 0.54\ \% \quad \text{(B.15)}$$
$$BR(Z' \to \tilde{e}_R\tilde{e}_R^*) = 0.54\ \% \quad \text{(B.16)}$$
$$BR(Z' \to W^+W^-) = 0.40\ \% \quad \text{(B.17)}$$
$$BR(Z' \to Zh_1) = 0.21\ \% \quad \text{(B.18)}$$
$$BR(Z' \to \tilde{\chi}_1^0\tilde{\chi}_2^0) = 0.07\ \% \quad \text{(B.19)}$$
$$BR(Z' \to \tilde{\chi}_1^0\tilde{\chi}_4^0) = 0.04\ \% \quad \text{(B.20)}$$
$$BR(Z' \to h_2A^0) = 0.03\ \% \quad \text{(B.21)}$$

B.2 BLVI

Width of the Z': $\Gamma_{Z'} = 19.6$ GeV

$$BR(Z' \to e^+e^-) = 10.27\ \% \quad \text{(B.22)}$$
$$BR(Z' \to \mu^+\mu^-) = 10.27\ \% \quad \text{(B.23)}$$
$$BR(Z' \to \tau^+\tau^-) = 10.27\ \% \quad \text{(B.24)}$$
$$BR(Z' \to d\bar{d}) = 8.95\ \% \quad \text{(B.25)}$$
$$BR(Z' \to s\bar{s}) = 8.95\ \% \quad \text{(B.26)}$$
$$BR(Z' \to b\bar{b}) = 8.95\ \% \quad \text{(B.27)}$$
$$BR(Z' \to \nu_e\nu_e) = 6.57\ \% \quad \text{(B.28)}$$
$$BR(Z' \to \nu_\mu\nu_\mu) = 6.57\ \% \quad \text{(B.29)}$$
$$BR(Z' \to \nu_\tau\nu_\tau) = 6.57\ \% \quad \text{(B.30)}$$
$$BR(Z' \to u\bar{u}) = 2.33\ \% \quad \text{(B.31)}$$
$$BR(Z' \to c\bar{c}) = 2.33\ \% \quad \text{(B.32)}$$
$$BR(Z' \to t\bar{t}) = 2.30\ \% \quad \text{(B.33)}$$
$$BR(Z' \to \tilde{\tau}_1\tilde{\tau}_1^*) = 1.89\ \% \quad \text{(B.34)}$$
$$BR(Z' \to \tilde{\mu}_R\tilde{\mu}_R^*) = 1.85\ \% \quad \text{(B.35)}$$
$$BR(Z' \to \tilde{e}_R\tilde{e}_R^*) = 1.85\ \% \quad \text{(B.36)}$$
$$BR(Z' \to \tilde{\tau}_2\tilde{\tau}_2^*) = 1.84\ \% \quad \text{(B.37)}$$
$$BR(Z' \to \tilde{\mu}_L\tilde{\mu}_L^*) = 1.83\ \% \quad \text{(B.38)}$$
$$BR(Z' \to \tilde{e}_L\tilde{e}_L^*) = 1.83\ \% \quad \text{(B.39)}$$
$$BR(Z' \to \tilde{\nu}_1^S\tilde{\nu}_1^P) = 0.95\ \% \quad \text{(B.40)}$$
$$BR(Z' \to \tilde{\nu}_2^S\tilde{\nu}_2^P) = 0.93\ \% \quad \text{(B.41)}$$
$$BR(Z' \to \tilde{\nu}_3^S\tilde{\nu}_3^P) = 0.93\ \% \quad \text{(B.42)}$$
$$BR(Z' \to \tilde{\chi}_2^+\tilde{\chi}_2^-) = 0.64\ \% \quad \text{(B.43)}$$
$$BR(Z' \to W^+W^-) = 0.39\ \% \quad \text{(B.44)}$$
$$BR(Z' \to \tilde{\chi}_3^0\tilde{\chi}_4^0) = 0.34\ \% \quad \text{(B.45)}$$
$$BR(Z' \to Zh_2) = 0.20\ \% \quad \text{(B.46)}$$
$$BR(Z' \to \tilde{\chi}_5^0\tilde{\chi}_5^0) = 0.12\ \% \quad \text{(B.47)}$$
$$BR(Z' \to \tilde{\chi}_1^\pm\tilde{\chi}_2^\mp) = 0.04\ \% \quad \text{(B.48)}$$
$$BR(Z' \to \tilde{\chi}_2^0\tilde{\chi}_3^0) = 0.02\ \% \quad \text{(B.49)}$$
$$BR(Z' \to \tilde{\chi}_1^0\tilde{\chi}_5^0) = 0.01\ \% \quad \text{(B.50)}$$

Appendix C

Mass matrices

Here we show the mass matrices for the sfermions not given in chapter 4.

C.1 Sneutrinos

We decompose the sneutrinos into the scalar and the pseudoscalar states

$$\tilde{\nu}_L^i = \frac{1}{\sqrt{2}}(\phi_L^i + i\chi_L^i) \quad \text{and} \quad \tilde{\nu}_R^i = \frac{1}{\sqrt{2}}(\phi_R^i + i\chi_R^i)\,. \tag{C.1}$$

In the basis (ϕ_L, ϕ_R) respectively (χ_L, χ_R) the mass matrices for the CP-even and CP-odd sneutrinos read [40]

$$m^2_{\tilde{\nu}^S} = \Re\begin{pmatrix} m^R_{LL} & m^{R,T}_{RL} \\ m^R_{RL} & m^R_{RR} \end{pmatrix}, \qquad m^2_{\tilde{\nu}^P} = \Re\begin{pmatrix} m^I_{LL} & m^{I,T}_{RL} \\ m^I_{RL} & m^I_{RR} \end{pmatrix}, \tag{C.2}$$

with $m^I_{LL} = m^R_{LL} = m_{LL}$ and

$$m_{LL} = M^2_{\tilde{L}} + \frac{v_u^2}{2}Y_\nu^\dagger Y_\nu + \frac{1}{8}\Big((g_1^2 + g_2^2 + \bar{g}^2 + \bar{g}g_{\mathrm{BL}})(v_d^2 - v_u^2) + 2(g^2_{\mathrm{BL}} + \bar{g}g_{\mathrm{BL}})(v_\eta^2 - v_{\bar{\eta}}^2)\Big)\mathbb{1} \tag{C.3}$$

$$m^{R,I}_{RL} = \frac{1}{\sqrt{2}}\Big(v_u T_\nu^* - v_d \mu Y_\nu^*\Big) \pm v_u v_\eta Y_x Y_\nu^* \tag{C.4}$$

$$\begin{aligned} m^{R,I}_{RR} = {} & M^2_{\tilde{\nu}} + \frac{v_u^2}{2}Y_\nu Y_\nu^\dagger + 2v_\eta^2 Y_x Y_x^* \pm \sqrt{2}v_\eta T_x \mp \sqrt{2}Y_x v_{\bar{\eta}}\mu'^* \\ & + \frac{1}{8}\Big(2g^2_{\mathrm{BL}}(v_{\bar{\eta}}^2 - v_\eta^2) + \bar{g}g_{\mathrm{BL}}(v_u^2 - v_d^2)\Big)\mathbb{1}\,. \end{aligned} \tag{C.5}$$

C.2 Squarks

C.2.1 Up-type squarks

The mass matrix in the basis $(\tilde{u}_L, \tilde{u}_R)$ reads [16]

$$m_{\tilde{q}}^2 = \begin{pmatrix} M_{LL} & \frac{1}{\sqrt{2}}\Big(v_u T_u - v_d \mu^* Y_u\Big) \\ \frac{1}{\sqrt{2}}\Big(v_u T_u^\dagger - v_d \mu Y_u^\dagger\Big) & M_{RR} \end{pmatrix} \tag{C.6}$$

$$M_{LL} = M_{\tilde{Q}}^2 + \frac{v_u^2}{2} Y_u^\dagger Y_u + \frac{1}{24}\Big((g_1^2 - 3g_2^2 + \bar{g}^2 + \bar{g} g_{\mathrm{BL}})(v_u^2 - v_d^2) + 2(g_{\mathrm{BL}}^2 + \bar{g} g_{\mathrm{BL}})(v_{\bar{\eta}}^2 - v_\eta^2)\Big)\mathbb{1} \tag{C.7}$$

$$M_{RR} = M_{\tilde{u}}^2 + \frac{v_u^2}{2} Y_u Y_u^\dagger + \frac{1}{24}\Big(- (4g_1^2 + 4\bar{g}^2 + \bar{g} g_{\mathrm{BL}})(v_u^2 - v_d^2) - 2(g_{\mathrm{BL}}^2 + 4\bar{g} g_{\mathrm{BL}})(v_{\bar{\eta}}^2 - v_\eta^2)\Big)\mathbb{1}\,. \tag{C.8}$$

C.2.2 Down-type squarks

The mass matrix in the basis $(\tilde{d}_L, \tilde{d}_R)$ reads [16]

$$m_{\tilde{q}}^2 = \begin{pmatrix} M_{LL} & \frac{1}{\sqrt{2}}\Big(v_d T_d - v_u \mu^* Y_d\Big) \\ \frac{1}{\sqrt{2}}\Big(v_d T_d^\dagger - v_u \mu Y_d^\dagger\Big) & M_{RR} \end{pmatrix} \tag{C.9}$$

$$M_{LL} = M_{\tilde{Q}}^2 + \frac{v_d^2}{2} Y_d^\dagger Y_d + \frac{1}{24}\Big((g_1^2 + 3g_2^2 + \bar{g}^2 + \bar{g} g_{\mathrm{BL}})(v_u^2 - v_d^2) + 2(g_{\mathrm{BL}}^2 + \bar{g} g_{\mathrm{BL}})(v_{\bar{\eta}}^2 - v_\eta^2)\Big)\mathbb{1} \tag{C.10}$$

$$M_{RR} = M_{\tilde{d}}^2 + \frac{v_d^2}{2} Y_d Y_d^\dagger + \frac{1}{24}\Big((2g_1^2 + 2\bar{g}^2 - \bar{g} g_{\mathrm{BL}})(v_u^2 - v_d^2) - 2(g_{\mathrm{BL}}^2 - 2\bar{g} g_{\mathrm{BL}})(v_{\bar{\eta}}^2 - v_\eta^2)\Big)\mathbb{1}\,. \tag{C.11}$$

References

[1] L. Evans and P. Bryant, "LHC Machine", *JINST* **3** (2008), S08001.

[2] J. Donoghue, E. Golowich, and B. R. Holstein, *Dynamics of the standard model*, Cambridge University Press, 1994.

[3] M. Bohm, A. Denner, and H. Joos, *Gauge theories of the strong and electroweak interaction*, Teubner Verlag, 2001.

[4] J. Wess and B. Zumino, "Supergauge Transformations in Four-Dimensions", *Nucl.Phys.* **B70** (1974), 39–50.

[5] J. Wess and B. Zumino, "A Lagrangian Model Invariant Under Supergauge Transformations", *Phys.Lett.* **B49** (1974), 52.

[6] H. Georgi and S. Glashow, "Unity of All Elementary Particle Forces", *Phys.Rev.Lett.* **32** (1974), 438–441.

[7] H. Georgi, H. R. Quinn, and S. Weinberg, "Hierarchy of Interactions in Unified Gauge Theories", *Phys.Rev.Lett.* **33** (1974), 451–454.

[8] P. Langacker, "Grand Unified Theories and Proton Decay", *Phys.Rept.* **72** (1981), 185.

[9] K. Hirata et al., "Experimental limits on nucleon lifetime for lepton + meson decay modes", *Phys.Lett.* **B220** (1989), 308.

[10] R. N. Mohapatra, *Unification and Supersymmetry*, 3rd edition, Springer, 2002.

[11] R. Mohapatra, "Supersymmetric grand unification: An Update", (1999), 336–394, `arXiv:hep-ph/9911272 [hep-ph]`.

[12] M. S. Carena, A. Daleo, B. A. Dobrescu, and T. M. Tait, "Z' gauge bosons at the Tevatron", *Phys.Rev.* **D70** (2004), 093009, `arXiv:hep-ph/0408098 [hep-ph]`.

[13] J. Erler, P. Langacker, S. Munir, and E. Rojas, "Improved Constraints on Z-prime Bosons from Electroweak Precision Data", *JHEP* **0908** (2009), 017, arXiv:0906.2435 [hep-ph].

[14] A. Leike, "The Phenomenology of extra neutral gauge bosons", *Phys.Rept.* **317** (1999), 143–250, arXiv:hep-ph/9805494 [hep-ph].

[15] K. Babu, C. F. Kolda, and J. March-Russell, "Implications of generalized Z - Z-prime mixing", *Phys.Rev.* **D57** (1998), 6788–6792, arXiv:hep-ph/9710441 [hep-ph].

[16] B. O'Leary, W. Porod, and F. Staub, "Mass spectrum of the minimal SUSY B-L model", *JHEP* **1205** (2012), 042, arXiv:1112.4600 [hep-ph].

[17] R. M. Fonseca, M. Malinsky, W. Porod, and F. Staub, "Running soft parameters in SUSY models with multiple U(1) gauge factors", *Nucl.Phys.* **B854** (2012), 28–53, arXiv:1107.2670 [hep-ph].

[18] P. Langacker, "The Physics of Heavy Z' Gauge Bosons", *Rev.Mod.Phys.* **81** (2009), 1199–1228, arXiv:0801.1345 [hep-ph].

[19] T. Appelquist, B. A. Dobrescu, and A. R. Hopper, "Nonexotic neutral gauge bosons", *Phys.Rev.* **D68** (2003), 035012, arXiv:hep-ph/0212073 [hep-ph].

[20] V. De Romeri, M. Hirsch, and M. Malinsky, "Soft masses in SUSY SO(10) GUTs with low intermediate scales", *Phys.Rev.* **D84** (2011), 18 pages, 12 figures, 5 tables, 053012, arXiv:1107.3412 [hep-ph].

[21] M. Ambroso and B. A. Ovrut, "The B-L/Electroweak Hierarchy in Smooth Heterotic Compactifications", *Int.J.Mod.Phys.* **A25** (2010), 60 pages, 6 figures, 2631–2677, arXiv:0910.1129 [hep-th].

[22] K. Nakamura *et al.* [Particle Data Group], "Review of Particle Physics", *J. Phys. G* **37** (2010), 075021.

[23] J. Alcaraz et al., "A Combination of preliminary electroweak measurements and constraints on the standard model", (2006), arXiv:hep-ex/0612034 [hep-ex].

[24] G. Cacciapaglia, C. Csaki, G. Marandella, and A. Strumia, "The Minimal Set of Electroweak Precision Parameters", *Phys.Rev.* **D74** (2006), 033011, arXiv:hep-ph/0604111 [hep-ph].

[25] ATLAS-collaboration, "Search for high-mass dilepton resonances with 5 fb^{-1} of pp collisions at $\sqrt{s} = 7$ TeV with the ATLAS experiment", ATLAS-CONF-2012-007 (2012).

[26] S. Chatrchyan et al., "Search for narrow resonances in dilepton mass spectra in pp collisions at $\sqrt{s} = 7$ TeV", (2012), arXiv:1206.1849 [hep-ex].

[27] S. Coleman and J. Mandula, "All Possible Symmetries of the S Matrix", *Phys. Rev.* **159** (5 1967), 1251–1256, URL: http://link.aps.org/doi/10.1103/PhysRev.159.1251.

[28] P. Binétruy, *Supersymmetry - Theory, Experiment, and Cosmology*, Oxford University Press, 2006.

[29] R. Haag, J. T. Lopuszanski, and M. Sohnius, "All Possible Generators of Supersymmetries of the S- Matrix", *Nucl.Phys.* **B88** (1975), 257.

[30] S. P. Martin, "A Supersymmetry primer", (1997), arXiv:hep-ph/9709356 [hep-ph].

[31] I. J. Aitchison, "Supersymmetry and the MSSM: An Elementary introduction", (2005), Notes of Lectures for Graduate Students in Particle Physics Oxford, 2004 and 2005, arXiv:hep-ph/0505105 [hep-ph].

[32] D. Bailin and A. Love, *Supersymmetric Gauge Filed Theory and String Theory*, Graduate Student Series in Physics, Institute of Physics Publishing, 1994.

[33] W. Porod, *lecture notes to Supersymmetry.*

[34] M. Drees, R. Godbole, and P. Roy, *Theory and Phenomenology of Sparticles*, World Scientific, 2004.

[35] H. Nishino et al., "Search for Proton Decay via $p \to e^+\pi^0$ and $p \to \mu^+\pi^0$ in a Large Water Cherenkov Detector", *Phys.Rev.Lett.* **102** (2009), 141801, arXiv:0903.0676 [hep-ex].

[36] A. Dabelstein, "The One loop renormalization of the MSSM Higgs sector and its application to the neutral scalar Higgs masses", *Z.Phys.* **C67** (1995), 495–512, arXiv:hep-ph/9409375 [hep-ph].

[37] L. Basso, "Phenomenology of the minimal B-L extension of the Standard Model at the LHC", (2011), arXiv:1106.4462 [hep-ph].

[38] L. Basso et al., "Z' discovery potential at the LHC in the minimal $B-L$ extension of the Standard Model", *Eur.Phys.J.* **C71** (2011), 1613, arXiv:1002.3586 [hep-ph].

[39] W. Buchmuller, K. Hamaguchi, O. Lebedev, and M. Ratz, "Supersymmetric Standard Model from the Heterotic String (II)", *Nucl.Phys.* **B785** (2007), 149–209, arXiv:hep-th/0606187 [hep-th].

[40] M. E. Krauss, B. O'Leary, W. Porod, and F. Staub, "Implications of gauge kinetic mixing on Z' and slepton production at the LHC", (2012), arXiv:1206.3513 [hep-ph].

[41] C.-F. Chang, K. Cheung, and T.-C. Yuan, "Supersymmetric Decays of the Z' Boson", *JHEP* **1109** (2011), 058, arXiv:1107.1133 [hep-ph].

[42] P. Fileviez Perez and S. Spinner, "The Fate of R-Parity", *Phys.Rev.* **D83** (2011), 035004, arXiv:1005.4930 [hep-ph].

[43] L. Basso, S. Moretti, and G. M. Pruna, "A Renormalisation Group Equation Study of the Scalar Sector of the Minimal B-L Extension of the Standard Model", *Phys.Rev.* **D82** (2010), 055018, arXiv:1004.3039 [hep-ph].

[44] F. Eysselein, *Renormierung des erweiterten Modells $SU(2) \times U(1) \times U(1)'$ der elektroschwachen Wechselwirkung*, Dissertation, Julius-Maximilians-Universität Würzburg, 1991.

[45] L. Basso, B. O'Leary, W. Porod, and F. Staub, "Dark matter scenarios in the minimal SUSY B-L model", (2012), arXiv:1207.0507 [hep-ph].

[46] F. Staub, "SARAH", (2008), arXiv:0806.0538 [hep-ph].

[47] F. Staub, "From Superpotential to Model Files for FeynArts and CalcHep/CompHep", *Comput.Phys.Commun.* **181** (2010), 1077–1086, arXiv:0909.2863 [hep-ph].

[48] F. Staub, "Automatic Calculation of supersymmetric Renormalization Group Equations and Self Energies", *Comput.Phys.Commun.* **182** (2011), 808–833, arXiv:1002.0840 [hep-ph].

[49] W. Porod, "SPheno, a program for calculating supersymmetric spectra, SUSY particle decays and SUSY particle production at e+ e- colliders", *Comput.Phys.Commun.* **153** (2003), 275–315, arXiv:hep-ph/0301101 [hep-ph].

[50] W. Porod and F. Staub, "SPheno 3.1: Extensions including flavour, CP-phases and models beyond the MSSM", (2011), arXiv:1104.1573 [hep-ph].

[51] W. Kilian, T. Ohl, and J. Reuter, "WHIZARD: Simulating Multi-Particle Processes at LHC and ILC", *Eur.Phys.J.* **C71** (2011), 1742, arXiv:0708.4233 [hep-ph].

[52] A. Pukhov, "CalcHEP 2.3: MSSM, structure functions, event generation, batchs, and generation of matrix elements for other packages", (2004), arXiv:hep-ph/0412191 [hep-ph].

[53] J. Alwall et al., "MadGraph 5 : Going Beyond", *JHEP* **1106** (2011), 128, arXiv:1106.0522 [hep-ph].

[54] F. Staub, T. Ohl, W. Porod, and C. Speckner, "A tool box for implementing supersymmetric models", (2011), arXiv:1109.5147 [hep-ph].

[55] P. Bechtle et al., "Constrained Supersymmetry after two years of LHC data: a global view with Fittino", (2012), arXiv:1204.4199 [hep-ph].

[56] D. Ghosh, M. Guchait, S. Raychaudhuri, and D. Sengupta, "How Constrained is the cMSSM?", (2012), arXiv:1205.2283 [hep-ph].

[57] B. Fuks et al., "Precision predictions for Z' - production at the CERN LHC: QCD matrix elements, parton showers, and joint resummation", *Nucl.Phys.* **B797** (2008), 322–339, arXiv:0711.0749 [hep-ph].

[58] E. Accomando et al., "Z' physics with early LHC data", *Phys.Rev.* **D83** (2011), 075012, arXiv:1010.6058 [hep-ph].

[59] J. Pumplin et al., "New generation of parton distributions with uncertainties from global QCD analysis", *JHEP* **0207** (2002), 012, arXiv:hep-ph/0201195 [hep-ph].

[60] C. Uhlemann and N. Kauer, "Narrow-width approximation accuracy", *Nucl.Phys.* **B814** (2009), 195–211, arXiv:0807.4112 [hep-ph].

[61] N. Kauer, "Narrow-width approximation limitations", *Phys.Lett.* **B649** (2007), 413–416, arXiv:hep-ph/0703077 [hep-ph].

[62] J. Terning, C. Wagner, and D. Zeppenfeld, *Physics in $D \geq 4$: Proceedings of the Theoretical Advanced Study Institute in Elementary Particle Physics*, World Scientific, 2004.

List of Figures

List of Tables

Acknowledgement

At that point it is time to thank some people which deserve to be mentioned here: I would like to thank:

- Prof. Dr. Werner Porod for including me in his SUSY work group, offering this interesting topic to me and for his patient help all through the time of this work.
- Dr. Ben O'Leary and Dr. Florian Staub, who were responsive night and day, stood aside to solve several mysteries and provided various helpful computing assistances.
- Lukas Mitzka for sharing his knowledge of `WHIZARD` and a lot of other stuff with me.
- my office colleagues Enrico Herrmann and Christof Weiß as well as my former office colleagues Asma Cheriguene and Martin Krauß for lots of interesting discussions and lots of fun.
- Maximilian Pietsch and all the other fellow students that accompanied me in the years of my study.
- once more Asma Cheriguene, Enrico Herrmann and particularly Ben O'Leary, who read this thesis carefully and helped me finding mistakes.
- Sven Heppel and Michael Hanselmann, for being valuable and reliable friends ever since I can remember.
- Last but not least my girlfriend Stefanie Damm for her love and patience as well as my family for their succour all over the time of my study.

Erklärung

Gemäß der allgemeinen Studien- und Prüfungsordnung für die Bachelor- und Masterstudiengänge an der Julius-Maximilians-Universität Würzburg erkläre ich hiermit, dass ich diese Arbeit selbstständig verfasst, keine anderen als die angegebenen Quellen und Hilfsmittel benutzt habe und diese Arbeit bisher keiner anderen Prüfungsbehörde unter Erlangung eines akademischen Grades vorgelegt habe.

Würzburg, den 10. Juli 2012

Manuel Krauß